Mechanisms for an ~7-kyr Climate and Sea-Level Oscillation During Marine Isotope Stage 3

Peter U. Clark[1], Steven W. Hostetler[2], Nicklas G. Pisias[3], Andreas Schmittner[3], and Katrin J. Meissner[4]

A number of climate proxies indicate that an ~7-kyr oscillation occurred during Marine Isotope Stage (MIS) 3, of which change in the Atlantic meridional overturning circulation (AMOC) and attendant change in cross-equatorial ocean heat transport played an integral role. The timing of Heinrich events and sea-level changes are clearly linked to this climate oscillation, indicating a coupled ice-ocean-atmosphere system with Heinrich events occurring in response to climate change. To explain this climate oscillation during MIS 3, we propose a causal chain of events involving transmission of a change in the AMOC through the ocean and atmosphere, with the timescale of the climate oscillation being set by the mass-balance response of Northern Hemisphere ice sheets. We begin at the point of an abrupt warming in the North Atlantic region that occurs in response to resumption of the AMOC and reduced sea ice extent. Warmer North Atlantic ocean and atmosphere temperatures cause a more negative Northern Hemisphere ice-sheet mass balance, with attendant increased freshwater flux inducing some reduction in the AMOC. By increasing cross-equatorial heat transport, a relatively active AMOC causes cooler sea surface temperatures (SSTs) in the South Atlantic, which are rapidly transmitted throughout the Southern Ocean by the Antarctic Circumpolar Current and are amplified by an increase in sea ice extent and a decrease in atmospheric CO_2. The heat content anomaly associated with the cooler SSTs in the Southern Ocean is transmitted equatorwards by the atmosphere and the shallow meridional circulation in the Pacific basin, where it cools equatorial SSTs. The effect of cooler equatorial Pacific SSTs is transmitted through the atmosphere and ocean to Northern Hemisphere ice sheets, leading to a more positive ice-sheet mass balance and ice-sheet growth. Ice-sheet expansion eventually

[1]Department of Geosciences, Oregon State University, Corvallis, Oregon, USA.
[2]U.S. Geological Survey, Department of Geosciences, Oregon State University, Corvallis, Oregon, USA.
[3]College of Oceanic and Atmospheric Sciences, Oregon State University, Corvallis, Oregon, USA.
[4]School of Earth and Ocean Sciences, University of Victoria, Victoria, British Columbia, Canada.

Ocean Circulation: Mechanisms and Impacts
Geophysical Monograph Series 173

10.1029/173GM15

results in increased calving, and thus an increase in the flux of freshwater to the North Atlantic which further reduces the AMOC. The subsequent reduction of ocean heat transport, amplified by an expansion of sea ice, cools the North Atlantic region. Reduced ocean heat transport in the Atlantic basin is balanced by warmer SSTs in the South Atlantic, which again are rapidly transmitted throughout the Southern Ocean by the Antarctic Circumpolar Current and amplified by a contraction of sea ice and an increase in atmospheric CO_2. The heat content anomaly associated with the warmer SSTs is transmitted equatorwards by the atmosphere and the shallow meridional circulation in the Pacific basin, where it warms SSTs in the tropics. The atmospheric bridge transmits warmer atmospheric temperatures to the Northern Hemisphere ice sheets, which increases ablation and runoff directed to the North Atlantic Ocean. This additional freshwater slows the AMOC further until, at some point, it ceases and thereby leads to peak expression of these atmospheric and oceanic responses. The collapsed AMOC results in subsurface warming in the North Atlantic which destabilizes ice shelves and triggers Heinrich events. The freshwater flux from a Heinrich event helps sustain the AMOC in greatly suppressed or off mode until subsurface warming erodes stratification of the upper ocean, and destabilizes the water column, which restarts the AMOC.

1. INTRODUCTION

Millennial-scale (10^3 yr) variability is an important component in the spectrum of climate change [*Mitchell*, 1976]. Although long documented from late-glacial and Holocene pollen records in Europe [*Jensen*, 1938; *Iversen*, 1954], the first convincing evidence of persistent large-amplitude millennial-scale change during the Pleistocene came from replication of stable isotope records measured in Greenland ice cores [*Dansgaard et al*., 1982, 1984; *Oeschger et al*., 1984]. Coincidently, the advent of ^{14}C dating by accelerator mass spectrometry in the early 1980s [*Wilson et al*., 1984] enabled the development of marine and terrestrial records that could resolve millennial-scale changes.

These developments ushered in a grand period of discovery, yielding a wide variety of climate proxies from highly resolved and well-dated Plio-Pleistocene records that now identify two fundamental characteristics of millennial-scale variability: (1) the amplitude of millennial-scale variability varies as a function of the amount of ice on the planet, with greatest amplitude being associated with intermediate ice volume [*Raymo et al*., 1998; *McManus et al*., 1999; *Schulz et al*., 1999; *Bartoli et al*., 2006], and (2) there are two spatially distinct signals, which *Bender* [1998] referred to as "northern" and "southern" responses in recognition of their association with the northern and southern hemispheres [*Alley and Clark*, 1999; *Clark et al*., 2002]. The northern response displays the same signature and timing of climate changes as those of the Greenland ice core records, wherein the so-called Dansgaard-Oeschger (D-O) events are characterized by abrupt warmings of 8-16 C [*Huber et al*., 2006] followed by gradual return to colder conditions (Figure 1a). *Bond et al*. [1993] first recognized that several successive D-O events of decreasing amplitude represented a longer term climate oscillation (Figure 1a), which have since become known as Bond cycles. In contrast, the southern response, best represented by Antarctic ice core records, exhibits less abrupt millennial changes with temperature changes of 1–3 C (Figure 1b). Synchronization of Greenland and Antarctic ice core records using the $\delta^{18}O$ of molecular O_2 [*Sowers and Bender*, 1995; *Bender et al*., 1994, 1999] and methane [*Blunier et al*., 1998; *Blunier and Brook*, 2001; *EPICA Community Members*, 2006] demonstrates that northern and southern signals are not in phase (Figure 1).

Change in the Atlantic meridional overturning circulation (AMOC) is most commonly invoked to explain these characteristics of millennial-scale change. Today, buoyancy forcing in the Nordic Seas drives the AMOC by inducing formation of North Atlantic Deep Water (NADW), which results in northerly cross-equatorial heat transport in the Atlantic basin that peaks at ~1.3 ± 0.3 PW at 25 N [*Ganachaud and Wunsch*, 2000]. The rate of overturning is sensitive to changes in the hydrological cycle, with decreased (increased) salinities at sites of deepwater formation causing a decrease (increase) in the AMOC [*Manabe and Stouffer*, 1988]; corresponding changes in poleward heat transport establish a so-called

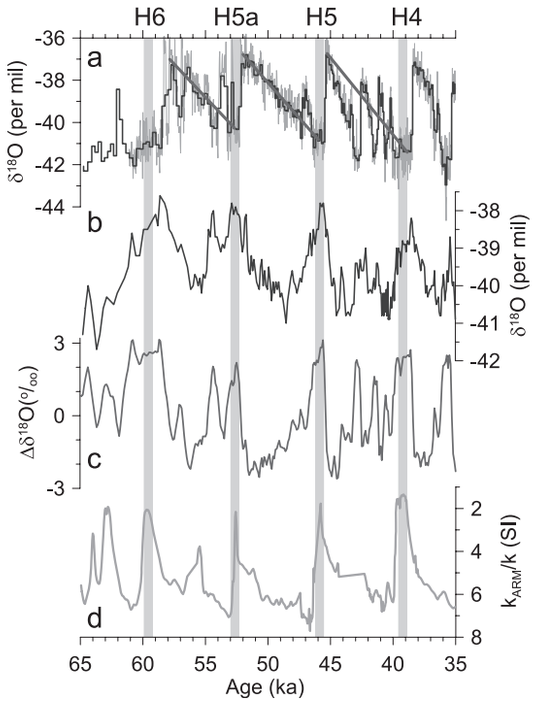

Figure 1. (a) The Greenland Ice Sheet Project 2 (GISP2) $\delta^{18}O$ record [*Grootes et al.*, 1993; *Stuiver and Grootes*, 2000]. The slanted lines represent the longer-term cooling trend followed by an abrupt warming, commonly referred to as Bond cycles. (b) The Byrd $\delta^{18}O$ record [*Johnsen et al.*, 1972], with the timescale synchronized to the GISP2 timescale by methane correlation [*Blunier and Brook*, 2001]. (c) Difference between the normalized GISP2 and Byrd $\delta^{18}O$ records. Heinrich events, shown by the vertical gray bars, occur at times of maximum cooling in Greenland and maximum warming in Antarctica. (d) Record of k_{ARM}/k (anhysteretic susceptibility/volume susceptibility) which identifies Heinrich layers [*Stoner et al.*, 2000].

bipolar seesaw [*Mix et al*., 1986; *Manabe and Stouffer*, 1988; *Crowley*, 1992] which is characterized by cooling (warming) in the North Atlantic and warming (cooling) in the South Atlantic (Figure 1). Warming and cooling is amplified by changes in the extent of sea ice.

Records of ice-rafted debris (IRD) suggest that Northern Hemisphere ice sheets also displayed substantial millennial-scale variability [*Bond et al*., 1992, 1999; *Bond and Lotti*, 1995]. While interpreting the significance of an IRD signal with respect to ice-sheet dynamics remains uncertain, the increase in IRD from multiple ice sheets during the cold phases of D-O events likely reflects a more-or-less uniform mass-balance response to cooling in the North Atlantic region [*Alley et al*., 1999; *Marshall and Koutnik*, 2006] On the other hand, IRD layers used to identify Heinrich events are dominated by sediment from Hudson Bay, and their rapid rate of deposition distinguishes them from other IRD layers and appears to require instability of the Laurentide Ice Sheet (LIS) [*Alley and MacAyeal*, 1994; *Marshall and Koutnik*, 2006]. The large flux of icebergs released from the LIS to the North Atlantic Ocean during a Heinrich event is commonly thought to have triggered a collapse of the AMOC with associated widespread climate responses [e.g., *Broecker*, 1994, 2003; *Ganopolski and Rahmstorf*, 2001; *Timmerman et al*., 2005].

These general characteristics of millennial-scale change are now fairly well established, but several important questions remain unanswered. What caused the changes in the AMOC that produced a bipolar seesaw? Do Heinrich events represent LIS instabilities triggered by internal ice dynamics or climate? What role did the tropical Pacific Ocean play in millennial-scale variability? We address these questions from the perspective of millennial-scale variability during marine isotope stage (MIS) 3, focusing on the interval from 30 ka to 65 ka. In doing so, we focus on the longer period, higher amplitude variability revealed by the relationship between Greenland and Antarctic ice core records and Heinrich events. The largest amplitude warming in Antarctica (the so-called A events) is contemporaneous with the terminal cooling of a Bond cycle in Greenland, and Heinrich events occur at this time of maximum temperature differential between the two polar hemispheres (Figure 1). Guided by these relations, we use additional data sets and model results to develop a conceptual model of an ocean-atmosphere-ice mechanism to explain the lower frequency (~7 kyr) climate oscillation during MIS 3. Heinrich events are clearly an integral part of this oscillation, but we propose that the events are a response to, rather than the cause of, collapse of AMOC.

2. DATA ANALYSIS

We analyze jointly 39 high-resolution time series to examine climate variability between 30 and 65 ka at a number of locations around the world (Figure 2, Table 1). The data include proxies of sea surface temperature (SST) and atmospheric temperature, deep-ocean circulation, monsoon strength, ice sheets, ocean productivity, and the hydrological cycle. The initial pattern recognition of northern and southern modes of variability proposed by *Bender* [1998] has been reinforced by the continued addition of new records [*Alley and Clark*, 1999; *Clark et al*., 2002; *Kiefer and Kienast*, 2005]. We first illustrate how these patterns have been inferred with some representative time series, and then discuss records in which the dominant signal in proxies occurs at times of Heinrich events.

We preface this discussion with some caveats. As we will show with specific examples, many records are attributed to one of the three modes of variability (northern, southern, and

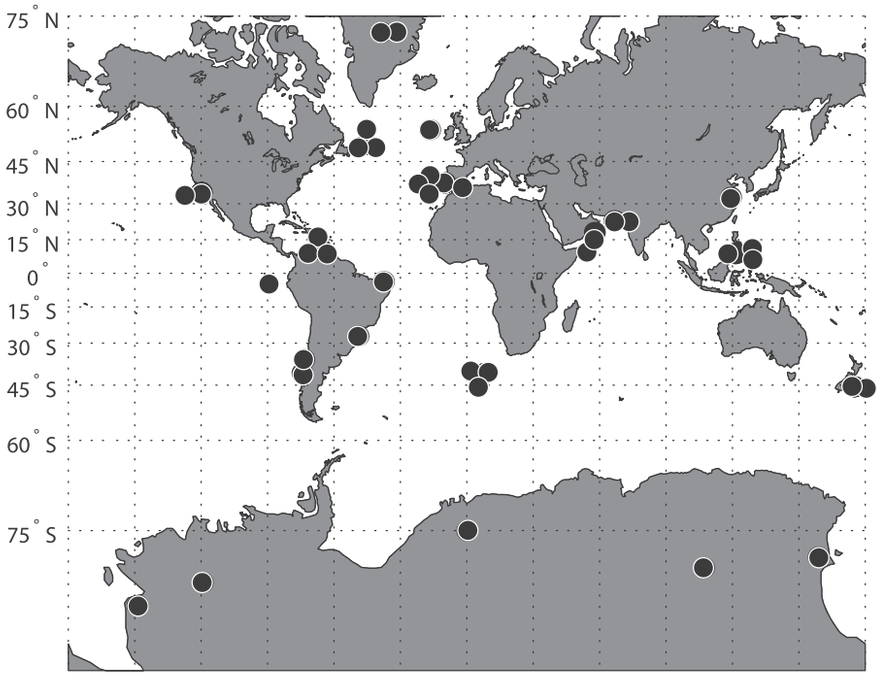

Figure 2. Map showing distribution of 39 time series used in the EOF analysis (see text).

Heinrich) because they share a common timescale of variability and may show some similar structure. To a first order, such correlations are supported by independent geochronology, but uncertainties in the dating control may approach the timescale of variability, preventing any firm conclusions regarding correlation and particularly phasing. The problem is exacerbated for those records that extend beyond the range of radiocarbon control (40-50 kyr) and which have few additional means of dating. In these cases, age models are commonly constructed by aligning common features ("wiggle-matching").

Our underlying assumption will be that one common mechanism is responsible for producing the similar spectral density present in each of the records, but we recognize that unrelated physical processes that have similar timescales of variability may produce time series with similar spectral densities [*Wunsch*, 2003, 2006]. Thus, even with perfect chronologies and their unequivocal correlations, it is still necessary to demonstrate that the proxies are responding to a common forcing.

We address some of these issues by using empirical orthogonal function (EOF) analysis of the MIS 3 time series to provide an objective characterization of modes of variability present within them. These results are still affected by chronological uncertainties, and we identify specific cases where this problem likely manifests itself in the EOF analysis. Nevertheless, this analysis supports the existence of three dominant modes of variability (northern, southern, and Heinrich), although improved chronological control will still be required for refining the EOF results and documenting phasing relationships. We use the clear temporal association between these three modes (Figure 1) to describe a general ~7-kyr climate oscillation that occurred during MIS 3.

2.1. The Northern Mode

The northern mode has the highest spectral densities relative to the two other modes and is therefore subject to the largest uncertainties in signal correlation. The canonical template for this mode is the dominant millennial-scale signal in Greenland ice cores represented by D-O events (Figure 3a). D-O events range from 1000 to 3000 years in duration, and have a characteristic pattern of abrupt (years to decades) warming into an interstadial which is followed by a cooling interval that initially is gradual (centuries to millennia) but abruptly transitions into a cold (stadial) interval.

Figure 3 presents several of the key records, shown on their published chronologies, which have been used to argue for a broad hemispheric distribution of the D-O pattern. With regard to a stadial phase of a D-O event in Greenland, these

Table 1. Results of EOF Analysis.

Latitude	Longitude	Proxy	Communalities	EOF1	EOF2	EOF3	EOF4	Reference
72.97	–38.8	CH_4	0.6604	–0.7484	0.1889	0.2515	0.0359	*Blunier and Brook* [2001]
72.97	–38.8	$\delta^{18}O$	0.6235	–0.7794	0.0276	0.1001	0.0723	*Stuiver and Grootes* [2000]
54.27	–16.78	*N. pachy*. (s.)%	0.7449	0.8326	–0.0289	–0.0605	0.126	*Bond et al*. [1993]
50.2	–45.68	Carbonate %	0.6855	0.0235	0.423	–0.5365	–0.4671	*Hillaire-Marcel et al*. [2000]
50.2	–45.68	K_{ARM}/k	0.7248	–0.2074	–0.6339	0.3906	0.3569	*Stoner et al*. [2000]
50.2	–45.68	$\delta^{18}O_p$	0.7567	0.1685	–0.739	0.2955	0.308	*Hillaire-Marcel et al*. [2000]
37.8	–10.17	$\delta^{13}C_b$	0.6795	–0.6189	–0.5129	–0.1818	–0.0202	*Shackleton et al*. [2000]
37.8	–10.17	$\delta^{18}O_p$	0.6867	0.7907	0.2407	–0.0335	–0.0485	*Shackleton et al*. [2000]
37.8	–10.17	$\delta^{18}O_b$	0.634	0.5561	–0.5674	0.0513	0.0072	*Shackleton et al*. [2000]
37.75	–9.83	SST	0.7629	–0.6924	–0.5295	–0.0396	–0.0391	*Pailler and Bard* [2002]
36.15	–2.62	SST	0.8503	–0.862	–0.3093	0.062	0.0882	*Cacho et al*. [1999]
34.28	–120.03	$\delta^{18}O_p$	0.7055	0.8194	0.1758	–0.0571	0.0051	*Hendy and Kennett* [2000]
34.28	–120.03	*N. pachy*. (d./s.)	0.4895	–0.6137	–0.1753	0.2101	–0.1951	*Hendy and Kennett* [2000]
32.5	119.17	$\delta^{18}O$	0.4856	0.4452	–0.3808	–0.3771	–0.0146	*Wang et al*. [2001]
23.12	66.5	TOC	0.7053	–0.6357	–0.5182	–0.1564	0.0902	*Schulz et al*. [1998]
18.25	57.66	$\delta^{15}N$	0.7834	–0.8437	–0.2382	–0.1182	0.0291	*Altabet et al*. [2002]
10.77	51.95	$\delta^{15}N$	0.7407	–0.8544	0.0769	–0.0601	–0.0349	*Ivanochko et al*. [2005]
10.77	51.95	Lithogenic dust	0.7271	0.7559	0.2108	0.2477	0.2234	*Ivanochko et al*. [2005]
10.7	–65.97	% Reflectance	0.4624	0.3715	0.5363	–0.1209	–0.1485	*Peterson et al*. [2000]
10.7	–65.97	Ti	0.4976	–0.3799	0.1881	0.5434	–0.1506	*Peterson et al*. [2000]
10.7	–65.97	Fe	0.6106	–0.5516	0.0171	0.5278	–0.1658	*Peterson et al*. [2000]
8.8	121.3	SST	0.3956	–0.2606	0.5281	–0.124	0.1826	*Dannenmann et al*. [2003]
6.33	125.8	$\delta^{18}O_p$	0.6956	0.7735	–0.1441	0.2376	0.1419	*Stott et al*. [2002]
6.33	125.8	SST	0.6944	–0.7731	0.1455	–0.2363	–0.1406	*Stott et al*. [2002]
–0.52	–92.4	SST	0.2913	–0.2213	0.089	0.0268	0.4834	*Lea et al.* [2006]
–3.67	–37.72	Fe/Ca	0.473	0.3046	0.3157	–0.0293	0.5288	*Arz et al*. [1998]
–27.22	–49.16	$\delta^{18}O$	0.6781	0.0458	0.2886	0.7697	–0.0133	*Cruz et al*. [2005]
–36.22	–73.68	$\delta^{15}N$	0.4592	0.0084	0.4545	–0.0964	0.4932	*Robinson et al*. [2007]
–41	–74.45	SST	0.6708	0.0764	0.7711	0.264	–0.0259	*Kaiser et al*. [2005]
–41.13	7.82	$\delta^{18}O_p$	0.3862	0.1627	–0.4874	–0.1967	0.2889	*Kanfoush et al*. [2000]
–41.13	7.82	SST	0.6211	–0.1464	0.3241	0.6811	–0.1756	*Sachs et al*. [2001]
–42	10	$\delta^{13}C_p$	0.6173	–0.4646	–0.5868	–0.2343	0.0467	*Charles et al*. [1996]
–45.53	174.93	alkenone conc.	0.762	–0.3343	0.7881	–0.0474	0.1639	*Sachs and Anderson* [2005]
–45.53	174.93	SST	0.7377	–0.1639	0.8304	0.0132	–0.1452	*Pahnke et al*. [2003]
–75	0	$\delta^{18}O$	0.7642	–0.3643	0.6829	–0.1689	0.3696	*EPICA Community Members* [2006]
–77.8	158.72	$\delta^{18}O$	0.5324	–0.5483	0.3929	0.0009	0.2783	*Steig et al*. [2000]
–78.78	106.92	δD	0.5298	–0.5496	0.3347	0.0399	–0.3377	*Petit et al*. [1999]
–80	–119.52	$\delta^{18}O$	0.7704	–0.0758	0.8562	–0.0594	0.1672	*Blunier and Brook* [2001]
–81.67	–148.82	δD	0.8247	–0.568	0.5352	–0.4353	0.1617	*Brook et al*. [2005]

records are interpreted to indicate weaker summer East Asian [*Wang et al*., 2001] (Figure 3b) and Arabian [*Schulz et al*., 1998] (Figure 3c) monsoon systems, strengthening of the North Pacific Aleutian Low [*Hendy and Kennett*, 2000] (Figure 3d), and drying in the tropics [*Blunier and Brook*, 2001; *Peterson et al*., 2000] (Figure 3e, 3f), possibly associated with a shift in the mean position of the Intertropical Convergence Zone (ITCZ) (*Ivanochko et al*., 2005] as a result of an increased pole-to-equator temperature gradient.

2.2. The Southern Mode

The canonical template for this mode is the dominant millennial-scale signal in Antarctic ice cores represented by A events (Figure 4a). These events differ from most D-O events in that they are longer duration (~4-5 kyr) and display a more symmetrical shape of gradual warming and cooling. The A events are the largest amplitude millennial-scale signals in Antarctic ice cores during stage 3. Correlation of Antarctic

and Greenland ice core records using methane records indicates that A events are not in phase with the longest D-O events (Figure 1) [*Blunier et al*., 1998; *Blunier and Brook*, 2001]: Antarctic warming begins during a Greenland stadial and continues until the abrupt onset of a Greenland interstadial. At that time, temperatures in both regions decrease, but more rapidly in Antarctica than Greenland. Based on correlation using the $\delta^{18}O$ of molecular O_2 of air in ice cores, *Bender et al*. [1999] proposed that the smaller Antarctic events are similarly correlative with the shorter D-O events. Recent methane correlation between the North Greenland Ice Sheet Project (NGRIP) ice core and the Dronning Maud Land (EDML) ice core support this proposal (EPICA Community Members, 2006), but whether these shorter events are correlative from one region of Antarctica to another has yet to be established.

Figure 4 illustrates several time series from which the southern mode has been inferred. The A events are clearly registered in the three Antarctic ice cores shown (Figures 4a-4c); age differences reflect differences in age-model construction. The

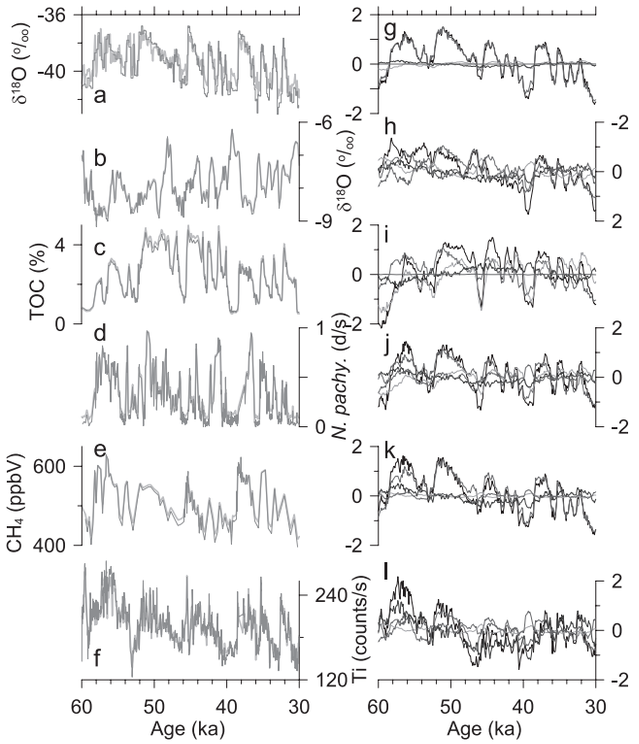

Figure 3. Climate records identified as representative of a "northern" signal. (a) The GISP2 $\delta^{18}O$ record [*Grootes et al.*, 1993; *Stuiver and Grootes*, 2000]. (b) The $\delta^{18}O$ record from the Chinese Hulu speleothem [*Wang et al.*, 2001]. (c) Total organic carbon from Arabian Sea sediments [*Schulz et al.*, 1998]. (d) Ratio of the planktonic foraminifera *N. pachyderma* [*Hendy and Kennett*, 2000]. (e) Methane record from the GISP2 ice core [*Blunier and Brook*, 2001]. (f) Record of Ti from the Cariaco Basin [*Peterson et al.*, 2000]. (g) through (l) Time-history of the first four EOFs for each of the time series shown in (a) through (f) (see Table 1). All time series in the EOF analysis were interpolated to a constant sampling interval of 100 years. Numerical experiments demonstrate that the results presented here are insensitive to factor-of-2 changes in the selected constant sampling interval. All data sets were then transformed to mean zero and standard deviation of one. The interpolated and normalized time series are shown on same panels as the original time series in (a) through (f) by light gray line.

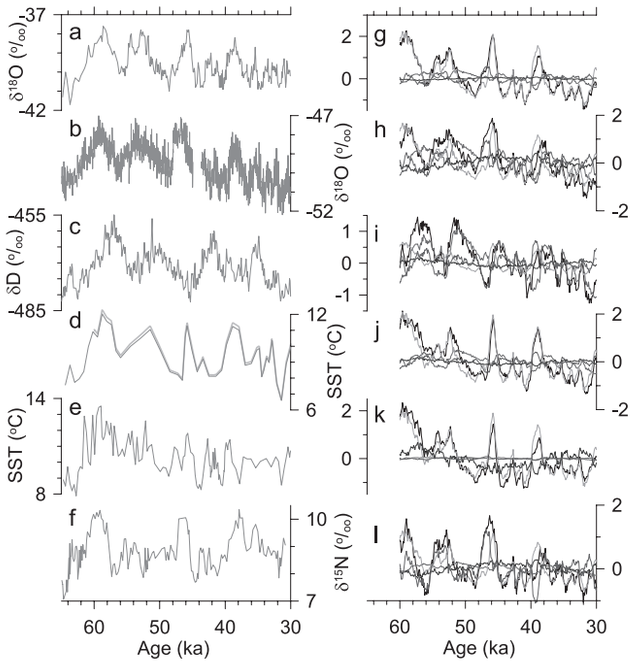

Figure 4. Climate records identified as representative of a "southern" signal. (a) The Byrd $\delta^{18}O$ record [*Johnsen et al.*, 1972], with the timescale synchronized to the GISP2 timescale by methane correlation [*Blunier and Brook*, 2001]. (b) The EDML $\delta^{18}O$ record (*EPICA Community Members*, 2006). (c) The Vostok δD record [*Petit et al*., 1999]. (d) SST record from the southwestern Pacific Ocean [*Pahnke et al*., 2003]. (e) SST record from the southeastern Pacific Ocean [*Kaiser et al.*, 2005]. (f) A $\delta^{15}N$ record from the southeastern Pacific Ocean [*Robinson et al.*, 2007]. (g) through (l) Time-history of the first four EOFs for each of the time series shown in (a) through (f) (see Table 1). All time series in the EOF analysis were interpolated to a constant sampling interval of 100 years. Numerical experiments demonstrate that the results presented here are insensitive to factor-of-2 changes in the selected constant sampling interval. All data sets were then transformed to mean zero and standard deviation of one. The interpolated and normalized time series are shown on same panels as the original time series in (a) through (f) by light gray line.

presence of the A events in two other Antarctic ice cores (Taylor Dome and Siple Dome) [*Steig et al*., 2000; *Brook et al*., 2005] indicates a coherent pattern over the continent. Changes in SSTs in the southwest Pacific (Figure 4d) [*Pahnke et al*., 2003], the southeast Pacific (Figure 4e) [*Kaiser et al*., 2005], and the South Atlantic [*Charles et al*., 1996; *Ninneman et al*., 1999] are all thought to be correlative to A events, suggesting a Southern Ocean response that extends at least to the mid-latitudes. *Robinson et al*. [2007] interpret increases in δ^{15}N from the southeast Pacific as an increased nutrient supply from the Southern Ocean induced by partial breakdown of stratification during A event warmings (Figure 4f).

2.3. Heinrich Modes

Heinrich [1988] first described six unusual layers of IRD deposited in the North Atlantic Ocean during the last glaciation (Figures 5a, b) that *Broecker et al*. [1992] subsequently named Heinrich layers 1 through 6. Later discovery of a seventh layer occurring between Heinrich layers 5 and 6 [*Stoner et al*., 1998; *Sarnthein et al*., 2001; *Rashid et al*., 2003] indicates temporal spacing of ~7-kyr between the layers (Figure 1). Heinrich layers are distinguished from other IRD layers in the North Atlantic by (1) their lithologic signature indicating a dominant source from the central regions of the LIS [*Gwiazda et al*., 1996; *Hemming et al*., 1998], (2) their increasing thickness westward towards Hudson Strait [*Dowdeswell et al*., 1995], and (3) their rapid sedimentation rates [*McManus et al*., 1998]. Each layer is also associated with a large decrease in planktonic δ^{18}O (Figure 5c) which is interpreted as a low-salinity signal derived from the melting of the icebergs [*Bond et al*., 1992; *Hillaire-Marcel and Bilodeau*, 2000; *Roche et al*., 2004]. Recent estimates suggest the duration of Heinrich events was on order of 500 yr [*Hemming*, 2004; *Roche et al*., 2004]. The above characteristics are consistent with the hypothesis of *Broecker et al*. [1992] and *Bond et al*. [1992] that Heinrich layers represent episodic "armadas" of icebergs which were rapidly released in association with a surge from the LIS [e.g., *Marshall and Koutnik*, 2006]. Less clear, however, is the amount of sea-level change associated with Heinrich events. Model results and δ^{18}O anomalies of North Atlantic surface water suggest sea-level changes of <3 m [*MacAyeal*, 1993; *Hemming*, 2004; *Roche et al*., 2004] and the well-constrained sea-level record of the last deglaciation shows no discernable rise at the time of Heinrich event 1 [*Hanebuth et al*., 2000; *Yokoyama et al*., 2000].

Figure 5 shows time series from several sites where the maximum mode of variability occurs during Heinrich events. During Heinrich events the hydrological cycle was enhanced over currently arid northeastern Brazil (Figure 5d) [*Arz et al*., 1998; *Wang et al*, 2004] and *Florida* [*Grimm et al*., 2006], while northeastern Africa became drier [*Ivanochko et al*., 2005]. In addition, surface-water productivity increased in the subpolar Southern Ocean (Figure 5e) [*Sachs and Anderson*, 2005]. Several records exhibiting D-O- and Heinrich-like variability show that cooling in the North Atlantic and Mediterranean [*Cacho et al*., 1999; *Shackleton et al*., 2000; *Pailler and Bard*, 2002], attenuation of the water

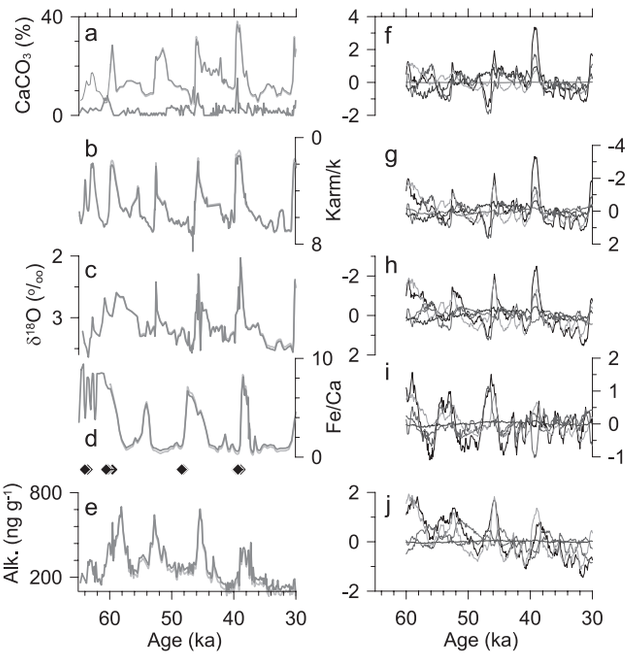

Figure 5. Climate records identified as representative of a "Heinrich" signal. (a) Upper time series is detrital carbonate record from northwestern Atlantic Ocean [*Hillaire-Marcel and Bilodeau*, 2000]. Lower time series is detrital carbonate record from northeastern Atlantic Ocean [*Bond et al.*, 1992, 1999]. (b) Record of k_{ARM}/k (anhysteretic susceptibility/volume susceptibility) [*Stoner et al*., 2000]. (c) Planktonic δ^{18}O record from the northwestern Atlantic Ocean [*Hillaire-Marcel and Bilodeau*, 2000]. (d) Record of Fe/Ca in marine sediments off the coast of northeastern Brazil [*Arz et al*., 1998]. Diamonds between (d) and (e) represent times of speleothem growth in Brazil [*Wang et al*., 2004]. (e) Alkenone concentrations in marine sediments from southwestern Pacific Ocean [*Sachs and Anderson*, 2005]. (f) through (j) Time-history of the first four EOFs for each of the time series shown in (a) through (e) (see Table 1). All time series in the EOF analysis were interpolated to a constant sampling interval of 100 years. Numerical experiments demonstrate that the results presented here are insensitive to factor-of-2 changes in the selected constant sampling interval. All data sets were then transformed to mean zero and standard deviation of one. The interpolated and normalized time series are shown on same panels as the original time series in (a) through (e) by light gray line.

balance in northern South America [*Peterson et al*., 2000], and suppression of Arabian and East Asian monsoons [*Schulz et al*., 1998; *Wang et al*., 2001] all were greatest at times of Heinrich events (Figure 3). Other records with D-O-like variability, including Greenland $\delta^{18}O$ records (Figure 3a), do not indicate any greater response during Heinrich than the responses recorded during intervening stadials or their equivalents.

2.4. Objectively Defined Modes of Variability

The apparent synchronous and asynchronous responses visible in the records above suggest regional and global climatic controls originating from common or distinct parts of the globe. We apply EOF analyses to extract the spatial and temporal modes of variability from multiple, geographically distributed time series. The EOFs are the eigenvectors of the correlation matrix of all time series. To maximize the resolution of all time series, we start by interpolating each of the 39 time series to a 100-year sampling interval on their original age models. Twenty-one time series (most of the ice core records, and sediment records from the Santa Barbara and Cariaco Basins) were undersampled with the 100-year sample interval, whereas most of the open-ocean deep-sea sediment sites were oversampled. The results presented here are essentially identical to analyses run with 200-year sample intervals.

Because the data variables include a diverse suite of proxies (e.g., SSTs, stable isotopes in sediments and ice cores, trace metals, etc.), we normalized all time series (zero mean and standard deviation equal to one). Each time series thus provides equal "weight" to the variance within an individual data set and among the time series included in the analysis. The first four EOFs of the combined data set account for 30%, 21%, 8% and 5% of the total variance. Higher order (>4) EOFs account for <4% of the total variance.

In Figure 2 we plot the communalities for each of the 39 time series (see also Table 1). The communalities indicate how well the variance of a normalized time series is characterized by the first four EOFs. A communality of 1 indicates that all the variance in the time series is accounted for by EOFs 1-4; lower communalities reflect progressively poorer fits to the data. Most of the time series have communalities >0.5, but several, particularly those from equatorial sites, have very low communalities. The lower communalities may indicate that the chronologies for the associated time series are demonstrably different from the methane synchronized GISP2 and Byrd age models (i.e., Vostok ice core, Hulu speleothem), although this difference does not necessarily guarantee a low value, as is demonstrated by the EDML ice core, which has a communality of 0.76 but is synchronized to the NGRIP ice core, which has a different timescale than GISP2. On the other hand, high communalities may reflect that the age model of a particular time series is based on correlation to the GISP2-Byrd age model, although again this approach may still return relatively low communalities (i.e., Cariaco reflectance at 0.46). These chronologic uncertainties will clearly apply equally to the EOF values, and we illustrate the sensitivity of our results to chronologic uncertainties with an example below. Accordingly, while we can explain some anomalous results, such as among the Antarctic ice cores, as reflecting chronologic differences, our results should be considered as preliminary until a consistent stratigraphic framework is established.

In the time domain, the first EOF (which accounts for 30% of the total variance) is equivalent to the Northern mode described above. The influence of this mode is greatest in the GISP2 ice core record (Figures 3a, g; Figure 6a). The Northern mode is also relatively strong in the eastern North Atlantic, in the Santa Barbara Basin and in the Arabian Sea, but much less so in the Southern Ocean (Figure 6a, Table 1). The importance of the Northern mode is less clear in the western Pacific At one site (MD98-2181, *Stott et al*., 2002), the mode is strong in both the $\delta^{18}O$ and SST record, but at a second site (MD97-2141, *Dannenmann et al*., 2003), it is much weaker. As discussed further below, however, these results may reflect chronologic uncertainties.

The second EOF (accounts for 21% of the total variance) is associated with the Southern mode. The Southern mode is most apparent in the Byrd ice core $\delta^{18}O$ record (Figures 4a, g; Figure 6b) but is less so in most other Antarctic ice core records. We partly attribute the lack of a strong influence in these other Antarctic ice cores to their differing chronologies or to uncertainties in the methane synchronization, and expect them to exhibit higher EOF2 values of Byrd when their age models are similarly synchronized. We do not discount the possibility, however, that regional variability across the Antarctic continent may also be a contributing factor. This mode is also expressed in the southeast and southwest Pacific (Figures 4 and 6b).

EOF2 also describes much of the variance related to the Heinrich mode (Figure 5), which is expected given the clear temporal association of the Antarctic A events with Heinrich events (Figure 1). Deepwater records of $\delta^{13}C$ and $\delta^{18}O$ at North Atlantic site MD95-2042 also contain a significant EOF2 component, indicating coeval changes in the AMOC and sea level with Antarctic temperature.

The third EOF accounts for 8% of the total variance in the data, and is associated with the subtropical $\delta^{18}O$ record from a Brazil speleothem [*Cruz et al*., 2005] and an alkenone-derived SST record from the southwest Pacific [*Sachs et al*., 2001] (Figure 6c). Sites where EOF3 is also an important mode of variance include the Cariaco trace-metal time series, the North Atlantic carbonate record, and the Siple

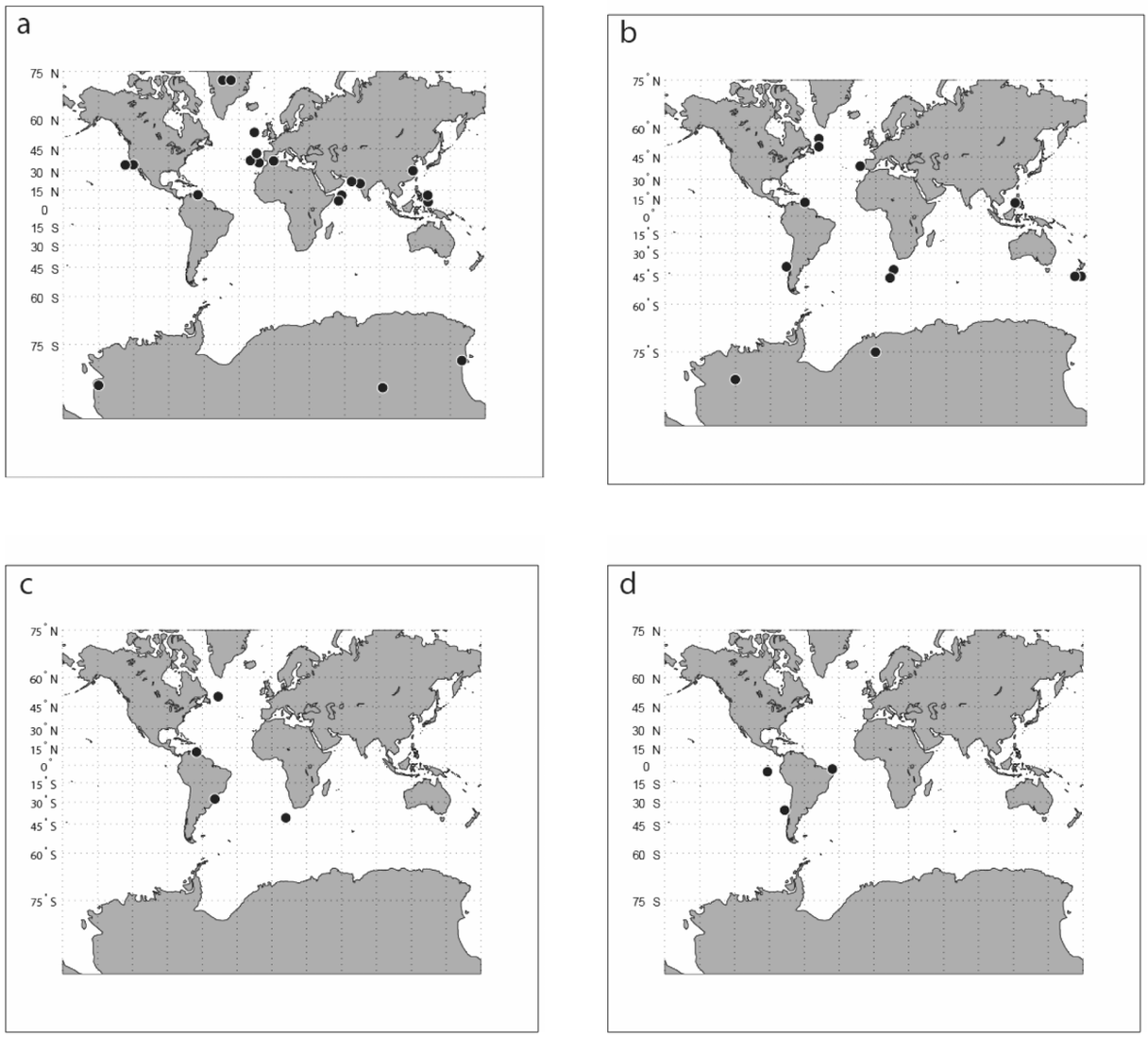

Figure 6. (a) Map showing distribution of time series in which most variance is explained by EOF 1. (b) Map showing variance in each time series explained by showing distribution of time series in which most variance is explained by EOF 2. (c) Map showing distribution of time series in which most variance is explained by EOF 3. (d) Map showing distribution of time series in which most variance is explained by EOF 4. See Table 1 for actual values.

Dome ice core δD record (Table 1). EOF3 is characterized by high-frequency variations that are superimposed on a longer wavelength change associated with solar forcing due to changes in Earth's orbital parameters [*Cruz et al*., 2005].

The fourth EOF, which accounts for about 5% of the data variance, is found in the North Atlantic carbonate record of MD95-2024 [*Hillaire-Marcel and Bilodeau*, 2000], the nitrogen isotope record of the southeast Pacific (ODP Site 1234) [*Robinson et al*., 2007], and in two equatorial sites [*Arz et al*., 1998; *Lea et al*., 2006] (Figure 6d; Table 1). We suspect that EOF4 may be substantially affected by chronologic uncertainties; however, comparison of EOF4 with EOF2 (Figures 6b, d) suggests an interesting insight into the climate system. Overall, the correlation between EOF2 and EOF4 is zero, but between 26 ka (the youngest end of the interval analyzed) and about 40 ka the two EOFs are negatively correlated. We calculated the correlations between the two EOFs by starting at 26 ka and stepping through the length of the records and

found that the maximum correlation between the two EOFs is –0.60 in the interval between 26 and 39.8 ka. In contrast, the correlation is positive (0.20) between 39.8 and 60 ka, and EOF4 leads EOF2. Cross-spectral analysis confirms this lead and shows that over the interval 39.8 and 60 ka the EOFs are highly coherent (maximum squared coherence = 0.65) at a period of 4 kyr and there is a phase shift of 49 ± 23 (0.5 kyr ± 0.25 kyr). An adjustment in chronology in the sites containing EOF4 of less than 1000 years would result in a phase of zero between the lower interval of EOF4 and EOF2.

This suggests that the response represented by EOF4 changed at about 40 ka. Prior to 40 ka the eastern equatorial Pacific response [*Lea et al*., 2006] represented by EOF4 was such that a warm Southern mode (EOF4 is positively correlated with EOF2) was associated with a warm eastern equatorial Pacific, whereas after 40 ka, a warm Southern mode was associated with a cool eastern equatorial Pacific.

We have assumed for this analysis that the published chronologies are "correct"; however, it is important to evaluate the robustness of EOF results to chronologic uncertainties. Detailed reanalysis is needed for a complete assessment, but we argue that the major modes of variability associated with EOFs 1-3 are reasonably robust to changes in chronology. The very different response of the Southern and Northern modes can be identified and quantified because the ice core records from Antarctica and Greenland provide independent stratigraphic frameworks that depend only on the assumption that the global atmosphere is well mixed with respect to methane. EOF3, most manifest in a well dated speleothem, but also found in less well dated marine records, reflects long wavelength variability whose character will not greatly change as improved chronologies are made available for this interval.

Even though the major patterns extracted from the composite data set by the EOF analysis are robust to improvements in chronologic control, this is not true for individual sites. The results differ in the western equatorial Pacific for the δ^{18}O and SST time series from site MD98-2181 [*Stott et al*., 2002] and the SST record from site MD97-2141 [*Dannenmann et al*., 2003]. The chronology for the MD98-2181 time series for the interval >41 ka was based on the assumption that this record could be correlated to the GISP2 ice core record [*Stott et al*., 2002]; however, within the dating constraints for this record, it is possible to adjust the chronology of this site with minimal wiggle-matching to provide a reasonable correlation to the Antarctic ice core data (Figure 7), which yields EOFs that become more similar to those for nearby site MD97-2141 (Table 1). Until better chronologies are available it is not yet possible to attribute variability in the western equatorial Pacific to either of the two primary modes of climate change identified within the studied time interval. Is the variability transmitted from the North Atlantic via the

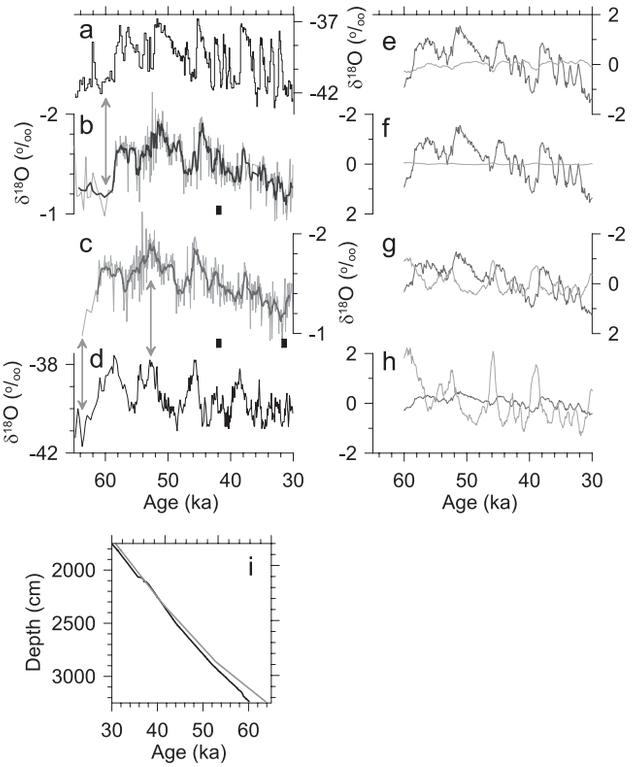

Figure 7. Example of sensitivity of EOF analysis to age model construction, based on site in the western Pacific (*Stott et al.*, 2002). (a) The GISP2 δ^{18}O record [*Grootes et al*., 1993; *Stuiver and Grootes*, 2000]. (b) The MD98-2181 δ^{18}O *Globigerinoides ruber* record on its original age model [*Stott et al*., 2002]. Age control for interval shown is provided by a calibrated ^{14}C of 29 cal ka (just off scale), and correlation first to the δ^{18}O maximum at 60 ka in the GISP2 record (shown by vertical double-headed arrow) and then by wiggle-matching to the GISP2 δ^{18}O record. Independent support for this correlation is provided by the presence of the Laschamp paleomagnetic excursion at 41 ka in MD98-2181 sediments (black rectangle). (c) The MD98-2181 δ^{18}O *G. ruber* record on a revised age model provided by the same ^{14}C age but recalibrated with a newer calibration data set [*Fairbanks et al*., 2005] to 30.1 cal ka (right black rectangle), by wiggle-matching to the Byrd δ^{18}O record, with tie points shown by double-headed arrows, and by the Laschamp paleomagnetic excursion at 41 ka in MD98-2181 sediments (left black rectangle). (d) The Byrd δ^{18}O record [*Johnsen et al*., 1972], with the timescale synchronized to the GISP2 timescale by methane correlation [*Blunier and Brook*, 2001]. (e) through (h) Time-history of the first two EOFs for each of the time series shown in (a) through (d). EOF1 is black, EOF2 is gray. (i) Age models for MD98-2181 sediments: black is original based on correlation to GISP2 ice core [*Stott et al.*, 2002], gray is revised based on correlation to Byrd ice core.

monsoon climate (suggested by the importance of the Northern mode in the northern Indian Ocean and Chinese speleothem sites)? Or, does the western equatorial Pacific, reflect the Southern mode via transmission from the South Pacific, where sites on both the eastern and western boundaries of the South Pacific strongly reflect the Southern mode? We return to these questions below.

Time series analysis of the EOFs is used to examine relationships between the Northern and Southern modes (Figure 8). The spectra of EOF1 and 2 show that both are "red" (i.e., they are dominated by low-frequency variation) with 96% of the variance occurring at periods longer than 1000 years (frequencies of 1 in Figure 8). There is a small spectral peak over this "red" background at a period of 1500 years. The squared coherence between EOF1 and 2 is statistically significant and >0.6 (60% of the variance at any given frequency band is related in the two time series) over the frequency band 0 to 1.2 cycles kyr^{-1} (to periods of about 870 years). There is a statistically significant, non-zero phase (if the signals were in-phase) and non 180 phase (if the signals were anti-phased), such that the Northern mode is leading the Southern mode throughout this frequency band. At the frequency of maximum coherence (0.177 or a period of 5.7 kyr) the phase is 65 ± 7 (95% confidence interval) or a phase shift in time of 1.02 kyr ± 0.11 kyr. The cross-correlation function, which can be also used to calculate the coherency and phase for these two EOFs, shows that on average, there is a 500-year lag, similar to what *Schmittner et al*. [2003] found, confirming an out-of-phase relationship between Northern and Southern modes. If the variability in the Northern and Southern modes were a simple "seesaw" (i.e., anti-phased) we would expect a phase of ±180 , but the phase relations established here imply a very different process, suggesting that the term "seesaw" is inappropriate for describing climate change at these timescales.

3. CHANGES IN THE AMOC AND CLIMATE

Proxy data indicate that changes in the rate of the AMOC were the source of millennial-scale climate change in the Atlantic basin through their effect on ocean heat transport. These data, taken together with ocean model simulations, suggest that millennial-scale changes are associated with three modes of the AMOC: (1) an active mode similar to the modern AMOC that induced interstadial warmth, (2) a glacial mode associated with NADW sinking to depths <2500 m and reduced heat transport that led to stadial cooling, and (3) a Heinrich mode in which the AMOC was effectively shut down [*Sarnthein et al*., 1994, 2001; *Alley and Clark*, 1999; *Ganopolski and Rahmstorf*, 2001].

The most widely used proxy of changes in the AMOC is $\delta^{13}C$ of dissolved inorganic carbon, which differentiates the location, depth and volume of NADW relative to underlying Antarctic bottom water [*Boyle and Keigwin*, 1982; *Curry and Lohman*, 1982; *Duplessy et al*., 1988], but does not yield a rate of change. Additional proxies that constrain changes in the rate of the AMOC support the inference from $\delta^{13}C$ that changes in depth and volume of NADW do reflect changes in the rate of the AMOC [*Lynch-Stieglitz et al*., 1999; *Rutberg et al*., 2000; *McManus et al*., 2004; *Piotrowski et al*., 2005]. Accordingly, we examine $\delta^{13}C$ records from the eastern North Atlantic basin that monitor changes in water masses across a depth transect from 1100 m to 3100 m to illustrate the modes of the AMOC during MIS 3 (Figure 9). While only two of these records cover the full time interval of interest, they do provide constraints on changes in the vertical gradient of $\delta^{13}C$ during the H4 and H5 events.

The Heinrich mode of the AMOC is readily distinguished from other times by a large reduction in $\delta^{13}C$ during Heinrich events, with the overlapping records for H4 indicating the near-complete replacement of nutrient-poor, high-$\delta^{13}C$ NADW with nutrient-rich, low-$\delta^{13}C$ Antarctic bottom water in this part of the Atlantic basin (Figure 9). On the other hand, we note that the $\delta^{13}C$ records make no clear distinction between interstadials and non-Heinrich stadials (in i.e., so called glacial and modern modes), possibly indicating a smaller direct role of the AMOC and a larger role from attendant feedbacks such as sea ice [*Li et al*., 2005] in causing D-O events.

Synchronization of Greenland and Antarctic ice core records indicates that the greatest warming in Antarctica (A events) occurred at times of Heinrich events (Figure 1), and thus at times of a near-collapse of the AMOC (Figure 9). In contrast, if the smaller warm events in Antarctica correspond to intervening Greenland stadials, as suggested by *Bender et al*. [1999] and *EPICA Community Members* (2006), then they are associated with some reduced strength of the AMOC which, although reduced relative to the modern mode, still remained active. Our interpretation contrasts with the conclusion by *EPICA Community Members* (2006) that correlation between the amplitude of Antarctica warming and the duration of Greenland stadials indicated that the times of greatest warming in Antarctica were associated with the duration of a reduced AMOC, rather than with the differences in the rate of the AMOC.

We further evaluate the effect of changing AMOC on climate by comparing proxy records. As noted previously, the Greenland records do not show any greater change in $\delta^{18}O$ at times of Heinrich events than those recorded during intervening stadials (Figure 1). Similarly, the amount of warming recorded in the GRIP ice core following a Heinrich event is comparable to the warming following a non-Heinrich event stadial [*Huber et al*., 2006]. We suggest that the absence of a greater change over Greenland during Heinrich events is a result of Greenland's distant location with respect to the area

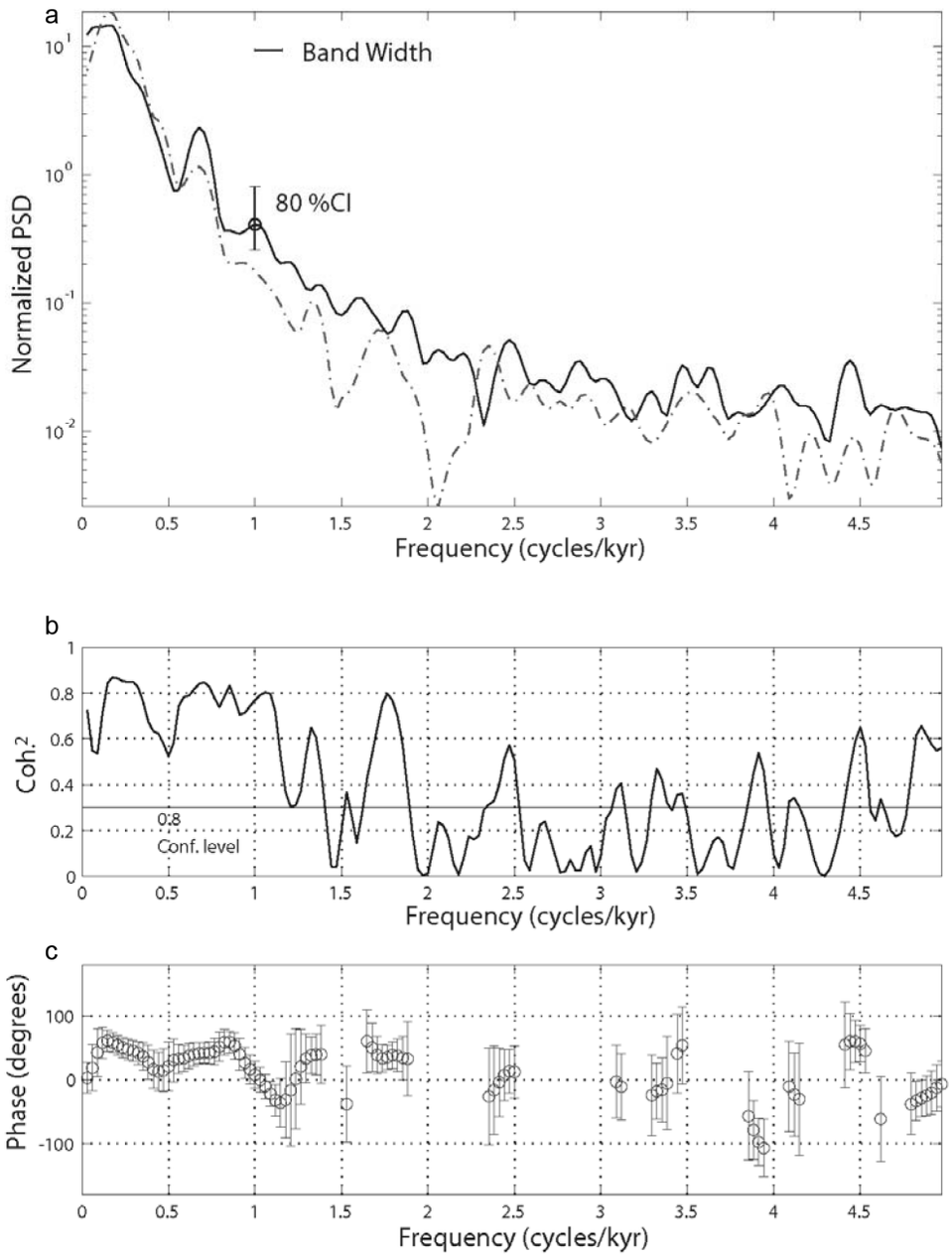

Figure 8. Cross-spectral analysis comparing the first and second EOF's from 30 climate time series. Cross-spectral analysis was completed using a fast Fourier transform. After transformation, spectral estimates were smoothed using a Hanning filter so that the spectral estimates have 11 degrees of freedom. (a) Normalized spectral variances (power spectral density: PSD) plotted on a log-linear scale. Area under the spectra is for EOF-1 (black) and EOF-2 (dashed). The bandwidth and 80% confidence interval are shown as horizontal and vertical bars. (b) Squared coherency between EOF 1 and EOF 2. Horizontal line is confidence interval; any values above the line are significantly greater than zero at the 80% confidence interval. (c) Phase spectra. Positive phase indicates that the EOF1 leads EOF2. 80% confidence intervals for phase are plotted where coherency is significantly different from zero.

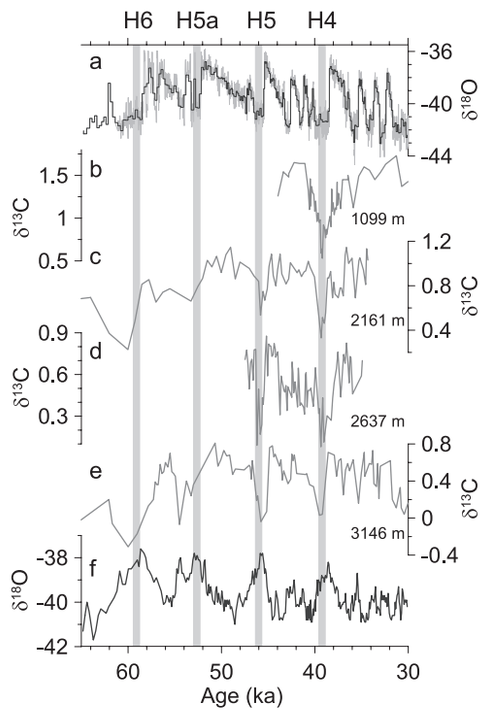

Figure 9. Relation of changes in the AMOC represented by $\delta^{13}C$ records to changes in climate. (a) The GISP2 $\delta^{18}O$ record [*Grootes et al*., 1993; *Stuiver and Grootes*, 2000]. (b) The $\delta^{13}C$ record from core SO75-26KL (1099 m water depth) in the eastern North Atlantic [*Zahn et al*., 1997]. (c) The $\delta^{13}C$ record from core Na 87-22 (2161 m water depth) in the eastern North Atlantic [*Elliot et al*., 2002]. (d) The $\delta^{13}C$ record from core MD01-2444 (2637 m water depth) in the eastern North Atlantic [*Skinner and Elderfield*, 2007]. (e) The $\delta^{13}C$ record from core MD95-2042 (3146 m water depth) in the eastern North Atlantic [*Shackleton et al.*, 2000]. (f) The Byrd $\delta^{18}O$ record [*Johnsen et al*., 1972], with the timescale synchronized to the GISP2 timescale by methane correlation [*Blunier and Brook*, 2001]. Vertical gray bars indicate timing of Heinrich events.

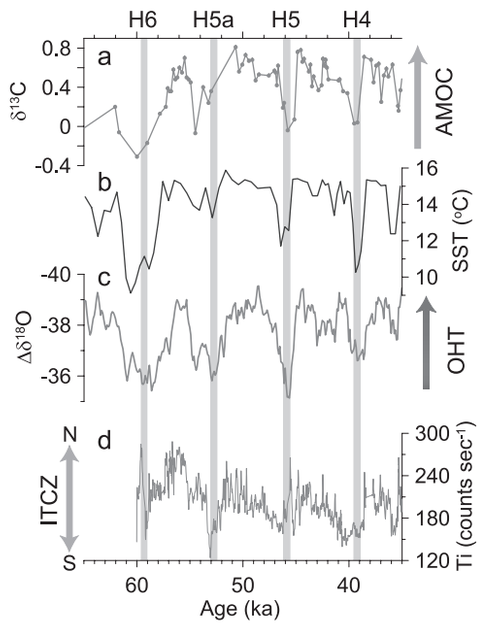

Figure 10. Relation of changes in the AMOC represented by benthic $\delta^{13}C$ to changes in climate. (a) The $\delta^{13}C$ record from core MD95-2042 (3146 m water depth) in eastern North Atlantic [*Shackleton et al.*, 2000]. (b) SST reconstruction from the Iberian Margin, eastern North Atlantic [*Pailler and Bard*, 2002]. (c) The difference between the Byrd $\delta^{18}O$ record [*Johnsen et al.*, 1972; *Blunier and Brook*, 2001] and the planktonic $\delta^{18}O$ record from the Iberian margin, eastern North Atlantic [*Shackleton et al*., 2000], taken to reflect changes in ocean heat transport (OHT). In order to account for the opposite sign of change in $\delta^{18}O$ with respect to temperature in the two records, the planktonic record was first multiplied by –1, and then subtracted from the Byrd record. (d) The Ti record from the Cariaco Basin, interpreted to reflect hydrologic changes associated with north-south changes in the position of the ITCZ (*Peterson et al.*, 2000). Timing of Heinrich events is shown by vertical gray bars.

most affected by reduced AMOC. Both stadial and Heinrich modes of AMOC cool North Atlantic surface waters and lead to southward expansion of sea ice, but models results indicate that the greatest cooling and sea ice expansion in the North Atlantic was at mid-latitudes, with little additional cooling being propagated to Greenland [*Ganopolski and Rahmstorf*, 2001].

In contrast, relative to intervening stadials, a number of other records with D-O-like variability display a greater response than Greenland during times of Heinrich events [*Schulz et al*., 1998; *Cacho et al*., 1999; *Shackleton et al*., 2000; *Peterson et al*., 2000, *Wang et al*., 2001; *Pailler and Bard*, 2002]. To illustrate this point, we compare the records of $\delta^{13}C$ changes in the AMOC (Figure 10a) with SSTs in the eastern North Atlantic (Figure 10b), with the differential between the Byrd $\delta^{18}O$ record and the North Atlantic planktic $\delta^{18}O$ record from the Iberian margin [*Shackleton et al*., 2000] (Figure 10c), and with the Cariaco Ti record [*Peterson et al*., 2000] (Figure 10c). Comparison of these records is robust because they are all on the same timescale (GISP2). To first order, the $\delta^{18}O$ difference reflects the gradient between SSTs in the eastern North Atlantic and atmospheric temperature over Antarctica, and thus is a crude measure of changes in ocean heat transport. The Cariaco Ti record reflects changes in the regional water balance linked to shifts in the mean position of the ITCZ [*Peterson et al*., 2000]. Comparison of these records suggests that the maxima in cooling in the North Atlantic (Figure 10b), reduction in ocean heat transport (Figure 10c), and southward displacement of

the ITCZ (Figure 10d) occurred during the largest reduction in the AMOC (Figure 10a). Similar changes in the Indian and Asian monsoon systems [*Schulz et al*., 1998; *Wang et al*., 2001; *Ivanochko et al*., 2005], and a southward shift of the ITCZ over South America [*Arz et al*., 1998; *Wang et al*., 2004] during times of Heinrich events can be explained as an atmospheric response to peak North Atlantic cooling and sea ice expansion associated with maximum decrease in the AMOC [*Barnett et al*., 1989; *Douville and Royer*, 1996; *Chiang et al*., 2003; *Zhang and Delworth*, 2005].

4. CHANGES IN ATMOSPHERIC CO_2

Stauffer et al. [1998] first determined that atmospheric CO_2 measured in the Byrd ice core increased during times of Heinrich events. Based on an improved CO_2 data set from the Taylor Dome ice core, *Indermuhle et al*. [2000] found that atmospheric CO_2 co-varied with Antarctic temperature during MIS 3, an expected outcome given the relation between A events and Heinrich events (Figure 1). *Ahn and Brook* [2007] have improved the synchronization of the Taylor Dome record with GISP2 as well as obtained new CO_2 measurements from the Byrd core. These new data allow direct comparison of CO_2 variations with the Byrd $\delta^{18}O$ record, which is also on the GISP2 timescale (Figure 11b). Comparison confirms the co-variation of CO_2 with A events with a time lag of 720 ± 370 yr. Moreover, these records indicate little, if any, variability in CO_2 associated with the smaller warm events in Antarctica. Given that the smaller warm events are roughly a third to a half the amplitude of the A events (Figure 11b), similarly scaled CO_2 variability associated with them would be evident if all of the warm events shared a common mechanism. Accordingly, whatever mechanism is responsible for the MIS 3 A events and CO_2 variations appears to differ from the mechanism responsible for smaller warm events which have no corresponding changes in CO_2.

Several mechanisms have been proposed for the CO_2 variability during MIS 3. *Indermuhle et al*. [2000] referred to modeling studies by *Marchal et al*. [1998], in which a shutdown of the AMOC causes an increase in CO_2 both through the solubility effect, wherein the effect of warming of the Southern Ocean exceeds that of cooling the North Atlantic, as well as changes in alkalinity and dissolved inorganic carbon concentration in the North Atlantic. *Martin et al*. [2005] attributed CO_2 variability to changes in deepwater temperature caused by increased NADW formation and solubility of CO_2. Schmittner et al. (this volume) used a coupled climate-carbon cycle model to show that cessation of the Atlantic overturning decreases stratification in the Southern Ocean, leading to increased outgassing of CO_2 and gradually increasing atmospheric CO_2 concentrations on a multi-millennial timescale. A consequence of this slow-response mechanism would be a lack of an association between higher frequency (centennial) variability (D-O events) and changes in atmospheric CO_2.

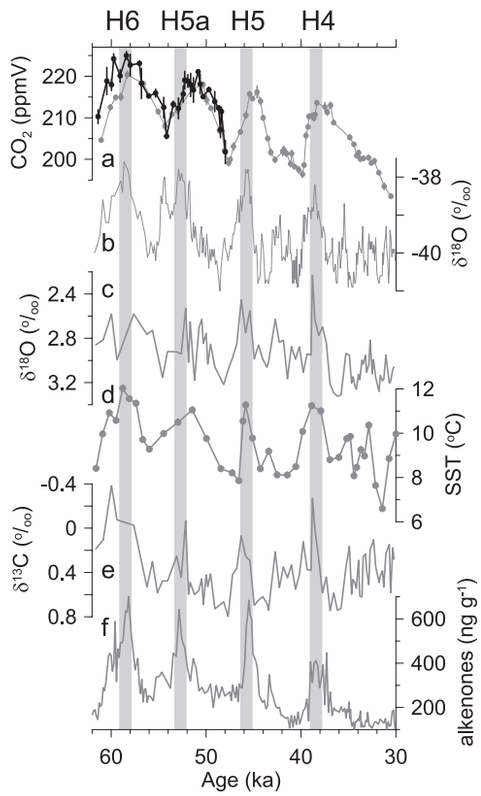

Figure 11. Changes in climate and ocean properties associated with changes in atmospheric CO_2. (a) The Taylor Dome (gray dots and curve) [*Indermuhle et al*., 2000] and Bryd (black dots and curve) CO_2 records, placed on the GISP2 timescale through synchronization with methane [*Ahn and Brook*, 2007]. (b) The Byrd $\delta^{18}O$ record [*Johnsen et al*., 1972], with the timescale synchronized to the GISP2 timescale by methane correlation [*Blunier and Brook*, 2001]. (c) Record of planktonic (*D bulloides*) $\delta^{18}O$ from the South Atlantic [*Charles et al.*, 1996]. (d) Record of changes in sea surface temperatures from the southwest Pacific [*Pahnke et al*., 2003]. (e) Record of planktonic (*Globigerina bulloides*) $\delta^{13}C$ from the South Atlantic (C. Charles, pers. comm.). (f) Record of alkenone concentrations from the southwest Pacific [*Sachs and Anderson*, 2005].

Figure 11 shows several proxy records from the Southern Ocean that, when combined with evidence for changes in the AMOC (Figure 9), place several constraints on possible mechanisms for CO_2 variability during MIS 3. Clearly there is an association with changes in Southern Ocean SSTs (Figures 11c, d), but model simulations that include the solubility pump only (without the effects of biology) cannot explain increasing atmospheric CO_2 levels after a disruption of the AMOC (*Marchal et al*., 1998; *Schmittner et al*., this

volume) and suggest a negligible role of solubility. *Martin et al*. [2005] postulated that the CO_2 changes may arise from deepwater temperature changes associated with an increase in NADW formation, but given that times of CO_2 increase occur when the AMOC had strongly decreased (Figure 9), the cause of the warming must be related to some other mechanism, such as from geothermal heating [*Adkins et al*., 2005].

A planktic $\delta^{13}C$ record from the South Atlantic [*Charles et al*., 1996] (Figure 11e) suggests that an additional source of atmospheric CO_2 during A events may have been the evasion of respired CO_2 from Southern Ocean deepwater. On average, $\delta^{13}C$ records indicate that Southern Ocean deepwater was a major reservoir of respired CO_2 during glaciations [*Hodell et al.*, 2003]. The South Atlantic planktic record indicates that surface waters became more depleted in $\delta^{13}C$ when SSTs were warm (Figure 11c) and CO_2 was high. Because only about half of the 0.6-0.8‰$\delta^{13}C$ changes can be explained by the 3-4 C SST changes through air-sea gas exchange [*Broecker and Maier-Reimer*, 1994], the $\delta^{13}C$ changes also indicate that nutrient-rich deepwaters reached the surface and degassed CO_2 to the atmosphere. Additional evidence for increased supply of nutrients to the surface of the Southern Ocean comes from alkenone concentrations and organic flux to the sea floor [*Sachs and Anderson*, 2005], which also increase markedly at times of high atmospheric CO_2 (Figure 11f). Because the increased productivity implied by these proxies also indicates an enhanced CO_2 sink, the net increase in atmospheric CO_2 suggests that sources from degassing exceeded that of the productivity sink.

In general, this reasoning is consistent with the mechanism proposed by *Toggweiler et al*. [2006] in which a shift of the Southern Hemisphere westerlies in response to cold (warm) climates induces a decrease (increase) in the degassing of respired CO_2 from the depths of the Southern Ocean. Similarly, this degassing mechanism is parallel to that proposed by *Schmittner et al.* (this volume), particularly with regard to a decrease in stratification in the Southern Ocean as a means to induce evasion of nutrient-rich deepwaters. Two issues, however, require additional exploration. First, their model simulation does not simulate the increase in nutrients suggested by depleted $\delta^{13}C$ values and alkenone concentrations. Secondly, the simulation was performed only for a case where the AMOC was shut down, and, although this is in agreement with proxy records of the AMOC at times of high CO_2 (i.e., the Heinrich mode of the AMOC) (Figure 9), these same proxy records suggest an active, albeit reduced, AMOC during the shorter intervening stadials with no corresponding CO_2 signal. Accordingly, it has yet to be established whether the absence or presence of a CO_2 signal during MIS 3 reflects the long response time to a collapsed AMOC with a short versus long duration, or differing responses to a glacial versus Heinrich mode of the AMOC.

5. THE ORIGIN OF HEINRICH EVENTS

Several mechanisms have been proposed to explain an ice-sheet instability that triggers a surge of the LIS through Hudson Strait into the North Atlantic Ocean, producing Heinrich events. *MacAyeal's* [1993] binge-purge mechanism involves an internal thermal oscillation of the LIS with a timescale similar to the ~7-kyr interval separating Heinrich events. *Bond et al*. [1993] disputed the mechanism proposed by *MacAyeal* [1993], however, by pointing out that Heinrich events occur only during stadials that follow prolonged cooling intervals in the North Atlantic region resulting from progressively cooler interstadials (Figure 1), thus implicating a causal relation between climate and Heinrich events. Existing sea-level records are additional evidence that dispute the binge-purge hypothesis by showing that sea-level rises (falls) during the predicted binge (purge) period [*Chappell*, 2002; *Siddall et al*., 2003].

Synchronization of Greenland and Antarctic ice core records reveals the possible relation of Heinrich events to climate by showing that they occur only at times of peak warming associated with Antarctic A events (Figure 1). This remarkable association strongly suggests that Heinrich events are an integral part of the bipolar seesaw that produces the out-of-phase response between the polar hemispheres, with the mechanism responsible for causing the seesaw somehow linked to, and possibly responsible for, Heinrich events. Temperature change at the surface of an ice sheet is greatly attenuated with ice-sheet depth, however, leaving open to question whether surface forcing could influence the basal temperatures of an ice sheet to the degree needed to produce a surge [*Oerlemans*, 1993; *Clarke et al*., 1999].

Hulbe et al. [2004] also implicated a climatic mechanism based on the presence of IRD layers from other circum-North Atlantic ice sheets that are found immediately prior to Heinrich layers, from which they inferred a common external forcing affecting these ice sheets. The long-term cooling trend prior to a Heinrich event established by *Bond et al*. (1993), however, can explain the presence of non-LIS IRD either through increased transit distances of icebergs in colder waters or through an increased flux of icebergs associated with mass-balance increase [*Marshall and Koutnik*, 2006]. Moreover, *Jullien et al*. [2006] found that this IRD relation only applied to H1 and H2. *Hulbe et al*. [2004] proposed that collapse of an ice shelf due to surface warming triggered surging of the LIS, but *Alley et al*. [2005] pointed out that Heinrich events occurred during the coldest intervals in the North Atlantic—the least likely time for surface forcing to cause an ice shelf to fragment.

Based on simulations with a simplified global climate model, *Shaffer et al*. [2004] proposed an additional mechanism by which climate change may trigger a Heinrich event

by ice-shelf fragmentation involving a subsurface warming that develops at intermediate depths in the North Atlantic in response to a reduction or collapse of the AMOC. Recent observations from Antarctica suggest that such oceanic forcing would be particularly effective at causing destabilization of ice shelves [*Rignot and Jacobs*, 2002] and attendant glacier surging [*De Angelis and Skvarca*, 2003; *Rignot et al*., 2004]. *Shaffer et al.'s* [2004] model simulations indicate that, without an active AMOC and cooling of the ocean interior by convection, downward diffusion of heat at low latitudes warms subsurface waters to a depth of ~2500 m. Some of the heat accumulated in the subsurface is transported poleward causing a temperature inversion in the northern North Atlantic. Development of a subsurface warming following collapse of the AMOC is also evident in other models, although for different reasons (e.g., *Schiller et al*., 1997, as reproduced in *Stocker and Johnsen*, 2003; *Knutti et al*., 2004; *Cheng et al*., this volume), and δ^{18}O of calcite ($\delta^{18}O_c$) records from benthic foraminifera living at these water depths are consistent with warming during Heinrich events [*Rasmussen et al*., 1996, 2003, 2004; *Dokken and Jansen*, 1999; *Olsen et al*., 2005].

Acknowledging subsurface warming as a possible amplifying mechanism, *Fluckiger et al*. [2006] implicate the ~1 m steric and dynamic sea-level rise that accompanies a collapse of the AMOC as the primary trigger for Heinrich events, with subsequent sea-level rise associated with ice-sheet surging acting as a positive feedback. Recent modeling, however, indicates that ice sheets are likely to be immune to such small sea-level forcing [*Alley et al*., 2007]. Moreover, as discussed further below (Section 6.3.3), existing sea-level reconstructions for MIS 3 indicate that significant sea-level rise (on the order of ≥10 m) occurred over a several thousand year period prior to Heinrich events [*Chappell*, 2002; *Siddall et al*., 2003], suggesting that if sea-level rise triggered Heinrich events, it was more likely this larger component that preceded a steric response to a collapsed AMOC [*Chappell*, 2002]. Existing records, however, indicate that the magnitude of sea-level rise varied from one Heinrich event to the next [*Chappell*, 2002; *Siddall et al*., 2003], suggesting that either the sensitivity of the LIS to sea-level forcing varied or that sea-level change did not trigger Heinrich events, but instead occurred in response to the same climate mechanisms that ultimately led to a collapse of the AMOC and a subsurface warming.

The plausible role of subsurface warming implies that some other factor caused the AMOC to slow down prior to Heinrich events, and that Heinrich events were thus responses to, rather than causes of, the shutdown of the AMOC, contrary to the widely held interpretation that Heinrich events cause AMOC shutdowns. This conjecture is consistent with the observation first made by *Bond et al*. [1993] that Heinrich events occur at the end of a long-term cooling trend; such a cooling is likely caused by a reduction in the AMOC and expansion of sea ice. The synchronization of Antarctic and Greenland ice cores further places the Heinrich events in the context of climate change occurring in response to a slowing AMOC. The classic bipolar seesaw pattern is most clearly expressed when Greenland is coldest and Antarctica is warmest, which is readily attributed to times of weakest AMOC [*Ganopolski and Rahmstorf*, 2001; *Stocker and Johnsen*, 2003]. Indeed, this is when Heinrich events occur (Figure 1).

In Figure 12, we show two Heinrich events, H1 and H4, for which corresponding data constraining AMOC strength exist. These data clearly support reduction in AMOC to its minimum strength before the Heinrich events occur [*Zahn et al*., 1997]. The question remains, however, as to the cause of the slowdown of the AMOC. Climate model simulations suggest that the answer may lie in the interaction between the AMOC and Northern Hemisphere ice-sheet mass balance. Specifically, *Schmittner et al*. [2002] found that an active AMOC induces an increase in freshwater flux from adjacent ice sheets through enhanced calving of marine ice margins and melting from mid-latitude ice margins, eventually triggering a rapid decrease in the AMOC. We also note that the increased freshwater flux is the result of a negative ice-sheet mass balance, which is supported by the sea-level record [*Chappell*, 2002; *Siddall et al*., 2003], but opposite that required by the binge-purge model [*MacAyeal*, 1993]. We describe below simulations with an atmospheric general circulation model (AGCM) that further elaborate on how climate-induced mass-balance changes may have increased the freshwater flux to the North Atlantic prior to a Heinrich event.

From the foregoing, we conclude that the available evidence supports neither an internal ice-sheet oscillation nor a surface climate forcing for triggering Heinrich events. A trigger involving subsurface warming of North Atlantic intermediate waters in response to a slowing AMOC, however, is consistent with the known timing of Heinrich events and changes in AMOC (Figure 12), and the high sensitivity of ice shelves to this warming is well established [*Rignot and Jacobs*, 2002]. In this regard, we view Heinrich events as occurring in response to climate change [*Bond et al*., 1993], rather than triggering it, although their hydrological effects likely act as a positive feedback in sustaining the AMOC in an off (Heinrich) mode.

6. A MIS 3 CLIMATE OSCILLATION

In the following, we outline a generalized conceptual framework to explain the ~7-kyr spacing of Heinrich events and their regular occurrence at times of minima in Northern

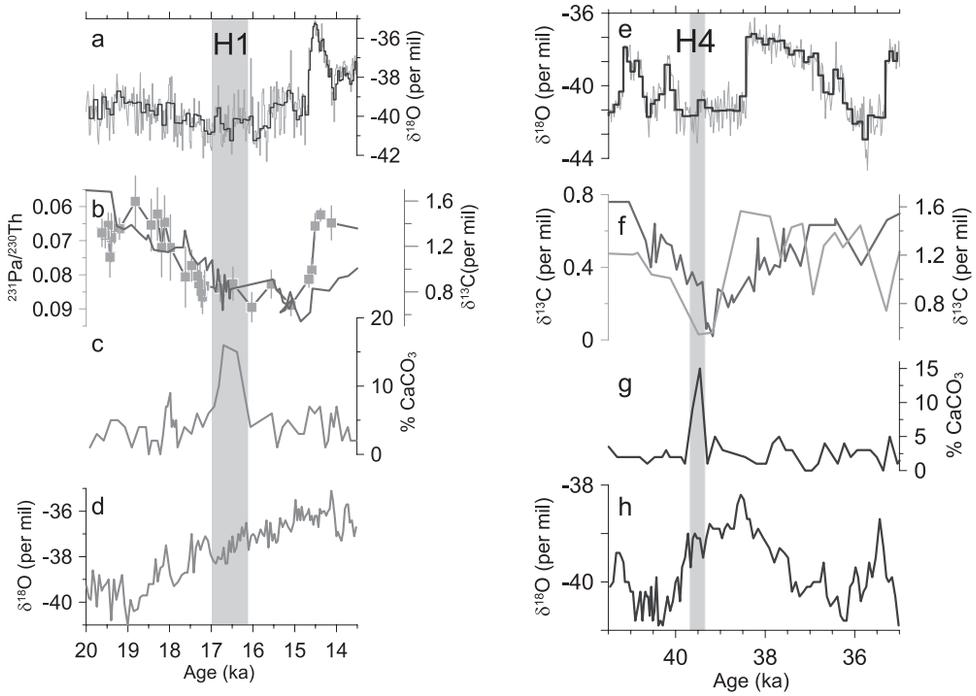

Figure 12. Records bracketing climate change around times of Heinrich events 1 and 4 (shown as vertical gray bars). (a) The GISP2 δ^{18}O record [*Grootes et al*., 1993; *Stuiver and Grootes*, 2000]. (b) The δ^{13}C record from core SO75-26KL (1099 m water depth) in eastern North Atlantic [*Zahn et al*., 1997] (black line), and record of ^{231}Pa/^{230}Th in marine sediments from Bermuda Rise, western North Atlantic [*McManus et al*., 2004] (gray symbols). (c) Record of changes in detrital carbonate in marine sediments from the North Atlantic [*Bond et al*., 1999]. (d) The Byrd δ^{18}O record [*Johnsen et al*., 1972], with the timescale synchronized to the GISP2 timescale by methane correlation [*Blunier and Brook*, 2001]. (e) The GISP2 δ^{18}O record [*Grootes et al*., 1993; *Stuiver and Grootes*, 2000]. (f) The δ^{13}C record from core SO75-26KL (1099 m water depth) in eastern North Atlantic [*Zahn et al*., 1997] (black line), and the δ^{13}C record from core MD95-2042 (3146 m water depth) in the eastern North Atlantic [*Shackleton et al*., 2000]. (g) Record of changes in detrital carbonate in marine sediments from the North Atlantic [*Bond et al.*, 1999]. (h) The Byrd δ^{18}O record [*Johnsen et al*., 1972], with the timescale synchronized to the GISP2 timescale by methane correlation [*Blunier and Brook*, 2001].

Hemisphere temperature and maxima in Southern Hemisphere temperature during MIS 3 (Figure 1). In doing so, we describe a quasi-periodic, repeating pattern that develops as a consequence of changes in the AMOC, the transmission of those changes through the atmosphere and ocean, and their effect on ice-sheet mass balance. We follow this with a more detailed description of each of the causal links as established by existing models and data. Lastly, we use climate models to simulate key aspects of the conceptual model.

6.1. General Outline

We begin at the point of an abrupt warming in the North Atlantic region that occurs in response to resumption of the AMOC and reduced sea ice extent. This initial warming increases melting of Northern Hemisphere ice sheets, with the increased freshwater flux inducing a slow reduction in the AMOC. Additional atmospheric responses to the warming include strengthening of the Indian and Asian monsoons [*Barnett et al*., 1989; *Douville and Royer*, 1996; *Timmermann et al*., 2005; *Zhang and Delworth*, 2005], weakening of the Aleutian Low [*Mikolajewicz et al*., 1997; *Zhang and Delworth*, 2005], and northward migration of the position of the ITCZ [*Schiller et al*., 1997; *Rind et al*., 2001; *Chiang et al*., 2003; *Zhang and Delworth*, 2005).

By increasing cross-equatorial heat transport, an active AMOC also causes cooler SSTs in the South Atlantic, which are rapidly transmitted throughout the Southern Ocean by the Antarctic Circumpolar Current (ACC) [*Vellinga and Wood*, 2002] and are amplified by an increase in sea ice extent and a decrease in atmospheric CO_2.

The heat content anomaly associated with the cooler SSTs in the Southern Ocean is subducted and transmitted by way

of the shallow meridional circulation in the Pacific basin, where it upwells at the equator and cools equatorial SSTs. The effect of cooler equatorial Pacific SSTs is transmitted through the atmosphere and ocean to the LIS, leading to a more positive ice-sheet mass balance and ice-sheet growth. Ice-sheet expansion eventually results in increased calving and thus an increase in the flux of freshwater to the North Atlantic, which further reduces the AMOC. The subsequent reduction of ocean heat transport, amplified by an expansion of sea ice, cools the North Atlantic region.

Reduced ocean heat transport in the Atlantic basin is balanced by warmer SSTs in the South Atlantic, which again are rapidly transmitted throughout the Southern Ocean by the ACC and amplified by a contraction of sea ice and an increase in atmospheric CO_2. The heat content anomaly associated with the warmer SSTs is subducted and transmitted equatorwards by way of the shallow meridional circulation in the Pacific basin, where it warms SSTs in the tropics. The atmospheric bridge transmits warmer atmospheric temperatures to the LIS, which increases ablation and runoff directed to the North Atlantic Ocean. This additional freshwater further slows the AMOC until, at some point, it ceases and thereby leads to peak expression of these atmospheric and oceanic responses. The collapsed AMOC results in subsurface warming in the North Atlantic, which destabilizes ice shelves and triggers Heinrich events. The freshwater flux from a Heinrich event helps sustain the AMOC in greatly suppressed or off mode until subsurface warming erodes stratification of the upper ocean and destabilizes the water column, which restarts the AMOC. (We note below other mechanisms by which this restart may occur and are equally consistent with this hypothesized sequence of events.)

6.2. Causal Linkages

In this section, we summarize previous work that has described the major pathways by which the response to a change in the AMOC is transmitted through the climate system to cause an ~7-kyr climate oscillation during MIS 3.

6.2.1. The North Atlantic–Southern Ocean connection: thermal bipolar seesaw. *Merz and Wuest* [1922] first recognized from temperature and salinity observations that the AMOC is associated with cross-equatorial flow (see review by *Longworth and Bryden*, this volume). Water transported northward in the upper ocean is warmer than that of the southward-flowing NADW, resulting in a net heat transport of ~1 PW from the Southern to the Northern Hemisphere. Any change in the overturning circulation that affects this interhemispheric mass flux is associated with interhemispheric heat transport and thus temperatures in the Southern Hemisphere. To our knowledge, this point was first made by *Mix et al*. [1986] based on paleoceanographic records and then reemphasized by *Crowley* [1992] based on the pioneering model simulations of *Manabe and Stouffer* [1988]. It has since been reproduced in coupled atmosphere-ocean models of varying complexity [e.g., *Stocker et al*., 1992; *Stocker*, 1998; *Schmittner and Stocker*, 1999; *Schmittner et al*., 2003; *Zhang and Delworth*, 2005]. The highest amplitude temperature signal occurs in the subsurface South Atlantic at a few hundred meters depth which, in the case of a complete cessation of the overturning, warms by up to 5 C.

Synchronization of Greenland and Antarctic ice core records enabled assessment of phasing between the Northern and Southern Hemisphere high latitudes [*Blunier et al*., 1998; *Blunier and Brook*, 2001]. Out-of-phase behavior during millennial timescale variations of the last ice age are consistent, at least qualitatively, with changes of the overturning and associated interhemispheric heat transport. However, the models display a range of response at high southern latitudes, and the mechanism by which the temperature anomaly is transmitted from the South Atlantic to the center of the Antarctic ice sheet remains unclear in detail [*Stocker*, 2002; *Schmittner et al*., 2003]. *Schmittner et al*. [2003] suggested that the lag of a few hundred years between Antarctic temperatures and opposing changes in Greenland (Figure 8) is caused by slow propagation of the signal through the ACC. They also proposed a very simple conceptual model that not only reproduces the large Antarctic A events from an idealized Greenland record, but also indicates that the amplitude of the response in Antarctica depends on the duration of the stadials and interstadials in Greenland. Both the model of *Schmittner et al*. [2003] and a similar model of *Stocker and Johnsen* [2003] produced smaller amplitude Antarctic temperature oscillations associated with higher frequency variations in Greenland similar to those in a higher resolution ice core record from Antarctica (*EPICA Community Members*, 2006). *Knutti et al*. [2004] suggested that additional freshwater input to the North Atlantic during a period of collapsed Atlantic overturning leads to an additional warming in the Southern Hemisphere; however, these results were an artifact of a freshwater compensation flux used in their model simulations (*R. Knutti and J. Fluckiger*, personal communication) and therefore must be dismissed.

6.2.2. The Southern Ocean–equatorial Pacific connection: equatorward advection. Time series analyses of long records from the tropical Pacific contain a significant component of orbital-scale variability that is in phase with high-latitude Southern Hemisphere temperature change, suggesting extratropical forcing of the tropics at these timescales [*Pisias and Mix*, 1997; *Lea et al*., 2000; *Feldberg and Mix*, 2003]. In addition to atmospheric teleconnections [*Liu and Yang*, 2003], several oceanic mechanisms exist by which a

change in Southern Ocean SSTs may be transmitted to the equatorial Pacific within decades or centuries. For millennial timescales, the Southern Ocean SST change is readily explained as a seesaw response to changes in the AMOC that synchronizes changes in Pacific SSTs with changes in the AMOC on a timescale of 100 yr. Accordingly, we can generalize the seesaw concept to include the tropical Pacific as well as the Southern Ocean in registering opposite temperature changes to those occurring in the North Atlantic.

Modeling experiments have identified additional mechanisms by which a change in the AMOC may induce a Pacific surface-ocean response with the same sign as that induced by transmission from the Southern Ocean. One means is by way of a rapid (10^1-10^2 yr) global baroclinic adjustment to a change in North Atlantic density, with an attendant change in the depth of the tropical Pacific thermocline [*Huang et al*., 2000; *Timmermann et al*., 2005]. Another mechanism involves a short-circuiting of the Southern Ocean pathway altogether, with a more direct linkage provided by the atmosphere across the Isthmus of Panama [*Zhang and Delworth*, 2005]. Specifically, a cooling of the tropical Atlantic adjacent to the isthmus enhances sea-level pressure in the eastern tropical Pacific, with attendant weakening of the Hadley circulation there, inducing anomalous southward surface winds across the equator in the Pacific. These anomalous surface winds induce ocean upwelling (cooling) in the eastern Pacific north of the equator and downwelling (warming) in the cold tongue south of the equator. These changes are self-reinforcing, and cause changes in tradewinds and thus the Walker circulation, with corresponding changes in the thermocline depth inducing an El Niño-like SST field south of the equator and a La Niña-like SST field north of the equator. In the following, we focus on mechanisms by which a Southern Ocean signal is transmitted to the tropical Pacific, but note that these additional physical mechanisms would amplify most the associated responses in the equatorial Pacific.

Equatorward transmission of a signal from the Southern Ocean may occur via surface waters and the shallow meridional overturning circulation in the Pacific basin. Much of the cool water along the eastern boundary of the South Pacific originates at high southern latitudes and is advected northward by the Chile and Peru Currents. Advection is also important in the shallow, wind-driven meridional overturning of the Pacific, through which subtropical surface waters subduct along isopycnal surfaces into the equatorial thermocline and then upwell in the equatorial Pacific. Similar subduction occurs in the North Pacific, but transmission of the heat anomalies to the eastern and central Pacific is either blocked by a ridge in the pycnocline at ~10 N caused by Ekman upwelling associated with the ITCZ [*Lu et al*., 1998] or diverted to the Indian Ocean through the Indonesia Throughflow [*Rodgers et al*., 1999]. Subantarctic Mode Water that forms in the ACC region subducts to form Antarctic Intermediate Water that ventilates waters below the thermocline. Geochemical data and modeling suggest that a significant component of the thermostad at the base of the Equatorial Undercurrent is comprised of waters originating from Subantarctic Mode Water formed in the southwest Pacific [*Toggweiler et al*., 1991; *Rodgers et al*., 2003; *Sarmiento et al*., 2004]. This water then upwells as cold, nutrient-rich water along the Peru coast, where it becomes entrained in the South Equatorial Current.

Coupled ocean-atmosphere models have demonstrated that a SST anomaly imposed in the South Pacific will subduct along isopycnal surfaces into the equatorial thermocline and upwell in the equatorial Pacific [*Gu and Philander*, 1997; *Bush and Philander*, 1998; *Weaver*, 1999; *Liu et al*., 2002; *Lee and Poulsen*, 2006]. Sensitivity studies with one climate model [*Liu et al*., 2002] suggest that the greatest response of the tropical Pacific to a given extratropical forcing is associated with a source-water temperature change between 30 and 50 S. Variations in sea ice extent are particularly important in controlling temperature changes of these mode waters, either through sea ice albedo feedback [*Liu et al*., 2002] or through sensible heat loss at the sea ice margin [*Lee and Poulsen*, 2006]. Advection of a thermal anomaly initiates a positive feedback between the tropical ocean and the atmosphere through the winds, thereby amplifying an initial perturbation [*Bush and Philander*, 1998]. Equatorward transmission of South Pacific SSTs may account for at least half of the changes in the tropical Pacific at the Last Glacial Maximum (LGM) [*Liu et al*., 2002] and throughout the last 150,000 years [*Feldberg and Mix*, 2003].

6.2.3. The equatorial Pacific–North American ice sheet connection: atmospheric bridging. Propagation of SST changes in the tropical and subtropical Pacific via atmospheric bridging occurs through both the ocean and atmosphere and their interactions and feedbacks. The nature of the bridging with regard to present-day teleconnections during the El Niño-Southern Oscillation (ENSO) is relatively well understood from analyses of data and from data-model experiments [*Lau and Nath*, 1996; *Trenberth et al*., 1998; *Hoerling et al*., 2002; *Alexander et al*., 2003, and studies cited therein). The bridge originates in the tropics where warm SST anomalies enhance deep convection. The additional heat and moisture is propagated poleward through an upper tropospheric wave train of alternating high and low changes in geopotential heights that develops and alters the position and intensity of the subtropical and mid-latitude jet streams and related storm tracks. Sinking motions in the subtropical high pressure region (~30 N) alter atmospheric moisture, heat and wind at the surface and, through air-sea

interactions, alter SST, salinity and mixed layer depth, resulting in atmospheric changes that influence the ice sheets through the westerlies. Although research has focused on the ENSO region of the Pacific, the mechanism also applies to the Atlantic and other oceans.

The potential importance of tropical climate (SST) changes on high latitudes has long been of interest in paleoclimate. A number of studies have explicitly or implicitly analyzed some or all of the components of atmospheric bridging in a paleoclimate context [*Dong and Valdez*, 1995, 1998; *Bush and Philander*, 1998; *Cane*, 1998; *Rind*, 1998; *Yin and Battisti*, 2001; *Rodgers et al*., 2003, 2004; *Zhao et al*., 2004; *Charbit et al*., 2005; *Justino et al*., 2005; *Hostetler et al*., 2006].

6.3. Modeling

In this section, we apply an Earth Model of Intermediate Complexity and an AGCM to further evaluate plausible causal linkages outlined in our conceptual framework that give rise to MIS 3 variability. As reviewed previously, each of the specific linkages, i.e., subsurface warming, the bipolar seesaw, the Southern Ocean-equatorial Pacific connection, and atmospheric bridging to the LIS, has been simulated in modeling experiments. Currently there is no Earth System model with all the components needed to evaluate the complete climate oscillation that we propose for MIS 3. In this section, however, we are able to use one modeling strategy that successfully simulates propagation of change in the AMOC through the ocean to the equatorial Pacific in a manner consistent with the data. The simulations also provide additional insights on the subsurface warming that develops in the North Atlantic in association with a collapse of the AMOC. Further modeling is needed, however, to evaluate fully whether this warming may have been a trigger of Heinrich events. We also present new results from climate modeling that quantify the response of Northern Hemisphere ice-sheet mass balance to changes in North Atlantic and equatorial SSTs, and discuss the implications of the associated changes in freshwater flux to changes in the AMOC and eustatic sea level.

6.3.1. The AMOC–Southern Ocean–equatorial Pacific linkages. We use the UVic Earth System Climate Model (ESCM) (Version 2.7) [*Weaver et al*. 2001], which consists of a global three-dimensional ocean circulation model, a dynamic thermodynamic sea ice model, a simple one-layer energy-moisture balance atmosphere model, and dynamic terrestrial vegetation and ocean ecosystem components. Changes in wind stress are considered through asynchronous coupling with the AGCM GENESIS [*Schmittner et al*., 2007]. A pre-industrial (interglacial) background climate and Earth's orbital parameters for year 1850 are used to calculate the seasonal cycle of insolation. Atmospheric CO_2 is calculated interactively. The Laurentide and Scandinavian ice sheets are not included in the model. See *Schmittner et al*. (this volume) for a more detailed description of the model used and the experimental setup.

A 0.2 Sv freshwater pulse is introduced into the North Atlantic over 500 years, which leads to reduced overturning circulation in the Atlantic (Figure 13). As a consequence of the reduced south-to-north heat flux in the ocean, the area of sea ice increases by ~40% in the North Atlantic and decreases by ~15% in the Southern Ocean, consistent both with previous results [*Schmittner et al*., 2003] and the concept of a bipolar temperature seesaw. A small warming of equatorial Pacific SSTs occurs in the simulation with fixed winds, but that warming increases to almost 1 C in the simulation that uses the seasonal cycle of wind stress from GENESIS (Figure 13), suggesting that changes in wind-driven circulation contribute almost half of the total signal there. Note that the initial rapid warming may be an artifact of the asynchronous coupling method which applies the wind-stress anomaly instantaneously at year 1. Subsequent warming is gradual on a millennial timescale (as is the warming in the simulation with fixed winds), as determined by the slow adjustment of thermocline and deep waters to the circulation changes.

Figure 14 displays surface and subsurface temperature anomalies at the end of the experiment, 3000 years after the cessation of NADW downwelling. With the exception of subsurface waters in the northwest Atlantic, surface and subsurface waters in the North Atlantic undergo strong cooling. Inspection of the velocity fields (not shown) indicates a weakening of the subpolar gyre and the southward transport of the cold water in the Labrador Current is replaced by northerly flow of subtropical waters off the coast of Newfoundland, producing the warm subsurface anomaly there. We attribute the subsurface warming to the collapse of the strong zonal temperature gradient that today supports the northward geostrophic flow in the North Atlantic Drift Current.

Warm anomalies are simulated in the South Atlantic and over of the Antarctic and Pacific Oceans (Figure 13). The amplitude of these anomalies is generally greater at subsurface depths but anomalies >1 C extend to the surface. In the North Pacific, strong warming is due to a shallow overturning circulation that develops there, consistent with the Atlantic-Pacific seesaw mechanism of anti-phased deep/intermediate water formation in the two basins [*Saenko et al*., 2004]. The response in the North Pacific is strongly dependent on the initial stratification there [*Schmittner and Clement*, 2002], and it appears to be model dependent [*Schmittner et al*., 2007]. Warming of the equatorial Pacific,

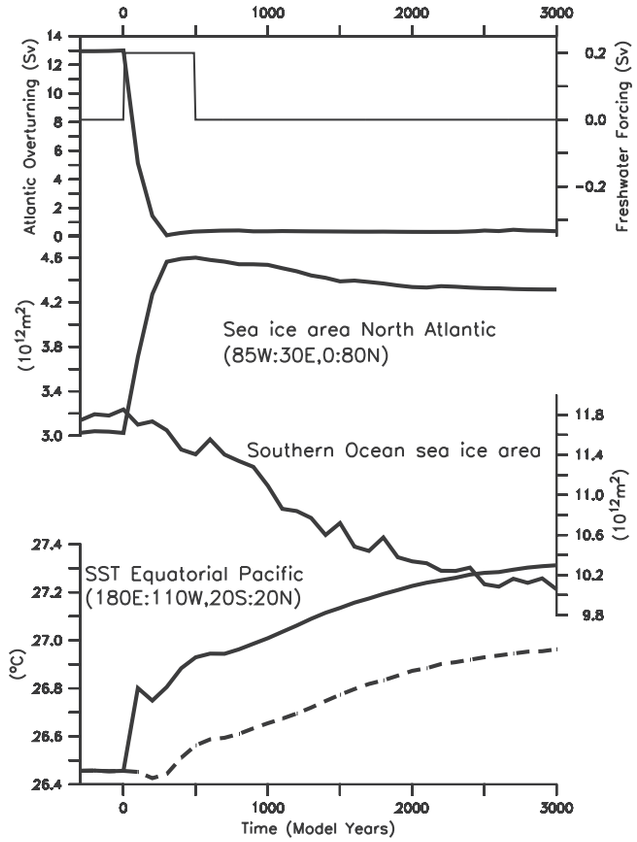

Figure 13. Time series of a model simulation in which the overturning in the North Atlantic (thick line in top panel) was shut down using a freshwater pulse (thin line in top panel) into the North Atlantic. The other panels show sea ice-covered area in the North Atlantic and Southern Ocean as well as equatorial Pacific SST. The solid lines correspond to the model experiment termed "wNPs NADW off + $\Delta\tau_{GENESIS}$" in *Schmittner et al*. (this volume), where a more detailed description can be found. This experiment considers changes in wind stress that were computed asynchronously using the GENESIS AGCM. The dashed line in the bottom panel is from a simulation identical to the one above except that wind stress was kept constant. The difference between the dashed and solid lines is therefore attributable to changes in the wind-driven circulation.

on the other hand, is robust among models when different North Pacific stratification and/or different wind-stress anomalies are applied (e.g., from the GFDL model, not shown), although the simulated amplitude of the warming varies somewhat among the models. Our ESCM results are also robust in a simulation with a colder (glacial) background climate (not shown).

6.3.2. North Atlantic subsurface warming. We performed additional experiments with the UVic ESCM to evaluate further the North Atlantic subsurface warming seen in Figure 14. A control run was integrated for several thousand years under LGM boundary conditions: atmospheric CO_2 concentration of 190 ppmv, orbital parameters corresponding to 21 ka BP, and prescribed continental ice sheets from *Peltier* [1994]. The maximum strength of the overturning streamfunction in the North Atlantic was 17 Sv at the end of our control run. We then added a freshwater flux of 0.12 Sv in the North Atlantic region for 200 years to cause a collapse of the meridional overturning in the North Atlantic. Figure 15 shows anomalies of potential temperature at selected depths after the collapse relative to the temperature before the collapse. The freshwater lens strengthens vertical stratification and thereby suppresses the heat flux between the ocean and atmosphere. The ocean loses less heat and so less (or no) cold water is convected into the deep ocean to be advected southward along the continental shelf. The result is a warming of the subsurface ocean water masses corresponding to NADW, similar to other model experiments [*Schiller et al*., 1997; *Shaffer et al*., 2004; *Knutti et al*., 2004; *Cheng et al*., this volume).

The subsurface warming of the LGM simulation (Figure 15) is more pronounced than that of the control simulation (Figure 14). This is mainly due to differences in the forcing climatologies and the diffusion and vertical mixing schemes: the horizontal isopycnal diffusion is lower for the control and LGM (4×10^2 m^2 s^{-1} and 2×10^3 m^2 s^{-1}, respectively). The LGM simulation uses the Bryan Lewis vertical profile mixing scheme whereas tidal mixing was used in the control simulation. Finally, the strength of the overturning for the LGM simulation is on the high end of estimates from data and other model experiments, so the simulated subsurface warming should be viewed as a "maximum estimate."

Existing proxy data of deep-ocean temperature are in good agreement with the magnitude of the subsurface warming in the North Atlantic simulated by the UVic model. High-resolution benthic $\delta^{18}O_c$ and faunal records from northeast of Newfoundland (1251 m water depth) and the Nordic Seas (1020 m and 1226 m depth) document substantial warming at intermediate water depths prior to each Heinrich event [*Dokken and Jansen*, 1999; *Rasmussen et al*., 2003] (Figure 16). Corresponding faunal changes support a significant temperature component to these $\delta^{18}O_c$ signals [*Rasmussen et al*., 1996, 2003, 2004; *Olsen et al*., 2005].

6.3.3. Pacific SST–North American ice sheet teleconnections. We applied the GENESIS (V2.2, GEN2) AGCM in a series of sensitivity tests to evaluate the response of the mass balances of the Northern Hemisphere ice sheets to changes in the tropical Pacific and North Atlantic SSTs. GEN2 uses a T31 atmospheric grid (~3.75 latitude by 3.75 longitude) with 18 vertical layers and a 2 latitude by 2 longitude grid

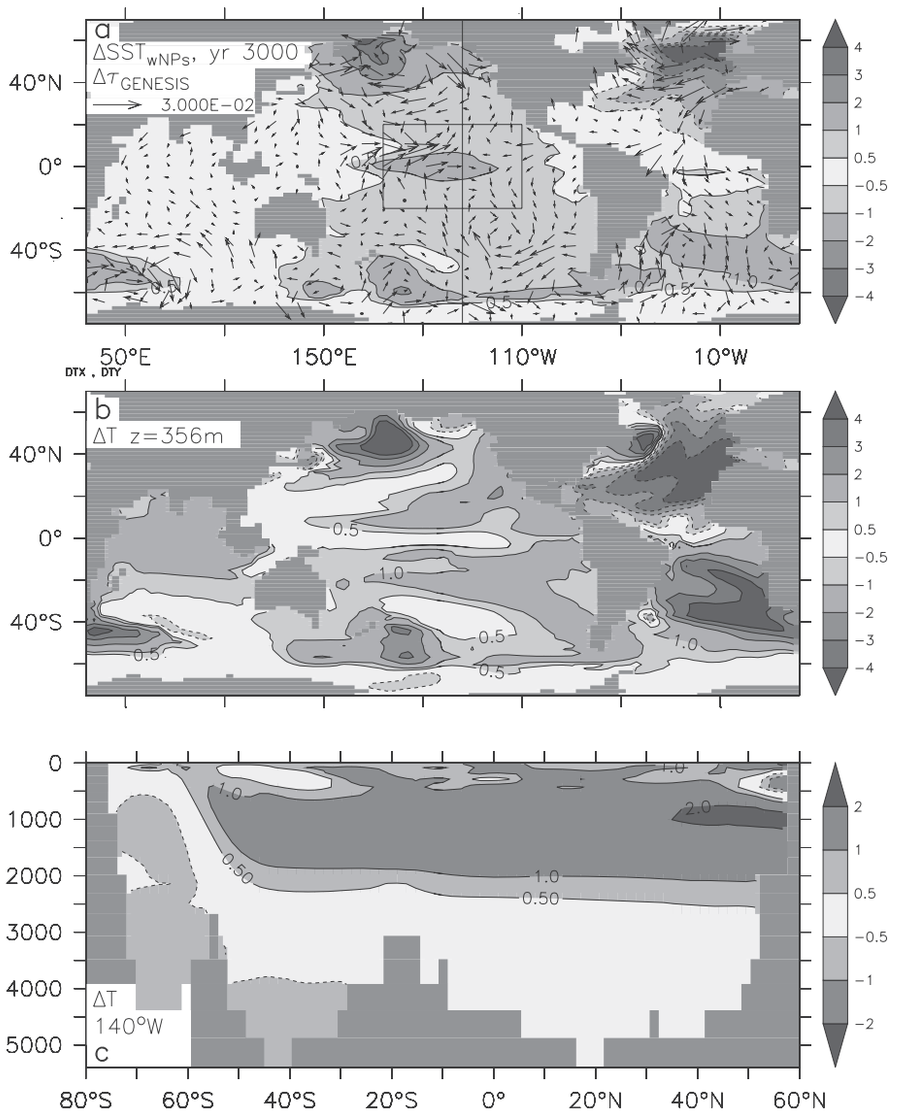

Figure 14. (a) SST and wind stress anomaly at year 3000 of the simulation described in Figure 13. Box in the equatorial Pacific shows the area of averaging used in bottom panel of Figure 13. The vertical line indicates 140 W. (b) Potential temperature anomaly at 356 m depth and (c) along a north-south section at 140 W in the Pacific ocean.

representation of the surface. The model includes a detailed land surface physics package, LSX [*Thompson and Pollard*, 1995] that explicitly computes the components of the ice-sheet mass-balance. The ice surface distribution and elevation are fixed (not dynamic) in the model. While the computed mass-balance numbers of our experiments are likely model dependent [*Pollard*, 2000], the relative changes in mass-balance among the simulations are internally consistent and thus provide a valid assessment of climatic forcing.

In the model simulations, we prescribed the appropriate global boundary conditions for the distribution of global ice sheets [*Licciardi et al*., 1998; *Peltier*, 1994], atmospheric composition (200 ppmV CO_2), orbital parameters (eccentricity = 0.0164, obliquity = 22.2366 , precession = 212.7878), and SST during MIS 3. The prescribed SST fields are the only boundary conditions that were varied in the simulations.

Although the chronology of changes in tropical SSTs during MIS 3 has yet to be adequately resolved [*Stott et al*., 2002;

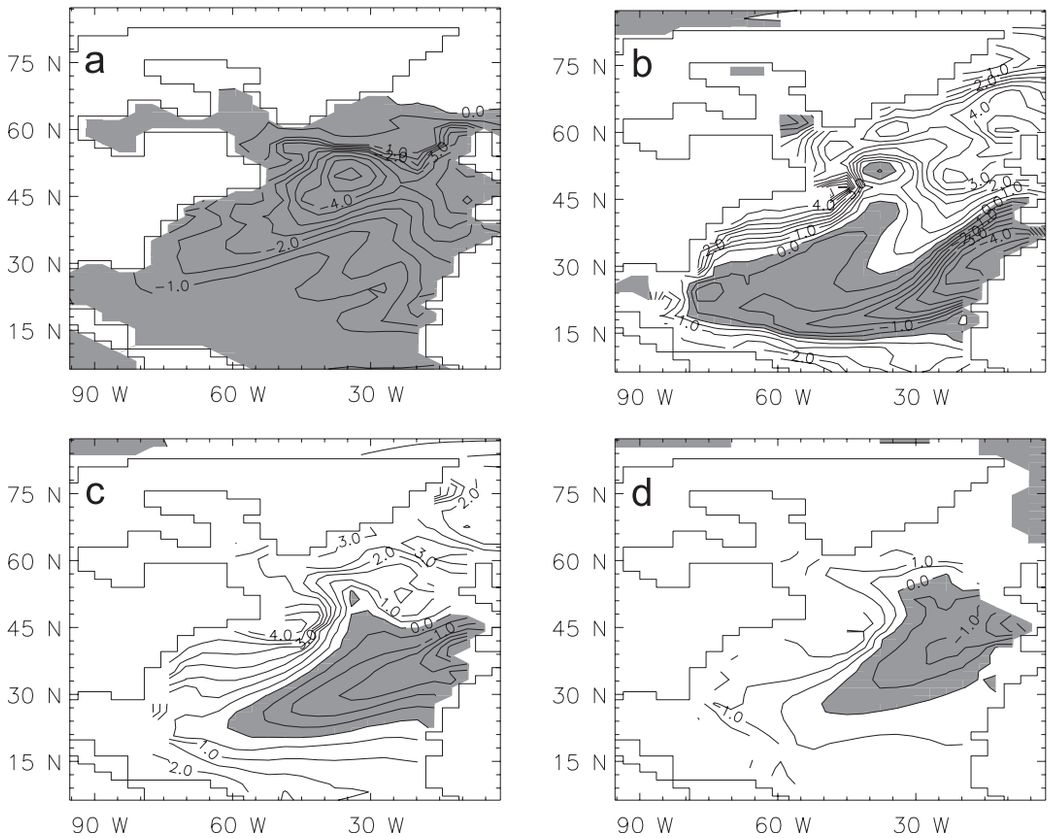

Figure 15. Subsurface temperature anomalies (relative to LGM) induced by a collapse of the overturning circulation in the UVic model at (a) 81 m, (b) 426 m, (c) 1005 m, and (d) 1521 m water depth.

Dannenmann et al., 2003] (Figure 7), the tropical Pacific SST record on orbital timescales [*Pisias and Mix*, 1997; *Lea et al*., 2000] and of the last deglaciation [*Visser et al*., 2001; *Lea et al*., 2006], and our simulation with the ESCM (Figure 14) indicates that the tropical Pacific did respond to forcing transmitted from the Southern Ocean. To evaluate the sensitivity of ice-sheet mass balance to tropical SSTs during MIS 3, we thus use the Byrd temperature record as a proxy for establishing the timing of tropical SST changes. Similarly, we use the GISP2 δ^{18}O record as a proxy for establishing the timing of well-established changes in North Atlantic SSTs.

On this basis, we identify four primary combinations of tropical and North Atlantic SSTs during each of the MIS 3 oscillations that we used to prescribe global SST fields in our simulations (Figure 17): (1) a "cold tropical" field, in which bias corrections were applied to the CLIMAP SSTs in (mainly) the tropical and subtropical Pacific to achieve greater LGM cooling while preserving the distribution of SST gradients, with SSTs and sea ice in the North Atlantic region set at full-glacial values [*Hostetler et al*., 2006], hereafter CTCNA; 2) a "warm tropical" field similar to that of CLIMAP which, relative to the field in (1), is warmer in the tropics and subtropics [*Mix et al*., 1999; *Hostetler and Mix*, 1999; *Hostetler et al*., 2006], hereafter WTCNA; (3) the field described in (2) with additional warming in the North Atlantic represented by setting the SSTs north of 30 N to values three fourths of the way from LGM to presentday values [*Hostetler et al*., 1999], hereafter WTWNA; and (4) the field described in (1) but with the same prescribed warming in the North Atlantic described in (3), hereafter CTWNA. We ran the GEN2 simulations for 50 years, and analyzed the last 40 years to evaluate the mass balances and climatic controls of the Northern Hemisphere ice sheets.

The volumetric net mass balance, B_n, is computed over all ice grid cells *i,* as:

$$B_n = \sum_i [p_i - e_i - (1 - \rho_i) r_i - d_i] \cdot A_i \qquad (1)$$

where p_i is precipitation, e_i is evaporation, p_i is the retention coefficient that determines the portion of precipitation and melt that is retained on the ice by refreezing and other processes, r_i is runoff from snow and ice melt, d_i is drainage

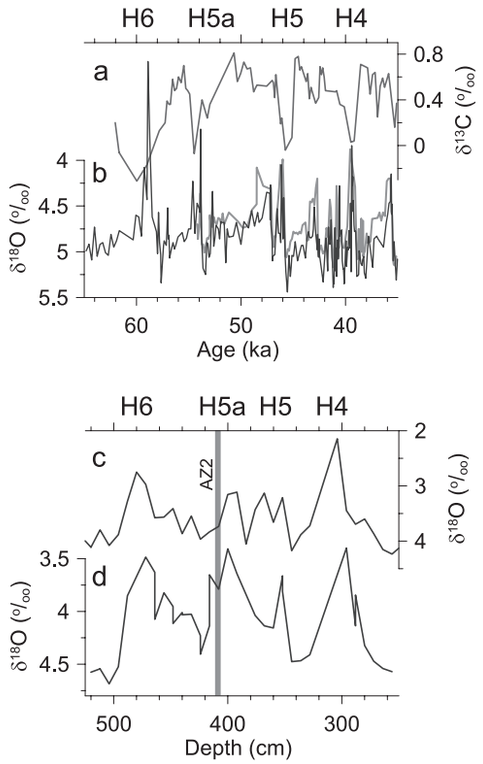

Figure 16. (a) The $\delta^{13}C$ record from core MD95-2042 (3146 m water depth) in the eastern North Atlantic [*Shackleton et al.*, 2000], a proxy for changes in the AMOC. (b) Benthic $\delta^{18}O$ records from intermediate depth sites in the Nordic Seas: ENAM93-21 (gray line) (1020 m water depth) and MD95-2010 (black line) (1226 m water depth) [*Dokken and Jansen*, 1999]. (c) Planktonic $\delta^{18}O$ record from site in western North Atlantic Ocean off Newfoundland (EW9302-2JPC) [*Rasmussen et al*., 2003]. Times of Heinrich events are identified by more negative anomalies in $\delta^{18}O$. (d) Benthic $\delta^{18}O$ record from same site as planktic record shown in (c) but at 1251 m water depth. Location of ash zone 2 (AZ2, ~53 ka) in core is shown by vertical gray bar.

of melt water into the ice sheet, and A_i the area of the grid cell. The temperature-dependent retention coefficient is computed using the method of *Huybrechts and deWolde* [1999]:

$$r_i = \min\left[\left(\frac{c}{L}\right)T_{air}\,\frac{d}{P};1.0\right] \qquad (2)$$

where c is specific heat capacity of ice, L is latent heat of fusion of ice, T_{air} is the 2-m air temperature, d is the depth of thermally active layer (2 m), and P is water-equivalent precipitation. Eq. 2 was derived by *Huybrechts and deWolde* [1999] over Greenland using mean annual average temperature and precipitation data; here we apply it using average monthly data.

The mass balances of the Laurentide, Greenland, and Scandinavian ice sheets (LIS, GIS, and SIS, respectively) (Table 2, Figure 18) are strongly controlled by changes in SSTs that are propagated to the ice sheets through the atmosphere. Warming the tropics and subtropics in the WTCNA experiment increases mean annual air temperature by >2.5 C over most of the LIS and by >1.0 C over the GIS and SIS (Figure 19b). The warmer tropical and subtropical SSTs enhance convection and increase the flux of water vapor out of the low latitudes and into higher latitudes in both hemispheres, resulting in a global increase in atmospheric moisture (Figure 20a). Precipitation increases associated with the warmer atmosphere, greater water vapor content, and change in the position of the storm tracks occur over much of the Northern Hemisphere (Figure 21b). Over the ice sheets, topographic and thermal forcing limit precipitation increases which do not offset the increase in temperature-related ablation (Figure 18b). All the ice sheets are sensitive to tropical and subtropical Pacific SSTs, with the LIS the most sensitive owing to the western extent of its margin and interior and the influence of the atmospheric bridge in the Pacific. The combined changes in the Northern Hemisphere ice-sheet mass balance in the WTCNA amount to an increase in freshwater flux to the North Atlantic ~1900 km^3 yr^{-1} (Table 2).

In the WTWNA experiment, warming the North Atlantic SSTs warms air temperature at latitudes above 30 N by up to 10 C in the basin, >2.5 C over most of Europe, and 1-2.5 C over Asia and western North America (Figure 19c). Over Greenland, air temperatures in the WTWNA are ~7 C warmer than those of the WTCNA experiment, in agreement with the estimated range (8-15 C) inferred from $\delta^{15}N$ records from Greenland ice cores [*Huber et al*., 2006]. Water vapor transport increases the atmospheric water vapor content over the southern margin of the LIS and the southern and western margin of the GIS (Figure 20b). Precipitation changes in the WTWNA experiment are largest over Greenland, smaller over the SIS, and negligible over the LIS, where desertification effects are strong (Figure 21c). Ablation is further enhanced over all the ice sheets in the WTWNA experiment (Figure 18c) resulting in mass balances that are substantially more negative as those of the WTCNA experiment and an additional increase in freshwater flux of ~2000 km^3 yr^{-1} (Table 2). Accumulation increases over the south and west of the GIS in response to the warming (Figure 18c), but the additional accumulation is offset by greater ablation, resulting in a more negative mass balance in the WTWNA simulation (Table 2, Figure 18c).

With a warm North Atlantic, cooling the tropics and subtropics cools the Northern Hemisphere, including most of the ice sheets (Figure 19d). Colder temperatures and reduced

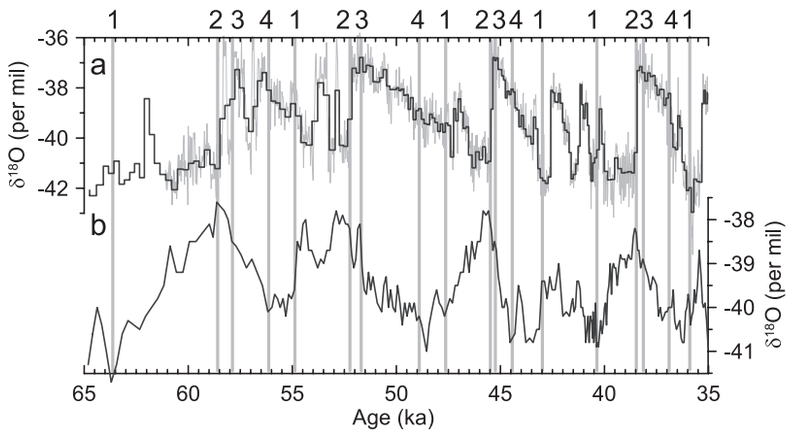

Figure 17. (a) The GISP2 δ^{18}O record [*Grootes et al*., 1993; *Stuiver and Grootes*, 2000]. (b) The Byrd δ^{18}O record [*Johnsen et al*., 1972], with the timescale synchronized to the GISP2 timescale by methane correlation [*Blunier and Brook*, 2001]. Vertical lines numbered 1 through 4 represent time slices identified from the two ice cores used to establish boundary conditions for climate modeling, with the GISP2 record used as a proxy for North Atlantic SSTs, and the Byrd record used as a proxy for changes in tropical SSTs. Time 1 identifies cold SSTs in the tropics and North Atlantic (model boundary condition CTCNA). Time 2 identifies warm SSTs in the tropics and cold SSTs in the North Atlantic (model boundary condition WTCNA). Time 3 identifies warm SSTs in the tropics and North Atlantic (model boundary condition WTWNA). Time 4 identifies cold SSTs in the tropics and warm SSTs in the North Atlantic (model boundary condition CTWNA).

water vapor transport from the tropics (inverse of Figure 20a) produce drying in the Northern Hemisphere (Figure 21d) in the CTWNA experiment. In response to colder temperatures, the mass balances of the ice sheets are substantially more positive than those of the WTWNA experiment and storage of freshwater in the ice sheets reduces the freshwater flux to the North Atlantic by 1800 km^3 yr^{-1} (Table 2).

6.3.4. Mass-balance-driven changes in eustatic sea level and freshwater fluxes. We derived time series of changes in eustatic sea level and freshwater flux to the North Atlantic by subdividing the interval from 65 to 35 ka based on the sequential changes in the four SST combinations described above (Figure 17). For each interval bracketed by two of the SST experiments, we took the average of the mass-balance difference and multiplied by the interval duration to derive the change in eustatic sea level (Figure 22) and the corresponding freshwater flux to the North Atlantic (Figure 23). Negative (positive) sea-level changes and freshwater fluxes are associated with those climatologies that led to a net increase (decrease) in ice-sheet mass balance during each interval.

Our modeled sea-level history is characterized by four fluctuations (Figure 22f). The magnitude and timing of these fluctuations is remarkably similar to those inferred from several other proxies of sea level change, including the New Guinea coral reef record dated by U-series [*Yokoyama et al*., 2001; *Chappell*, 2002] (Figure 22c), benthic $\delta^{18}O_c$ records that sample intermediate waters in the Southwest Pacific (Figure 22d) [*Pahnke and Zahn*, 2005] and deep waters in the eastern North Atlantic basin (Figure 22e) [*Shackleton et al*., 2000], both of which are on the same (GISP2) timescale as our modeled record, and the *Siddall et al*. [2003] δ^{18}O record from the Red Sea (Figure 22b) with chronology based on correlation to the Byrd δ^{18}O record, and thus also on the GISP2 timescale. Our record also shares a similar structure, within dating uncertainties, to another Red Sea sea-level reconstruction from δ^{18}O that has an independent chronology based on radiocarbon and paleomagnetic excursions (Figure 22a) [*Arz*

Table 2. Sensitivity of Northern Hemisphere ice–sheet mass balance to sea surface temperatures.

	CTCNA (km^3 yr^{-1})	WTCNA (km^3 yr^{-1})	WTWNA (km^3 yr^{-1})	CTWNA (km^3 yr^{-1})	# grids
Laurentide	–656	–1888	–3088	–944	340
Scandinavian	–145	–471	–841	–494	35
Greenland	–107	–447	–831	–465	54
Sum	–908	–2806	–4760	–1703	429

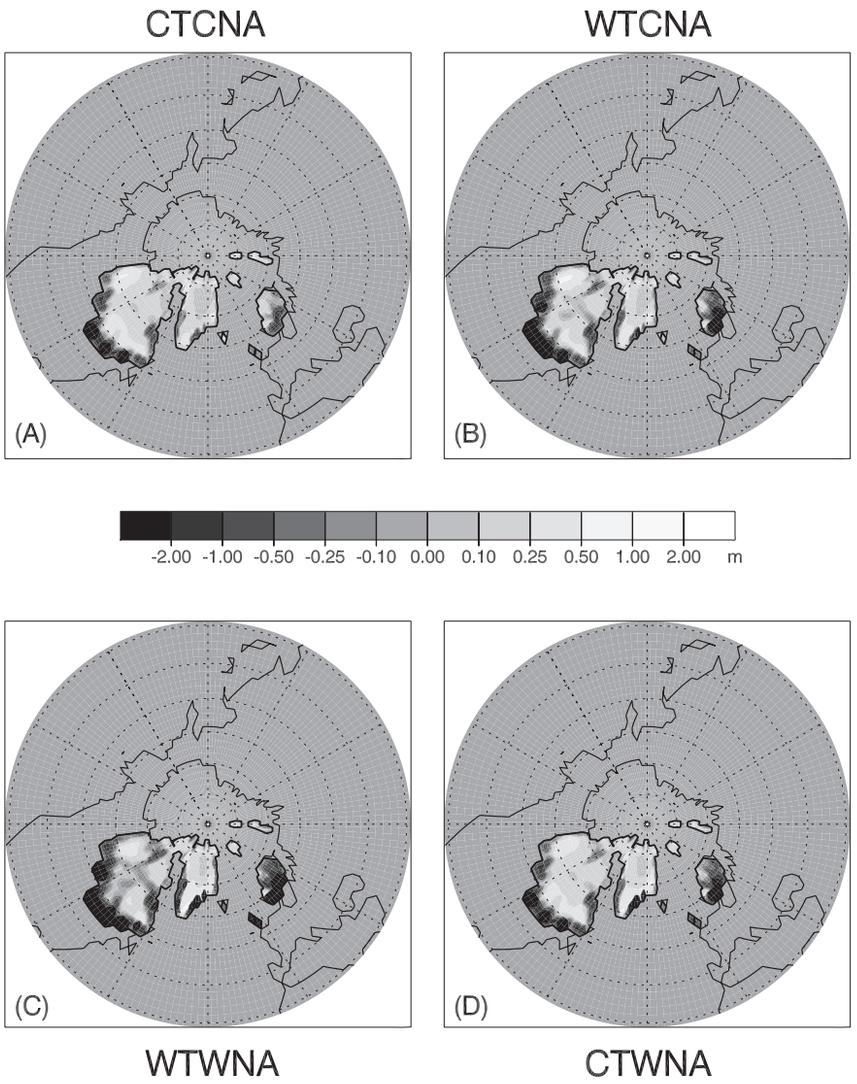

Figure 18. Simulated mass balance of Northern Hemisphere ice sheets for each of the four boundary conditions described in the text and in Figure 17.

et al., 2006]. Our modeled sea-level changes (on the order of 10 m) are similar to those derived from the New Guinea coral record (10-15 m) (Figure 22c) [*Yokoyama et al*., 2001; *Chappell*, 2002], but are significantly smaller than those inferred from the Red Sea records (up to 25 m) (Figures 22a, 23b), although we note that these latter estimates are subject to large uncertainties (±12 m). In any event, our modeled sea-level changes and those from New Guinea are substantially less than needed to explain the benthic $\delta^{18}O_c$ records (Figures 22d, 22e), suggesting either a greater ice-sheet contribution than we have modeled or the need for parallel changes in NADW and Antarctic Intermediate Water temperature (*Chappell*, 2002; *Siddall et al*., in review).

Our results are consistent with other modeling studies that demonstrate the sensitivity of the ice sheets to changes in North Atlantic SSTs [*Schmittner et al*., 2002; *Zweck and Huybrechts*, 2005; *Arz et al*., 2006]. Not surprisingly, modeled sea levels rise rapidly to their highest levels when tropical Pacific and North Atlantic SSTs (as inferred from the Byrd and GISP2 records in Figure 17) are at their warmest. Otherwise the sea-level history reflects the equally strong sensitivity of mass balance to tropical Pacific SSTs. Accordingly, the sea-level response to abrupt warming in the North Atlantic is short-lived because, although North Atlantic SSTs remain relatively warm, sea level starts to drop in response to the rapid cooling of the tropical SSTs.

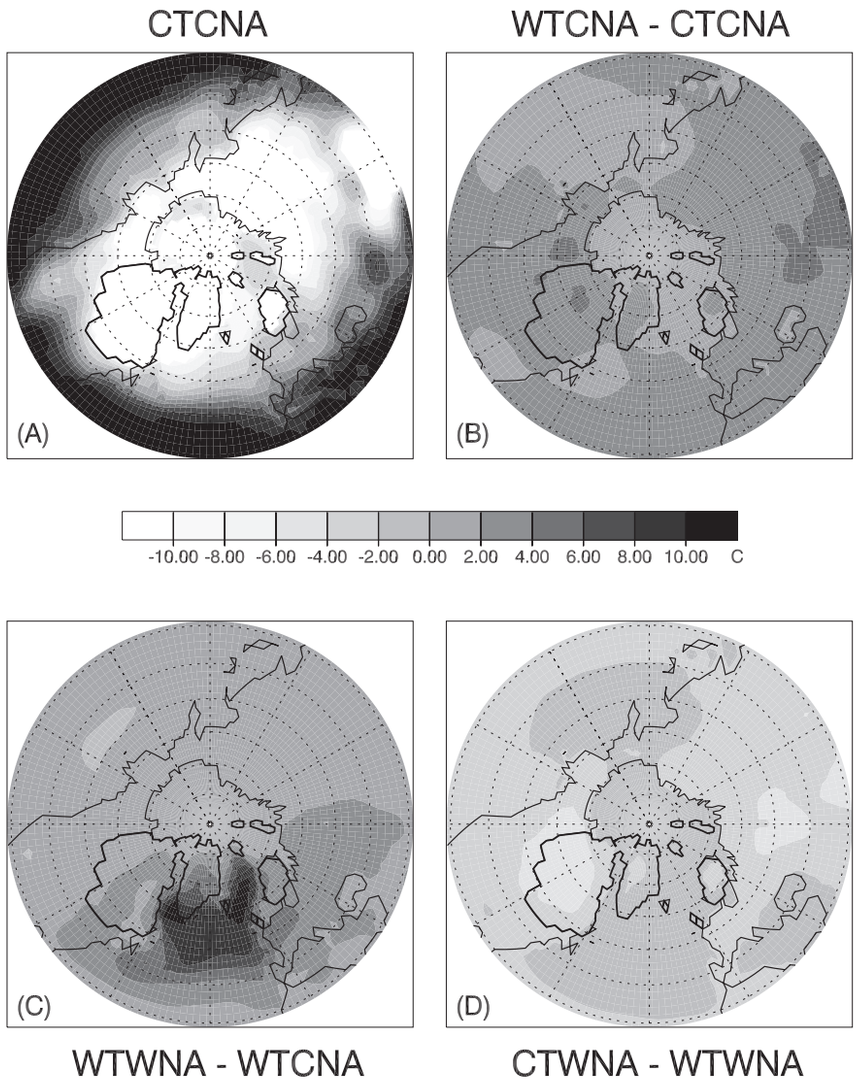

Figure 19. (a) Simulated 2-m air temperature for the boundary condition with cold tropical and North Atlantic SSTs (CTCNA). (b) Simulated anomalies in 2-m air temperature for WTCNA relative to CTCNA, illustrating the effect of warming tropical ocean SSTs. (c) Simulated anomalies in 2-m air temperature for WTWNA relative to WTCNA, illustrating the effect of warming North Atlantic SSTs. (d) Simulated anomalies in 2-m air temperature for CTWNA relative to WTWNA, illustrating the effect of cooling tropical ocean SSTs.

Similarly, at a time when North Atlantic SSTs are at their coldest, sea level starts to rise in response to the warming of tropical Pacific SSTs. Changes in North Atlantic SSTs that parallel changes in Pacific SSTs cause parallel sea-level changes, but the primary trajectory and magnitude of each fluctuation is determined by the history of Pacific SSTs.

Because we have assumed that the timings of Pacific SST changes are contemporaneous with those of Antarctica (Figure 17), the estimated sea-level changes are nearly in phase with Antarctic temperature changes (Figure 22f). Simulated mass-balance changes over the Antarctic ice sheet in response to our four SST scenarios are minimal (<10 km^3 yr^{-1}), but our AGCM experiments have not included the effect of seesaw changes in Southern Ocean SSTs and sea ice extent relative to those in the North Atlantic, leaving open the question of how much sea-level change the Antarctic ice sheet may have contributed in response to the MIS 3 climate oscillations [e.g., *Rohling et al*., 2004; *Arz et al*., 2006]. Based on sensitivity studies of Antarctic ice-sheet mass balance to temperature change [*Huybrechts et al*., 2004], however, we expect that

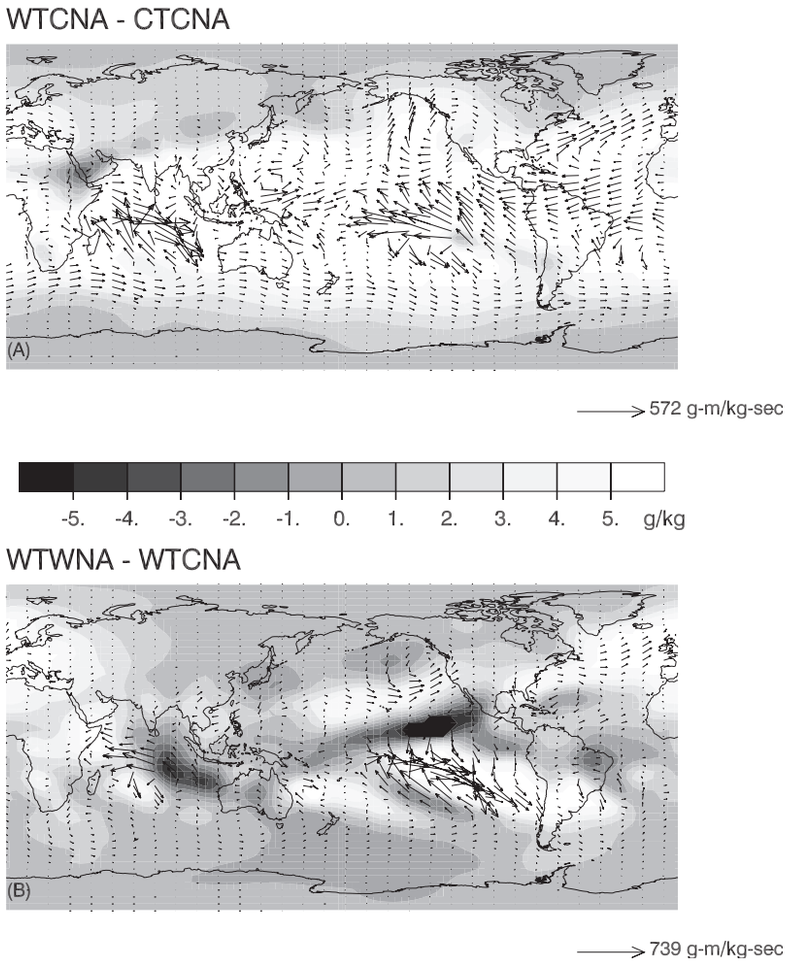

Figure 20. Anomalies of annual total atmospheric water vapor and water vapor transport (vectors) for (a) WTCNA-CTCNA and (b) WTWNA-WTCNA experiments. Total water vapor computed for the 18 vertical layers of the model. Transport computed over the 18 vertical model layers as $\sqrt{(q \cdot u)^2 + (q \cdot v)^2}$, where q is the specific humidity and u and v are the eastward and northward wind components, respectively.

the warming (cooling) over Antarctica during MIS 3 will cause the ice sheet to grow (shrink), so that corresponding sea-level changes will be directly opposite to those originating from Northern Hemisphere ice sheets. Given that reconstructed sea-level changes are in the opposite direction than if driven from the Antarctic ice sheet (Figure 22), we thus conclude that Antarctic contributions to MIS 3 sea-level changes were relatively modest, with the dominant signal originating from the Northern Hemisphere ice sheets.

The modeled time series of freshwater fluxes demonstrates how mass-balance changes forced by changes in tropical Pacific and North Atlantic SSTs cause corresponding changes in freshwater flux to the North Atlantic (Figure 23b) and thus in the AMOC. Our simulated fluxes (0.03-0.09 Sv) are comparable to those found by many models to induce changes in the AMOC [*Rahmstorf*, 1995; *Schmittner et al*., 2002; *Stouffer et al*., 2006]. Freshwater fluxes peak when tropical Pacific and North Atlantic SSTs are at their warmest, which may explain the subsequent reduction in the AMOC and cooling of North Atlantic SSTs (Figure 23c). The duration of peak flux is short, however, and the subsequent decrease reflects the influence of cooling tropical SSTs relative to warm North Atlantic SSTs in forcing more positive mass balance of the ice sheets. A reduced flux of freshwater should have acted as a positive feedback in sustaining a strong AMOC, but the North Atlantic temperature and $\delta^{13}C$ records suggest that the AMOC continued to decline slowly at first, and then more rapidly until it eventually collapsed. Cooling further decreased the freshwater flux (Figure 23b). We speculate that the cause of the decrease in the AMOC and

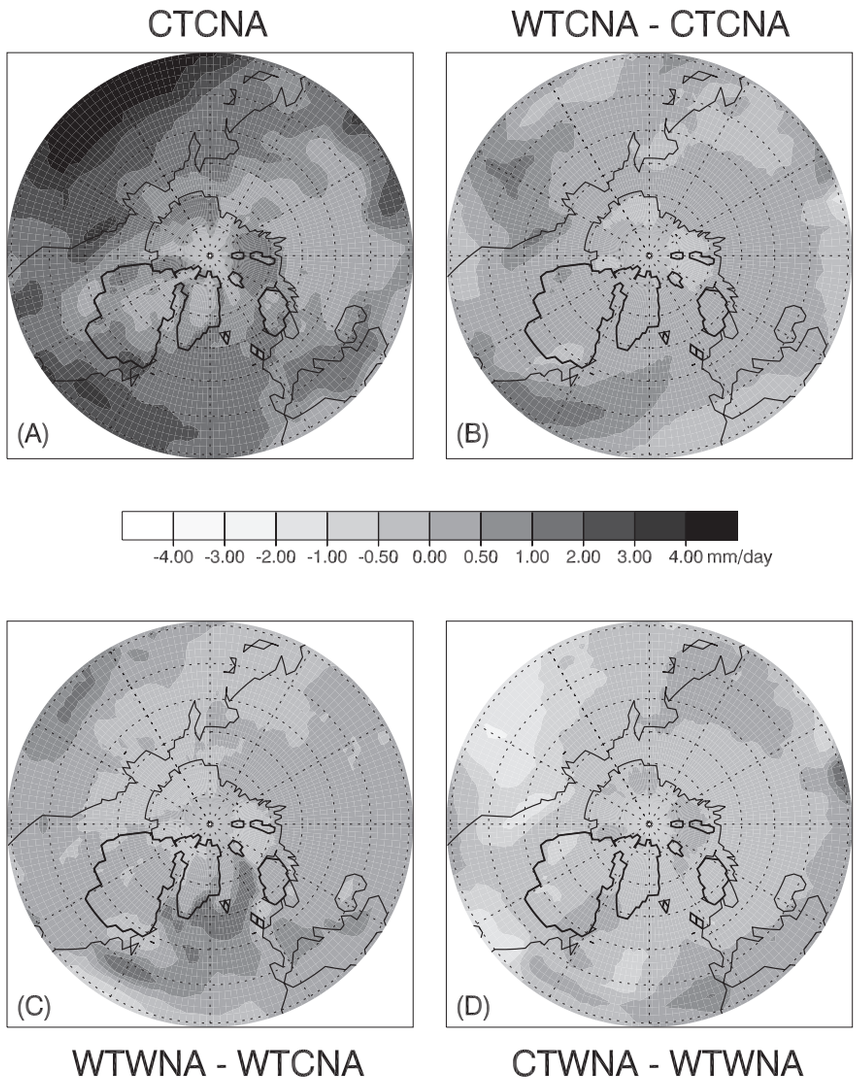

Figure 21. (a) Simulated precipitation (*P*) for the boundary condition with cold tropical and North Atlantic SSTs (CTCNA). (b) Simulated anomalies in *P* for WTCNA relative to CTCNA, illustrating the effect of warming tropical ocean SSTs. (c) Simulated anomalies in P for WTWNA relative to WTCNA, illustrating the effect of warming North Atlantic SSTs. (d) Simulated anomalies in *P* for CTWNA relative to WTWNA, illustrating the effect of cooling tropical ocean SSTs.

North Atlantic temperatures was the growth of the Northern Hemisphere ice sheets that occurred during this time (Figure 22); when their margins advanced to North Atlantic coastlines, the ice sheets again began to deliver icebergs to the ocean, thereby increasing the freshwater flux to the ocean. It thus was the more positive ice-sheet mass balance in response to the cooling of North Atlantic SSTs, combined with the cooler Pacific SSTs, that together acted as a positive feedback on the AMOC decline.

Eventual collapse of the AMOC resulted in seesaw warming in the Pacific and a decrease in ice-sheet mass balance. Although the corresponding retreat of ice margins from North Atlantic coastlines would have reduced calving to the North Atlantic, there was a corresponding increase in freshwater flux derived from the increase in melt from the ice sheets (Figure 23). This response would have acted as a positive feedback by sustaining a collapsed AMOC, and thus continued seesaw warming in the Pacific Ocean.

A $\delta^{18}O$ record in seawater ($\delta^{18}O_{sw}$) from the Gulf of Mexico [*Hill et al*., 2006] provides supporting evidence of our modeled changes in freshwater flux. Changes in $\delta^{18}O_{sw}$ at this locality (Figure 24c) likely reflect changes in the flux of

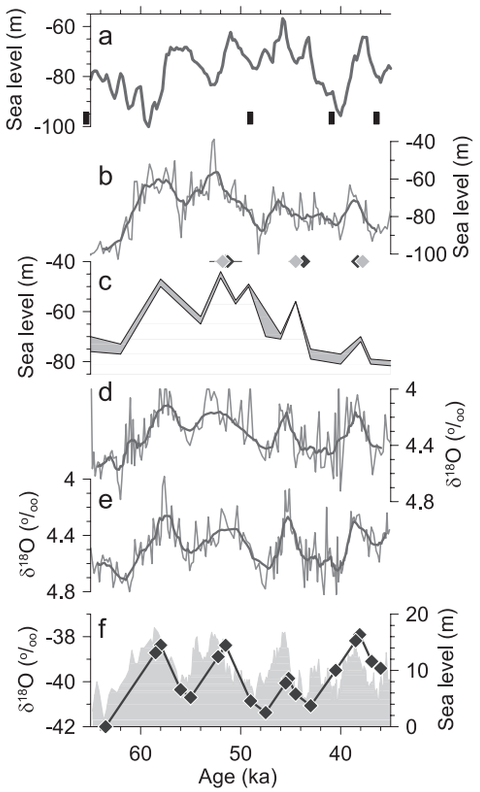

Figure 22. Reconstructions of eustatic sea level compared to our modeled sea level based on changes in ice-sheet mass balance. (a) Record from the Red Sea [*Arz et al*., 2007]. Age control shown by black rectangles. (b) Record from the Red Sea (gray line) [*Siddall et al*., 2003]. Age model based on correlation by wiggle-matching to the Byrd δ^{18}O record [*Johnsen et al*., 1972], with the timescale synchronized to the GISP2 timescale by methane correlation [*Blunier and Brook*, 2001]. Thick black line is 9-point running average of the data. (c) Sea level reconstructed from flights of raised marine terraces on New Guinea [*Chappell*, 2002] (uncertainty in sea level indicated by thickness of gray line). Age control for high sea-level stands established by uranium-series dating: light gray diamonds from *Chappell* [2002]; black diamonds from *Yokoyama et al*. [2001]. (d) Record of benthic δ^{18}O from core MD95-2042 (3146 m water depth) in the eastern North Atlantic [*Shackleton et al*., 2000]. Thick black line is 9-point running average of the data. (e) Record of benthic δ^{18}O from core MD97-2120 (1210 m water depth) in the southwestern Pacific Ocean [*Pahnke and Zahn*, 2005]. Thick black line is 9-point running average of the data. (f) The Byrd δ^{18}O record (gray screen) [*Johnsen et al*., 1972], with the timescale synchronized to the GISP2 timescale by methane correlation [*Blunier and Brook*, 2001] with our modeled sea level record superimposed (black line, with black diamonds corresponding to each of the time slices identified in Figure 17).

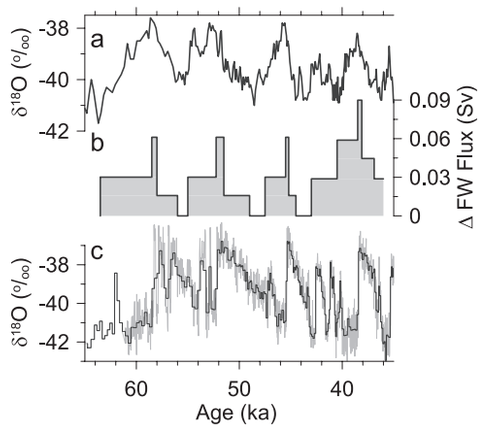

Figure 23. (a) The Byrd δ^{18}O record [*Johnsen et al*., 1972], with the timescale synchronized to the GISP2 timescale by methane correlation [*Blunier and Brook*, 2001]. (b) Changes in freshwater flux (in Sv) to the North Atlantic Ocean in response to changes in ice-sheet mass balance. (c) The GISP2 δ^{18}O record [*Grootes et al*., 1993; *Stuiver and Grootes*, 2000].

meltwater delivered to the Gulf of Mexico from the southern margin of the LIS. As noted by *Hill et al*. [2006], the $\delta^{18}O_{sw}$ record displays a fluctuation in isotopically light meltwater occurring at the same time as the A1 warm event in Antarctica (Figure 24d). Our modeling provides an explanation for this association in that it illustrates how an Antarctic signal may have propagated to the LIS through oceanic ventilation to the tropical Pacific and then atmospheric bridging (Figure 24b).

7. THE LAST DEGLACIATION

Compared to their MIS 3 counterparts, climate records spanning the last deglaciation are subject to fewer uncertainties in their age control, and climate signals tend to be robust, thus providing an excellent opportunity to evaluate specific aspects of the causal linkages described above. This is particularly the case for the availability of records from the tropical Pacific, which otherwise remains one of the largest sources of uncertainty for MIS 3. The millennial-scale climatic structure of the last deglaciation is similar to that of MIS 3 in showing northern and southern responses that are consistent with changes associated with changes in the strength of the AMOC. *Clark et al*. [2002] presented an EOF analysis of 18 high-resolution records that shows that the dominant mode of variability (EOF1) is associated with the global warming from glacial to interglacial conditions that evolved over a timescale of ~10 kyr. Included in this EOF is the interruption of the warming trend by the Younger Dryas cold interval. The second EOF quantifies the spatial and temporal expression of millennial changes centered at 16 and 12 ka BP, corresponding to the Oldest Dryas-Bølling/Allerød-Younger Dryas sequence in the north, and the warming-Antarctic Cold Reversal-warming sequence in the south. The

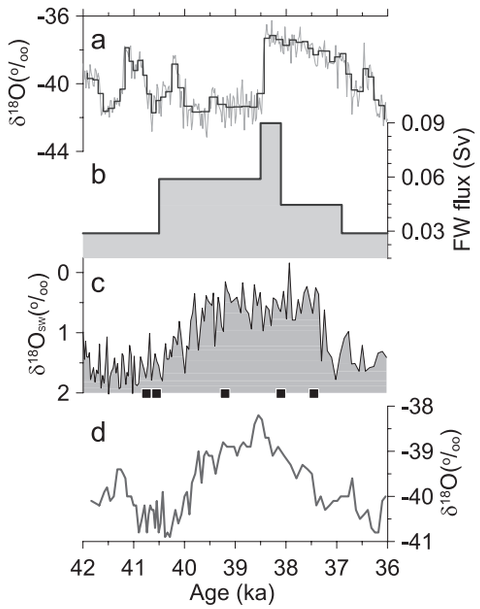

Figure 24. (a) The GISP2 $\delta^{18}O$ record [*Grootes et al.*, 1993; *Stuiver and Grootes*, 2000]. (b) Change in freshwater flux based on our simulated change in ice-sheet mass balance. (c) Record of the $\delta^{18}O$ of surface seawater from the Gulf of Mexico [*Hill et al*., 2006]. Age control based on calibrated ^{14}C ages shown by black squares. (d) The Byrd $\delta^{18}O$ record [*Johnsen et al*., 1972], with the timescale synchronized to the GISP2 timescale by methane correlation [*Blunier and Brook*, 2001].

spatial pattern of EOF2, with negative scores over Antarctica and in the South Atlantic and positive scores at all other sites, is consistent with an atmospheric transmission of the North Atlantic signal except for those areas in the Southern Hemisphere where during the last deglaciation the seesaw produced an anti-phased response as indicated by a large change in the AMOC [*Crowley*, 1992; *Stocker et al*., 1992; *Stocker*, 1998; *Schmittner and Stocker*, 1999; *Schmittner et al*., 2003; *Zhang and Delworth*, 2005].

Here we evaluate our conceptual framework for transmission of a change in the AMOC through the climate system with 14 high-resolution deglacial records that are representative of many of the components thought to be involved in the transmission (*Clark et al.*, 2004). Because other mechanisms were clearly involved in causing the last deglaciation, we focus on that interval between 19 and 14.5 ka BP, which corresponds to a time and duration similar to one of the MIS 3 climate oscillations when the AMOC collapsed [*McManus et al*., 2004]. We speculate, however, that the climate system at this time may have been poised to switch out of a glacial state, and that the responses induced by the AMOC collapse provided critical feedbacks that helped push the system into the interglacial state.

In Figure 25, we organize these deglacial records into three rows, with the top row representing processes in the North Atlantic associated with changes in the AMOC, the middle row representing processes involved in the bipolar seesaw, and the bottom row representing processes by which a Southern Ocean signal is transmitted via the ocean to the equatorial Pacific, and then via the atmosphere to the LIS.

Progressing from left to right in the top row of Figure 25, these records suggest that (25a) a decrease in the AMOC at ~19 ka BP was accompanied by (25b) cooling over Greenland. Subsequent collapse of the AMOC at ~17 ka BP coincides with (25c) a large SST cooling in the subtropical Atlantic. As discussed previously, Heinrich event 1 (25d) does not occur until the AMOC collapsed and subsurface warming had occurred [*Rasmussen and Thomsen*, 2004].

Deglacial time series in the middle row of Figure 25 represent the well-documented responses of the Southern Hemisphere to a reduced AMOC and changes in interhemispheric ocean heat transport, i.e., the thermal bipolar seesaw. As North Atlantic climate cooled (25b), the tropical Atlantic (25e) and Southern Ocean (25f) warmed, with a corresponding decrease in sea ice (25g) leading to additional warming through sea ice albedo feedback and exposure of the underlying ocean to the atmosphere. At the same time, the Antarctic continent also warmed (25h), despite a decrease in austral summer insolation from changes in the Earth's orbit (25h). The onset of CO_2 rise (25i) lags behind Southern Hemisphere temperature rise, although the magnitude of the temporal offset is subject to uncertainties in ice core chronologies (e.g., *Brook et al*., 2005).

The bottom row of Figure 25 shows deglacial time series that suggest transmission of geochemical and thermal anomalies out of the Southern Ocean to the equatorial Pacific by the shallow meridional overturning circulation. Specifically, Southern Ocean warming and sea ice meltback led to enhanced upwelling of nutrient-rich, isotopically light ($\delta^{13}C$) Southern Ocean deep water [*Sigman and Boyle*, 2000]. Newly upwelled waters with their light $\delta^{13}C$ composition were transmitted to shallow intermediate waters, which subsequently reached the equatorial Pacific to produce the signal measured in planktonic foraminifera (25j). Upwelled Southern Ocean water transmitted to the equator in the shallow subsurface would also have been supersaturated with respect to CO_2. The partial pressure of CO_2 (PCO_2) of equatorial Pacific surface waters thus should have thus risen in association with warming of these isotopically lighter, CO_2-enriched waters. Indeed, a record from the western equatorial Pacific identifies changes of PCO_2 of surface waters that are synchronous with changes $\delta^{13}C$ (25k). The 6-8 C warming of Southern Ocean SSTs in the region of mode water formation today (25f) is accompanied by 3-4 C warming of equatorial Pacific SSTs (25l, 25m), remarkably similar to the response of the tropical Pacific to an imposed warm anomaly at these

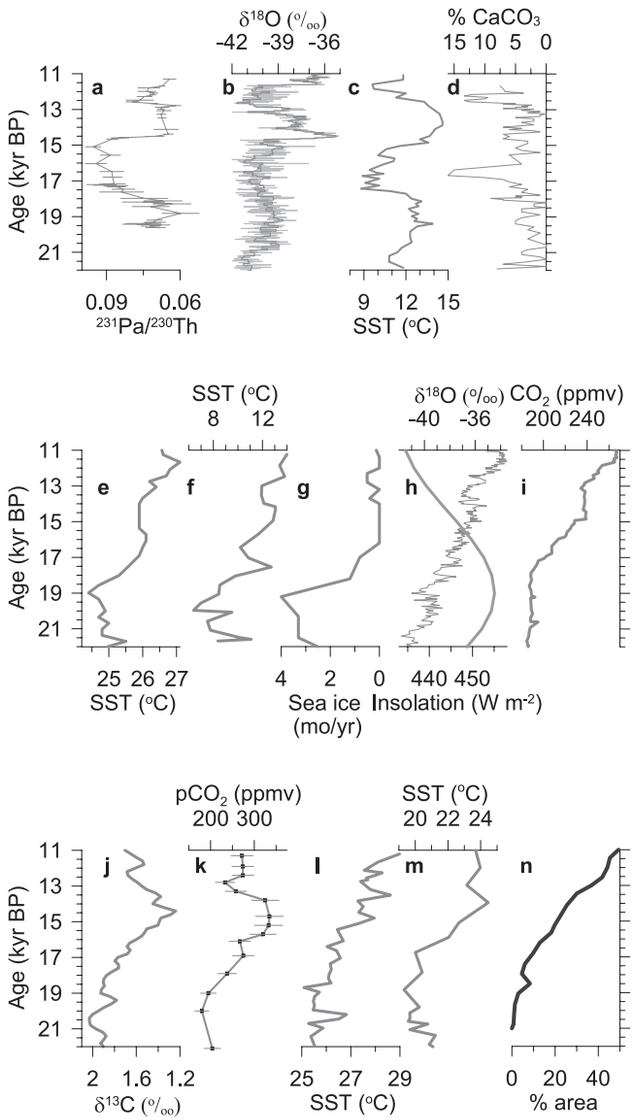

Figure 25. Records spanning the last deglaciation. (a) The record of $^{231}Pa/^{230}Th$ in marine sediments from Bermuda Rise, western North Atlantic (*McManus et al.*, 2004). (b) The GISP2 $\delta^{18}O$ record [*Grootes et al*., 1993; *Stuiver and Grootes*, 2000]. (c) Record of SSTs from the eastern North Atlantic [*Bard et al*., 2000]. (d) Record of changes in detrital carbonate in marine sediments from the North Atlantic [*Bond et al.*, 1999]. (e) Record of SSTs from the tropical North Atlantic [*Ruhlemann et al*., 1999]. (f) Record of SSTs from the southwest Pacific Ocean [*Pahnke et al*., 2003]. (g) Record of duration of sea ice (months per year) from the South Atlantic [*Shemesh et al*., 2002]. (h) Mid-month January insolation at 65 S [*Berger and Loutre*, 1991] and the Byrd $\delta^{18}O$ record [*Johnsen et al*., 1972], with the timescale synchronized to the GISP2 timescale by methane correlation [*Blunier and Brook*, 2001]. (i) The record of atmospheric CO_2 from the Siple Dome ice core [*Ahn et al*., 2004]. (j) Record of $\delta^{13}C$ from the planktonic foraminifera *Neogloboquadrina dutertrei* from eastern tropical Pacific Ocean [*Clark et al*., 2004]. (k) Record of PCO_2 from marine sediments in the western equatorial Pacific Ocean [*Palmer and Pearson*, 2003]. (l) Record of SSTs from western equatorial Pacific Ocean [*Visser et al*., 2003]. (m) Record of SSTs from eastern equatorial Pacific Ocean [*Martinez et al*., 2003]. (n) Record of integrated ice-margin retreat of the LIS, expressed as percent area remaining from its full-glacial extent [*Dyke*, 2004].

same latitudes (30-50 S) simulated with an ocean model [*Liu et al*., 2002]. Finally, the near-synchronous warming of equatorial SSTs (25l, 25m) and retreat of the LIS (25n) is consistent with the simulated response of the ice sheet to a tropical forcing [*Hostetler et al*., 2006].

8. CONCLUSIONS

Our EOF analysis of 39 high-resolution time series supports the premise that a large fraction of millennial-scale global climate variability during MIS 3 is characterized by a spatially distinct pattern referred to as a Northern mode and a Southern mode. The Northern mode is best represented in the Greenland ice cores by the D-O timescale of variability, and is largely restricted to proxies of components of the climate system in the Northern Hemisphere that are sensitive to atmospheric forcing from changes in SSTs and sea ice extent in the North Atlantic region. The Southern mode is best represented in Antarctic ice cores by the longer wavelength A events, and is seen largely in proxies of components that are sensitive to collapses of the AMOC. Accordingly, this signal is present not only throughout much of the Southern Hemisphere but in many records from the Northern Hemisphere as well. The signal may be present in surface-water proxies from the tropical Pacific, but chronological uncertainties prevent any firm conclusions as to the dominant mode of variability in this important region.

Bond et al. [1993] first noted the existence of lower-frequency variability in North Atlantic ice and marine records, whereby a long-term cooling characterized by successively smaller D-O events culminates in a Heinrich event (Figure 1). From this relationship, they argued that the cause of Heinrich events is linked to climate change rather than internal ice-sheet dynamics. Synchronization of Greenland and Antarctic records with methane [*Blunier et al*., 1998; *Blunier and Brook*, 2001] further established a clear association between climate change and Heinrich events in demonstrating that the events only occur when Greenland is at its coldest and Antarctica is at its warmest, i.e., the Atlantic meridional temperature gradient is at its greatest (Figure 1). This seesaw climate realization is the expected outcome of a collapse in the AMOC with an attendant reduction in the meridional ocean heat transport, and

is documented by the $\delta^{13}C$ proxy of the AMOC in showing the near-complete replacement of NADW with Antarctic bottom water in the eastern North Atlantic basin at the times of Heinrich events.

Despite their consistent relation to an ongoing climate oscillation, Heinrich events have commonly been identified as a trigger of abrupt climate change by forcing collapse of the AMOC [e.g., *Broecker*, 1994, 2003; *Timmermann et al*., 2005]. We argue instead that Heinrich events may themselves have occurred in response to a collapse of the AMOC. Surface-temperature forcing of the ice sheets can be ruled out because of strong attenuation through an ice sheet and because it is of the wrong sign to cause the disintegration of an ice shelf. A number of ocean models, however, simulate the development of a strong subsurface warming in response to a collapsed AMOC at the depths where the grounding lines of marine-based ice margins fringing the North Atlantic would occur, and benthic $\delta^{18}O$ and faunal records suggest a signal of subsurface warming at the time of Heinrich events. In view of the demonstrated sensitivity of ice shelves to oceanic thermal forcing, and because Heinrich events occurred at times of maximum expression of subsurface warming, we agree with *Shaffer et al*. [2004] in attributing the cause of Heinrich events to subsurface warming.

In view of this perspective on the origin of Heinrich events, many responses in the geologic record previously attributed to the influence of Heinrich events on climate instead represent a common response to a collapse of the AMOC triggered by some mechanism other than a Heinrich event. The atmospheric response to the extreme cooling in the North Atlantic and maximum expansion of sea ice produces the largest attenuations of the Asian and Indian monsoons and the most southerly displacement of the mean position of the ITCZ. One of the best-documented oceanic responses is the interhemispheric seesaw associated with the large reduction in cross-equatorial ocean heat transport. Warming of the South Atlantic, amplified by a reduction in sea ice extent there, is rapidly transmitted throughout the Southern Ocean by the ACC. SST warming and reduced sea ice extent may have allowed a southward shift of the mid-latitude westerlies, the combined effect of which was a breakdown in stratification and upwelling of CO_2-rich deepwater. Several mechanisms exist by which a collapse of the AMOC might lead to a warming of tropical Pacific SSTs, including a baroclinic adjustment of the thermocline or transmission of the Southern Ocean seesaw signal through the atmosphere or by shallow meridional overturning.

Modeling studies identify several mechanisms to explain the abrupt resumption of the AMOC and Northern Hemisphere warming after a Heinrich event: (1) a negative freshwater forcing [*Ganopolski and Rahmstorf*, 2001; *Schmittner et al*., 2002], (2) destabilization of the stratified water column due to the subsurface warming that developed when the AMOC collapsed [*Marotzke*, 1989; *Weaver and Sarachik*, 1991; *Winton*, 1997], (3) salt buildup during times of reduced AMOC [*Broecker et al*., 1990; *Schmidt et al*., 2006], and (4) changes in the surface salinity and temperature of the Southern Ocean in response to a warmer climate [*Knorr and Lohman*, 2003; *Weaver et al*., 2003]. Our simulations of ice-sheet mass balance suggest that a negative freshwater forcing is unlikely since warming in the tropical Pacific caused an increase in freshwater flux prior to an abrupt warming seen in the Greenland ice core record. Evidence for a subsurface warming in the North Atlantic [*Rasmussen and Thomsen*, 2004], for salt buildup in the subtropical North Atlantic [*Schmidt et al*., 2006], and for Southern Hemisphere warming in response to the collapsed AMOC [*Broecker*, 1998], however, suggests that some combination of these mechanisms may be responsible for causing the AMOC to resume.

What set the timescale of the 7-kyr climate oscillation? Of all the Earth system components that we argue were involved in this oscillation, the only one with a suitably long time constant is the ice sheets. Our mass-balance simulations identify a plausible mechanism for how the coupled system interacted to produce the changes in Northern Hemisphere ice sheets that set this timescale. We propose that the system will oscillate with this timescale only when the ice sheets are at an intermediate size. When they are larger, such as they were during MIS 4 or 2, their seaward-facing margins extend to and beyond North Atlantic coastlines, where they deliver a steady flux of icebergs which maintains the AMOC in a glacial mode. When at an intermediate size, however, seaward-facing margins may retreat from coastlines and thus reduce the freshwater flux from icebergs. Subsequent fluctuations in size then change the freshwater flux to the North Atlantic through modulation of icebergs' discharge and ablation. Changes in freshwater flux cause changes in the AMOC, which are then transmitted through the ocean and atmosphere to feed back on ice-sheet mass balance and cause additional changes in freshwater flux.

During MIS 3, an initial collapse of the AMOC occurred [*Shackleton et al*., 2000] perhaps in response to insolation forcing and the associated decrease from large-size MIS 4 to intermediate-size MIS 3 ice sheets. Seesaw warming in the tropical Pacific Ocean induced a more negative mass balance over Northern Hemisphere ice sheets, causing additional retreat that sustained a relatively high freshwater flux. Subsequent abrupt resumption of the AMOC initially spiked the freshwater flux to the North Atlantic by further increasing ice-sheet ablation, inducing the start of a gradual reduction in the AMOC (i.e., the start of the cooling phase of a Bond cycle). The seesaw cooling that shortly followed peak warming then caused the ice sheets to start to grow again,

reducing freshwater fluxes. However, seaward-facing margins of growing ice sheets eventually reached North Atlantic coastlines, thus again increasing freshwater fluxes from icebergs and causing the AMOC to collapse, which initiated the next climate oscillation. This conceptual framework suggests that the strength of the AMOC will be limited by positive and negative mass balances of the circum-North Atlantic ice sheets: a colder climate increases freshwater flux to the North Atlantic through increased calving, while a warmer climate also increases freshwater flux through increased melting and runoff.

Acknowledgments. We thank J. Ahn, H. Arz, E. Bard, G. Bond, E. Brook, C. Charles, T. Dokken, L. Edwards, M. Elliot, I. Hendy, T. Ivanochko, J. Kaiser, D. Lea, J. McManus, A. Mix, T. Rasmussen, J. Sachs, M. Siddall, L. Skinner, J. Stoner, L. Stott, H. Wang, and R. Zahn for providing their outstanding data sets, and the NOAA Paleoclimatology Program for maintaining an extraordinary data base of paleoclimate records. Anders Carlson and Robbie Toggweiler provided helpful comments, and thorough reviews by Chris Charles and Zhengyu Liu greatly improved the paper. Funded by the Paleoclimate Program of the U.S. National Science Foundation.

REFERENCES

Adkins J.F., A.P Ingersoll, and C. Pasquero, Rapid climate change and conditional instability of the glacial deep ocean from the thermobaric effect and geothermal heating, *Quat. Sci. Rev*., 24, 581-594, 2005.

Ahn, J., M. Wahlen, B.L. Deck, E. Brook, P.A. Mayewski, K.C. Taylor, and J.W.C. White, A record of atmospheric CO2 during the last 40,000 years from the Siple Dome, Antarctica ice core, *Jour. Geophys. Res.*, 109, D13305, doi:10.1029/2003JD004415, 2004.

Ahn, J., and E.J. Brook, Atmospheric CO2 and climate from 65 to 30 ka B.P., *Geophys. Res. Let.*, 34, L10703, doi:10.1029/2007GL029551, 2004.

Alexander, M.A., I. BladÈ, M. Newman, J.R. Lansante, N-C. Lau, and J.D. Scott, The atmospheric bridge: The influences of ENSO teleconnections on the air-sea interaction over the global oceans, *J. Climate*, 15, 2205-2231, 2003.

Alley, R.B., and P.U. Clark, The deglaciation of the northern hemisphere: A global perspective, *Ann. Rev. Earth Planet. Sci.*, 27, 149-182, 1999.

Alley, R.B., and D.R. MacAyeal, Ice-rafted debris associated with binge/purge oscillations of the Laurentide Ice Sheet, *Paleoceanography*, 9, 503-11, 1994.

Alley, R.B., P.U. Clark, L.D. Keigwin, and R.S. Webb, Making sense of millennial-scale climate change, in *Mechanisms of Global Climate Change at Millennial Time Scales*, *Geophys. Monogr. Ser*., vol. 112, edited by P.U. Clark, R.S. Webb, and L.D. Keigwin, pp. 385-394, AGU, Washington, D.C, 1999.

Alley, R.B., J.T. Andrews, D.C. Barber, and P.U. Clark, Comment on "Catastrophic ice shelf breakup as the source of Heinrich event icebergs" by C.L. Hulbe et al., *Paleoceanography*, 20, PA1009, doi:10.1029/2004PA001086, 2005.

Alley, R.B., S. Anandakrishnan, T.K. Dupont, B.R. Parizek, and D. Pollard, Effect of sedimentation on ice-sheet grounding-line stability, *Science*, 315, 1838-1841, 2007.

Altabet, M.A., M.J. Higginson, and D.W. Murray, The effect of millennial-scale changes in Arabian Sea denitrification on atmospheric CO_2, *Nature*, 415, 159-162, 2002.

Arz, H., J. Patzold, and G. Wefer, Correlated millennial-scale changes in surface hydrography and terrigenous sediment yield inferred from last-glacial marine deposits off northeastern Brazil, *Quat. Res.*, 50, 157-166, 1998.

Arz, H.W., F. Lamy, A. Ganopolski, N. Nowaczyka, and J. Patzold, Dominant Northern Hemisphere climate control over millennial-scale glacial sea-level variability, *Quat. Sci. Rev*., 26, 312-321, 2007.

Bard, E., F. Rostek, J.-L. Turon, and S. Gendreau, Hydrological impact of Heinrich events in the subtropical northeast Atlantic, *Science*, 289, 1321-1324, 2000.

Barnett, T.P., L. Dumenil, U. Schlese, E. Roeckner, and M. Latif, The effect of Eurasian snow cover on regional and global climate variations, *J. Atmos. Sci.*, 46, 661-685, 1989.

Bartoli, G., M. Sarnthein, and M. Weinelt, Late Pliocene millennial-scale climate variability in the northern North Atlantic prior to and after the onset of Northern Hemisphere glaciation, *Paleoceanography*, 21, PA4205, doi:10.1029/2005PA001185, 2006.

Bender, M.L., Interhemispheric phasing of millennial-duration climate events during the last 100 ka. AGU Chapman Conference on Mechanisms of Millennial-Scale Global Climate Change, Abstracts with Program, p. 10, 1998.

Bender, M, T. Sowers, M.-L. Dickson, J. Orchardo, P. Grootes, P.A. Mayewski, and D.A. Meese, Climate correlations between Greenland and Antarctica during the past 100,000 years, *Nature*, 372, 663-666, 1994.

Bender, M.L., B. Malaize, J. Orchardo, T. Sowers, and J. Jouzel, High-precision correlations of Greenland and Antarctic ice core records over the last 100 kyr, in *Mechanisms of Global Climate Change at Millennial Time Scales*, *Geophys. Monogr. Ser*., vol. 112, edited by P.U. Clark, R.S. Webb, and L.D. Keigwin, pp. 149-164, AGU, Washington, D.C, 1999.

Berger, A.L., and M.F. Loutre, Insolation values for the climate of the last 10 million years, *Quat. Sci. Rev*., 10, 297-317, 1991.

Blunier, T., and E.J. Brook, Timing of millennial-scale climate change in Antarctica and Greenland during the last glacial period, *Science*, 291, 109-112, 2001.

Blunier, T. *et al.*, Asynchrony of Antarctic and Greenland climate change during the last glacial period, *Nature*, 394, 739-743, 1998.

Bond, G., and R. Lotti, Iceberg discharges into the North Atlantic on millennial time scales during the last glaciation, *Science*, 267, 1005-1010, 1995.

Bond, G.C. *et al.*, Evidence of massive discharges of icebergs into the North Atlantic Ocean during the last glacial period, *Nature*, 360, 245-249, 1992.

Bond, G.C., W.S. Broecker, S. Johnsen, J. McManus, L. Labeyrie, J. Jouzel, and G. Bonani, Correlations between climate records from North Atlantic sediments and Greenland ice, *Nature*, 365, 143-147, 1993.

Bond, G.C., W. Showers, M. Elliot, M. Evans, R. Lotti, I. Hajdas, G. Bonani, and S. Johnsen, The North Atlantic's 1–2 kyr climate rhythm: relation to Heinrich events, Dansgaard/Oeschger cycles and the little ice age, in *Mechanisms of Global Climate Change at Millennial Time Scales*, *Geophys. Monogr. Ser*., vol. 112, edited by P.U. Clark, R.S. Webb, and L.D. Keigwin, pp. 35-58, AGU, Washington, D.C, 1999.

Boyle E.A., and L.D., Keigwin, Deep circulation of the North Atlantic over the last 200,000 years: geochemical evidence, *Science*, 218, 784-787, 1982.

Broecker, W.S., Massive iceberg discharges as triggers for global climate change, *Nature*, 372, 421-424, 1994.

Broecker, W.S., Paleocean circulation during the last deglaciation: a bipolar seesaw? *Paleoceanography*, 13, 119-121, 1998.

Broecker, W.S., Does the trigger for abrupt climate change reside in the ocean or the atmosphere? *Science*, 300, 1519-1522, 2003.

Broecker W.S., and E. Maier-Reimer, The influence of air and sea exchange on the carbon isotope distribution in the sea, *Global Biogeochem. Cycles*, 6, 315-320, 1992.

Broecker, W.S., G. Bond, M. Klas, G. Bonani, and W. Wolfli, A salt oscillator in the North Atlantic? 1. The concept, *Paleoceanography*, 5, 469-477, 1990.

Broecker, W.S., G.C. Bond, M. Klas, E. Clark, and J. McManus, Origin of the northern Atlantic's Heinrich events, *Clim. Dyn.*, 6, 265-273, 1992.

Brook, E.J., J.W.C. White, A.S.M. Schilla, M.L. Bender, B. Barnett, J.P. Severinghaus, K.C. Taylor, R.B. Alley, and E.J. Steig, Timing of millennial-scale climate change at Siple Dome, West Antarctica, during the last glacial period, *Quat. Sci. Rev*., 24, 1333-1343, 2005.

Bush, A.B.G., and S.G.H. Philander, The role of ocean-atmosphere interactions in tropical cooling during the Last Glacial Maximum, *Science*, 279, 1341-1344, 1998.

Cacho, I., J.O. Grimalt, C. Pelejero, M. Canals, F.J. Sierro, J.A. Flores, and N.J. Shackleton, Dansgaard–Oeschger and Heinrich event imprints in the Alboran Sea palaeotemperatures, *Paleoceanography*, 14, 698-705, 1999.

Calov, R., A. Ganopolski, V. Petoukhov, and M. Claussen, rge-scale instabilities of the Laurentide ice sheet simulated in a fully coupled climate-system model, *Geophys. Res. Lett.*, 29, 2216, doi:10.1029/2002GL016078, 2002.

Cane, M.A., A role for the tropical Pacific, *Science*, 282, 59-61, 1998.

Chappell, J., Sea-level changes forced ice breakouts in the Last Glacial cycle: New results from coral terraces, *Quat. Sci. Rev.*, 21, 1229-1240, 2002.

Charbit, S., M. Kageyama, D. Roche, C. Ritz, and G. Ramstein, Investigating the mechanisms leading to the deglaciation of past continental northern hemisphere ice sheets with the CLIMBER-GRMLINS coupled model, *Global Planetary Change*, 48, 253-273, 2005.

Charles, C.D., J. Lynch-Stieglitz, U.S. Ninneman, and R.G. Fairbanks, Climate connections between the hemispheres revealed by deep-sea sediment/ice core correlations, *Earth Planet. Sci. Let.*, 142, 19-27, 1996.

Chiang, J.C.H., M. Biasutti, and D.S. Battisti, Sensitivity of the Atlantic Intertropical Convergence Zone to Last Glacial Maximum boundary conditions, *Paleoceanography*, 18, 1094, doi:10.1029/2003PA000916, 2003.

Clark, P.U., N.G. Pisias, T.S. Stocker, and A.J. Weaver, The role of the thermohaline circulation in abrupt climate change, *Nature*, 415, 863-869, 2002.

Clark, P.U., A.M. McCabe, A.C. Mix, and A.J. Weaver, The 19-kyr B.P. meltwater pulse and its global implications, *Science*, 304, 1141-1144, 2004.

Clarke, G.K.C., S.J. Marshall, C. Hillaire-Marcel, G. Bilodeau, and C. Veiga-Pires, A glaciological perspective on Heinrich events, in *Mechanisms of Global Climate Change at Millennial Time Scales*, *Geophys. Monogr. Ser*., vol. 112, edited by P.U. Clark, R.S. Webb, and L.D. Keigwin, pp. 243-262, AGU, Washington, D.C, 1999.

Crowley, T.J., North Atlantic Deep Water cools the southern hemisphere, *Paleoceanography*, 7, 489-497, 1992.

Cruz, Jr., F.W., S.J. Burns, I. Karmann, W.D. Sharp, M. Vuille, A.O. Cardoso, J.A. Ferrari, P.L. Silva Dias, and O. Viana, Jr., Insolation-driven changes in atmospheric circulation over the past 116,000 years in subtropical Brazil, *Nature*, 434, 63-66, 2005.

Curry W.B., and G.P. Lohmann, Carbon isotopic changes in benthic foraminifera from the western South Atlantic: reconstructions of glacial abyssal circulation patterns, *Quat. Res*., 18, 218-235, 1982.

Dannenmann, S., B.K. Linsley, D.W. Oppo, Y. Rosenthal, and L. Beaufort, East Asian monsoon forcing of suborbital variability in the Sulu Sea during Marine Isotope Stage 3: Link to Northern Hemisphere climate, *Geochemistry, Geophysics, Geosystems*, 4, 1001, doi:10.1029/2002GC000390, 2003.

Dansgaard, W., H.B. Clausen, N. Gundestrup, C.U. Hammer, S.J. Johnsen, P.M. Kristinsdottir, and N. Reeh, A new Greenland deep ice core, *Science*, 218, 1273-1277, 1982.

Dansgaard W., S.J. Johnsen, H.B. Clausen, D. Dahl-Jensen, N. Gundestrup, C.U. Hammer, and H. Oeshger, North Atlantic climatic oscillations revealed by deep Greenland ice cores, in *Climate Processes and Climate Sensitivity*, *Geophys. Monogr. Ser*., vol. 29, edited by J.E. Hansen, T. Takahashi, pp. 288-298, AGU, Washington, D.C.

De Angelis, H., and P. Skvarca, Glacier surge after ice shelf collapse, *Science*, 299, 1560-1562, 2003.

Dokken, T.M., and E. Jansen, Rapid changes in the mechanism of ocean convection during the last glacial period, *Nature*, 401, 458-461, 1999.

Dong, B.W., and P.J. Valdes, Sensitivity studies of northern hemisphere glaciation using an atmospheric general circulation model, *J. Climate*, 8, 2471-2496, 1995.

Dong, B.W., and P.J. Valdes, Simulations of the Last Glacial Maximum climates using a general circulation model: prescribed versus computed sea surface temperatures, *Climate Dynamics*, 14, 571-591, 1998.

Douville, H., and J.-F. Royer, Sensitivity of the Asian summer monsoon to an anomalous Eurasian snow cover with the Meteo-France GCM, *Climate Dynamics*, 12, 449-466, 1996.

Dowdeswell, J.A., M.A. Maslin, J.T. Andrews, and I.N. McCave, Iceberg production, debris rafting, and the extent and thickness of Heinrich layers (H-1, H-2) in North Atlantic sediments, *Geology*, 23, 301-304, 1995.

Duplessy J.-C., N.J. Shackleton, R.G. Fairbanks, L. Labeyrie, D. Oppo, and N. Kallel, Deepwater source variations during the last climatic cycle and their impact on the global deepwater circulation, *Paleoceanography*, 3, 343-360, 1988.

Dyke, A.S., An outline of North American deglaciation with emphasis on central and northern Canada, in *Quaternary Glaciations-Extant and Chronology, Part II*, edited by J. Ehlers and P.L. Gibbard, pp. 373-424, Elsevier Science and Technology Books, Amsterdam, 2004.

Dyke, A.S., J.T. Andrews, P.U. Clark, J.H. England, G.H. Miller, J. Shaw, and J. Veillette, The Laurentide and Innuitian Ice Sheets during the Last Glacial Maximum, *Quat. Sci. Rev.*, 21, 9-32, 2002.

EPICA Community Members, One-to-one coupling of glacial climate variability in Greenland and Antarctica, *Nature*, 444, 195-198, 2006.

Fairbanks, R.G., R.A. Mortlock, T.-C. Chiua,, L. Caoa, A. Kaplan, T.P. Guilderson, T.W. Fairbanks, A.L. Bloom, P.M. Grootes, and M.-J. Nadeau, Radiocarbon calibration curve spanning 0 to 50,000 years BP based on paired $^{230}Th/^{234}U/^{238}U$ and ^{14}C dates on pristine corals, *Quat. Sci. Rev*., 24, 1781-1796, 2005.

Feldberg, M.J., and A.C. Mix, Planktonic foraminifera, sea surface temperatures, and mechanisms of oceanic change in the Peru and south equatorial currents, 0–150 ka BP, *Paleoceanography*, 18, PA1016, doi:10.1029/2001PA000740, 2003.

Flueckiger, J., R. Knutti, and J.W.C. White, Oceanic processes as potential trigger and amplifying mechanisms for Heinrich events, *Paleoceanography*, 21, PA2014, doi:10.1029/2005PA001204, 2006.

Ganachaud, A., and C. Wunsch, Improved estimates of global ocean circulation, heat transport and mixing from hydrographic data, *Nature*, 408, 453-457, 2000.

Ganopolski, A., and S. Rahmstorf, Rapid changes of glacial climate simulated in acoupled climate model, *Nature*, 409, 153-158, 2001.

Giorgi, F., M.R. Marinucci, and G.T. Bates, Development of a second-generation regional climate model (RegCM2). Part I: Boundary-layer and radiative transfer processes, *Monthly Weather Review*, 121, 2794-2813, 1993.

Grimm, E.C., W.A. Watts, G.L. Jacobson, Jr., B.C.S. Hansen, H. Almquist, and A.C. Dieffenbacher-Krall, Evidence for warm wet Heinrich events in Florida, *Quat. Sci. Rev.*, 25, 2197-2211, 2006.

Grootes, P.M., M. Stuiver, J.W.C. White, S.J. Johnsen, and J. Jouzel, Comparison of oxygen isotope records from the GISP2 and GRIP Greenland ice cores, *Nature*, 366, 552-554, 1993.

Gu, D., and S.G.H. Philander, Interdecadal climate fluctuations that depend on exchanges between the tropics and extratropics, *Science*, 275, 805-807, 1997.

Gwiazda, R.H., S.R. Hemming, and W.S. Broecker, Tracking the sources of icebergs with lead isotopes: The provenance of ocean-rafted debris in Heinrich Layer 2, *Paleoceanography*, 11, 77-93, 1996.

Hanebuth, T., K. Stattegger, and P.M. Grootes, Rapid flooding of the Sunda shelf: A late-glacial sea-level record, *Science*, 288, 1033-1035, 2000.

Hemming, S.R., W.S. Broecker, W.D. Sharp, G.C. Bond, R.H. Gwiazda, J.F. McManus, M. Klas, and I. Hajdas, Provenance of Heinrich layers in core V28–82, northeastern Atlantic: ^{40}Ar-^{39}Ar ages of ice-rafted hornblende, Pb isotopes in feldspar grains, and Nd-Sr-Pb isotopes in the fine sediment fraction, *Earth Planet. Sci. Lett.*, 164, 317-333, 1998.

Hemming, S.R., Heinrich events: Massive late Pleistocene detritus layers of the North Atlantic and their global climate imprint, *Rev. Geophysics*, 42, RG1005, doi:10.1029/2003RG000128, 2004.

Hendy, I.L., and J.P. Kennett, Dansgaard-Oeschger cycles and the California Current System: Planktonic foraminiferal response to rapid climate change in Santa Barbara Basin, Ocean Drilling Program hole 893A, *Paleoceanography*, 15, 30-42, 2000.

Hill, H.W., B.P. Flower, T.M. Quinn, D.J. Hollander, and T.P. Guilderson, Laurentide Ice Sheet meltwater and abrupt climate change during the last glaciation, *Paleoceanography*, 21, doi:10.1029/2005PA001186, 2006.

Hillaire-Marcel, C., and G. Bilodeau, Instabilities in the Labrador Sea water mass structure during the last climatic cycle, *Can. Jour. Earth Sci.*, 37, 795-809, 2000.

Hodell, D.A., K.A. Venz, C.D. Charles, and U.S. Ninnemann, Pleistocene vertical carbon isotope and carbonate gradients in the South Atlantic

sector of the Southern Ocean, *Geochemistry, Geophysics, Geosystems*, 4, doi:10.1029/2002GC000367, 2003.

Hoerling, M.P., and A. Kumar, Atmospheric response patterns associated with tropical forcing, *J. Climate*, 15, 2184-2203, 2002.

Hostetler, S.W., and A.C. Mix, Ice age cooling of the tropics reassessed, *Nature*, 399, 673-676, 1999.

Hostetler, S.W., P.U. Clark, P.J. Bartlein, A.C. Mix, and N.G. Pisias, Atmospheric transmission of North Atlantic Heinrich Events, *Jour. Geophys. Res.*, 104, 3947-3952, 1999.

Hostetler, S.W., N.G. Pisias, and A.C. Mix, Sensitivity of the Last Glacial climate to uncertainties in tropical and subtropical ocean temperatures, *Quat. Sci. Rev.*, 25, 1168-1185, 2006.

Huber, C., M. Leuenberger, R. Spahni, J. Fluckiger, J. Schwander, T.F. Stocker, S. Johnsen, A. Landais, and J. Jouzel, Isotope calibrated Greenland temperature record over Marine Isotope Stage 3 and its relation to CH4. *Earth and Planetary Science Letters*, 243, 504-519, 2006.

Hulbe, C.L., D.R. MacAyeal, G.H. Denton, J. Kleman, and T.V. Lowell, Catastrophic ice shelf breakup as the source of Heinrich event icebergs, *Paleoceanography*, 19, PA1004, doi:10.1029/2003PA000890, 2004.

Huybrechts, P., and J. de Wolde, The dynamic response of the Greenland and Antarctic ice sheets to multiple-century climatic warming, *Jour. Climate*, 12, 2169-2188, 1999.

Huybrechts, P., J. Gregory, I. Janssens, and M. Wild, Modelling Antarctic and Greenland volume changes during the 20th and 21st centuries forced by GCM time slice integrations, *Global and Planetary Change*, 42, 83-105, 2004.

Indermuhle, A., E. Monnin, B. Stauffer, and T.F. Stocker, Atmospheric CO_2 concentration from 60 – 20 kyr BP from the Taylor Dome ice core, Antarctica, *Geophys. Res. Lett.*, 27, 735-738, 2000.

lversen, J., The late glacial flora of Denmark and its relation to climate and soil, *Damn. Geol. Unders. Ser. H.*, 80, 87-119, 1954.

Ivanochko, T., R.S. Ganeshram, G.-J.A. Brummer, G. Ganssen, S.J.A. Jung, S.G. Moreton, and D. Kroon, Variations in tropical convection as an amplifier of global climate change at the millennial scale, *Earth Plan. Sci. Let.*, 235, 302-314, 2005.

Jensen, K., Some west Baltic pollen diagrams, *Quartar.*, 1, 124-139, 1938.

Johnsen, S.J., W. Dansgaard, H.B. Clausen, and C.C. Langway, Jr., Oxygen isotope profiles through the Antarctic and Greenland ice sheets, *Nature*, 235, 429-434, 1972.

Jullien, E., F.E. Grousset, S.R. Hemming, V.L. Peck, I.R. Hall, C. Jeantet, and I. Billy, Contrasting conditions preceding MIS3 and MIS2 Heinrich events, *Global and Planetary Change* 54, 225-238, 2006.

Justino, F., A. Timmermann, U. Merkel, and E.P. Souza, Synoptic reorganization of atmospheric flow during the Last Glacial Maximum, *Jour. Clim.*, 18, 2826-2846, 2005.

Kaiser J., F. Lamy, and D. Hebbeln, A 70-kyr sea surface temperature record off southern Chile (Ocean Drilling Program Site 1233), *Paleoceanography*, 20, PA4009, doi:10.1029/ 2005PA001146, 2005.

Kiefer, T., and M. Kienast, Patterns of deglacial warming in the Pacific Ocean: a review with emphasis on the time interval of Heinrich event 1, *Quat. Sci. Rev.*, 24, 1063-1081, 2005.

Knorr, G., and G. Lohman, Southern Ocean origin for the resumption of Atlantic thermohaline circulation during deglaciation, *Nature*, 424, 532-536, 2003.

Knutti, R., J. Fluckiger, T.F. Stocker, and A. Timmermann, Strong hemispheric coupling of glacial climate through freshwater discharge and ocean circulation, *Nature*, 430, 851-856, 2004.

Lau, N.-C., and M.J. Nath, The role of the "Atmospheric Bridge" in linking tropical Pacific ENSO events to extratropical SST anomalies, *Jour. Clim.*, 9, 2036-2057, 1996.

Lea, D.W., D.K. Pak, and H.J. Spero, Climate impact of late Quaternary equatorial Pacific sea surface temperature variations, *Science*, 289, 1719-1724, 2000.

Lea, D.W., D.K. Pak, C.L. Belanger, H.J. Spero, M.A. Hall, and N.J. Shackleton, Paleoclimate history of Galapagos surface waters over the last 135,000 years, *Quat. Sci. Rev.*, 25, 1152-1167, 2006.

Lee, S.-Y., and C.J. Poulsen, Sea ice control of Plio–Pleistocene tropical Pacific climate evolution, *Earth Planet. Sci. Let.*, 248, 238-247, 2006.

Licciardi, J.M., P.U. Clark, J.W. Jenson, and D.R. MacAyeal, Deglaciation of a soft-bedded Laurentide Ice Sheet, *Quat. Sci. Rev.,* 17, 427-448, 1998.

Liu, Z., S.I. Shin, B. Otto-Bliesner, J.E. Kutzbach, E.C. Brady, and D.E. Lee, Tropical cooling at the Last Glacial Maximum and extratropical ocean ventilation, *Geophys. Res. Let.*, 29, doi:10.1029/2001GL013939, 2002.

Liu, Z., and H. Yang, Extratropical control of tropical climate, the atmospheric bridge and oceanic tunnel, *Geophys. Res. Let.*, 30, doi:10.1029/ 2002GL016492, 2003.

Lu, P., J. McCreary, and B.A. Klinger, Meridional circulation cells and the source waters of the Pacific equatorial undercurrent, *Jour. Phys. Ocean.*, 28, 62-84, 1998.

Lynch-Stieglitz, J., W.B. Curry, and N. Slowey, Weaker Gulf Stream in the Florida Straits during the last glacial maximum, *Nature*, 402, 644-648, 1999.

MacAyeal, D.R., Binge/purge oscillations of the Laurentide ice sheet as a cause of the North Atlantic's Heinrich events, *Paleoceanography*, 8, 775-784, 1993.

Manabe, S., and R.J. Stouffer, Two stable equilibria of a coupled ocean-atmosphere model, *Jour. Clim.*, 1, 841-866, 1988.

Marchal, O., T.F. Stocker, and F. Joos, Impact of oceanic reorganizations on the ocean carbon cycle and atmospheric carbon dioxide content, *Paleoceanography*, 13, 225-244, 1998.

Marotzke, J., Instabilities and multiple steady states of the thermohaline circulation, iu *Ocean Circulation Models: Combining Data and Dynamics,* edited by D.L.T. Anderson, and J. Willebrand, pp. 501-511, NATO ASI Ser., vol. I., 1989.

Marshall, S.J., and G.K.C. Clarke, A continuum mixture model of ice stream thermomechanics in the Laurentide Ice Sheet, 2. Application to the Hudson Strait Ice Stream, *Jour. Geophys. Res.*, 102, 20,615-20,638, 1997.

Marshall, S.J., and G.K.C. Clarke, Ice sheet inception: subgrid hypsometric parameterization of mass balance in an ice sheet model, *Clim. Dyn.*, 15, 533-550, 1999.

Marshall, S.J., and M.R. Koutnik, Ice sheet action versus reaction: Distinguishing between Heinrich events and Dansgaard-Oeschger cycles in the North Atlantic, *Paleoceanography*, 21, PA2021, doi:10.1029/ 2005PA001247, 2006.

Martin, P., D. Archer, and D.W. Lea, Role of deep sea temperature in the carbon cycle during the last glacial, *Paleoceanography*, 20, PA2015, doi:10.1029/2003PA000914, 2005.

Martinez, I., L. Keigwin, T.T. Barrows, Y. Yokoyama, and J. Southon, La Nina-like conditions in the eastern equatorial Pacific and a stronger Choco jet in the northern Andes during the last glaciation, *Paleoceanography*, 18, 1033, doi:10.1029/2002PA000877, 2003.

McManus, J.F., R.F. Anderson, W.S. Broecker, M.Q. Fleisher, and S.M. Higgins, Radiometrically determined sedimentary fluxes in the sub-polar North Atlantic during the last 140,000 years, *Earth Planet. Sci. Lett.*, 155, 29-43, 1998.

McManus, J.F., D.W. Oppo, and J.L. Cullen, A 0.5-million-year record of millennial-scale climate variability in the North Atlantic, *Science*, 283, 971-975, 1999.

McManus, J.F., R. Francois, J.-M. Gherardi, L.D. Keigwin, and S. Brown-Leger, Collapse and rapid resumption of the Atlantic meridional circulation linked to deglacial climate changes, *Nature*, 428, 834-837, 2004.

Merz, A., and G. Wuest, Die Atlantische Vertikalzirkulation, Zeitschrift der Gesellschaft fuer Erdkunde zu Berlin, *Jahrgang*, 1922, 1-35, 1922.

Mikolajewicz, U., T.J. Crowley, A. Schiller, and R. Voss, Modelling teleconnections between the North Atlantic and North Pacific during the Younger Dryas, *Nature*, 387, 384-387, 1997.

Mitchell, J.M., An overview of climatic variability and its causal mechanisms, *Quat. Res.*, 6, 481-493, 1976.

Mix, A.C., W.F. Ruddiman, and A. McIntyre, Late Quaternary paleoceanography of the tropical Atlantic, 1: Spatial variability of annual mean sea-surface temperatures, 0-20,000 years B.P., *Paleoceanography*, 1, 43-66, 1986.

Mix, A.C., D.C. Lund, N.G. Pisias, P. Boden, L. Bornmalm, M. Lyle, and J. Pike, Rapid climate oscillations in the Northeast Pacific during the last deglaciation reflect northern and southern hemisphere sources, in *Mechanisms of Global Climate Change at Millennial Time Scales*, *Geophys. Monogr. Ser*., vol. 112, edited by P.U. Clark, R.S. Webb, and L.D. Keigwin, pp. 127-148, AGU, Washington, D.C, 1999.

Mix, A.C., A.E. Morey, N.G. Pisias, and S.W. Hostetler, Foramininiferal faunal estimates of paleotemperature: Circumventing the no-analog problem yields cool ice age tropics, *Paleoceanography*, 14, 350-359, 1999.

Ninnemann, U.S., C.D. Charles, and D.A. Hodell, Origin of millennial scale climate events: Constraints from the Southern Ocean deep sea sedimentary record, in *Mechanisms of Global Climate Change at Millennial Time Scales*, *Geophys. Monogr. Ser*., vol. 112, edited by P.U. Clark, R.S. Webb, and L.D. Keigwin, pp. 99-112, AGU, Washington, D.C, 1999.

Oerlemans, J., Evaluating the role of climate cooling in iceberg production and the Heinrich events, *Nature*, 364, 783-786, 1993.

Oeschger H., J. Beer, U. Siegenthaler, B. Stauffer, W. Dansgaard, and C.C. Langway, Late glacial climate history from ice cores, in *Climate Processes and Climate Sensitivity*, *Geophys. Monogr. Ser*., vol. 29, edited by J.E. Hansen, T. Takahashi, pp. 299-306, AGU, Washington, D.C, 1984.

Olsen, S.M., G. Shaffer, and C.J. Bjerrum, Ocean oxygen isotope constraints on mechanisms for millennial-scale climate variability, *Paleoceanography*, 20, PA1014, doi:10.1029/2004PA001063, 2005.

Pahnke, K., R. Zahn, H. Elderfield, and M. Schulz, 340,000-year centennial-scale marine record of Southern Hemisphere climatic oscillation, *Science*, 301, 948-952, 2003.

Pahnke, K., and R. Zahn, Southern Hemisphere water mass conversion linked with North Atlantic climate variability, *Science*, 307, 1741-1746, 2005.

Pailler, D., and E. Bard, High frequency palaeoceanographic changes during the past 140 000 yr recorded by the organic matter in sediments of the Iberian Margin, *Palaeogeography, Palaeoclimatology, Palaeoecology*, 181, 431-452, 2002.

Palmer, M.R., and P.N. Pearson, A 23,000-year record of surface water pH and pCO_2 in the western equatorial Pacific Ocean, *Science*, 300, 480-482, 2003.

Petit, J.R. *et al.*, Climate and atmospheric history of the past 420,000 years from the Vostok ice core, Antarctica, *Nature*, 399, 429-436, 1999.

Pelteir, W.P., Ice age paleotopography, *Science*, 265, 195-201, 1994.

Peterson, L.C., G.H. Haug, K.A. Hughen, and U. Rohl, Rapid changes in the hydrologic cycle of the tropical Atlantic during the last glacial, *Science*, 290, 1947-1951, 2000.

Piotrowski, A.M., S.L. Goldstein, S.R. Hemming, and R.G. Fairbanks, Temporal relationships of carbon cycling and ocean circulation at glacial boundaries, *Science*, 307, 1933-1938, 2005.

Pisias, N.G., and A.C. Mix, Spatial and temporal oceanographic variability of the eastern equatorial Pacific during the late Pleistocene: Evidence from radiolaria microfossils, *Paleoceanography*, 12, 381-393, 1997.

Pollard, D., and S.L. Thompson, Climate and ice-sheet mass balance at the Last Glacial Maximum from GENESIS version 2 global climate model, *Quat. Sci. Rev.*, 16, 841-863, 1997.

Pollard, D., and PMIP Participating Groups, Comparisons of ice-sheet surface mass budgets from Paleoclimate Modeling Intercomparison Project_PMIP/simulations, *Global Planet. Change*, 24, 76-106, 2000.

Rahmstorf, S., Bifurcations of the Atlantic thermohaline circulation in response to changes in the hydrological cycle, *Nature*, 378, 145-149, 1995.

Rashid, H., R. Hesse, and D.J.W. Piper, Evidence for an additional Heinrich event between H5 and H6 in the Labrador Sea, *Paleoceanography*, 18, 1077, doi:10.1029/ 2003PA000913, 2003.

Rasmussen, T.L., E. Thomsen, T.C.E. van Weering, and L. Labeyrie, Rapid changes in surface and deep water conditions at the Faeroe Margin during the last 58,000 years, *Paleoceanography*, 11, 757-771, 1996.

Rasmussen, T.L., D.W. Oppo, E. Thomsen, and S.J. Lehman, Deep-sea records from the SE Labrador Sea: ocean circulation changes and ice-rafting events during the last 160,000 years, *Paleoceanography*, 18, 1018 (doi: 1029/2001PA000736), 2003.

Rasmussen, T.L., and E. Thomsen, The role of the North Atlantic Drift in the millennial timescale glacial climate fluctuations, Palaeogeogr. Palaeoclimatol. Palaeoecol., 210(1), 101-116, 2004.

Raymo, M.E., K. Ganley, S. Carter, D.W. Oppo, and J. McManus, Millennial-scale climate instability during the early Pleistocene epoch, *Nature*, 392, 699-702, 1998.

Rignot, E., and S.S. Jacobs, Rapid bottom melting widespread near Antarctic ice sheet grounding lines, *Science*, 296, 2020 –2023, 2002.

Rignot, E., G. Casassa, P. Gogineni, W. Krabill, A. Rivera, and R. Thomas, Accelerated ice discharge from the Antarctic Peninsula following the collapse of Larsen B ice shelf, *Geophys. Res. Lett*., 31, L18401, doi:10.1029/ 2004GL020697, 2004.

Rind, D., Latitudinal temperature gradients and climate change, *Jour. Geophys. Res.*, 103, 5943-5971, 1998.

Rind, D., G. Russell, G. Schmidt, S. Sheth, D. Collins, P. deMenocal, and J. Teller, Effects of glacial meltwater in the GISS coupled atmosphere-ocean model 2., A bipolar seesaw in Atlantic Deep Water production, *Jour. Geophys. Res.*, 106, 27,355-27,365, 2001.

Robinson, R.S., A. Mix, and P. Martinez, Southern Ocean control on the extent of denitrification in the southeast Pacific over the last 70 ka, *Quat. Sci. Rev.*, 26, 201-212, 2007.

Roche, D., D. Paillard, and E. Cortijo, Constraints on the duration and freshwater release of Heinrich event 4 through isotope modelling, *Nature*, 432, 379-382, 2004.

Rodgers, K., M.A. Cane, N. Naik, and D. Schrag, The role of the Indonesian throughflow in equatorial Pacific thermocline ventilation, *Jour. Geophys. Res.*, 104, 20,551-20,570, 1999.

Rodgers, K.B., B. Blanke, G. Madec, O. Aumont, P. Ciais, and J.-C. Dutay, Extratropical sources of Equatorial Pacific upwelling in an OGCM, *Geophys. Res. Let.*, 30, 1084, doi:10.1029/2002GL016003, 2003.

Rodgers, K.B., G. Lohmann, S. Lorenze, R. Schneider, and G.M. Henderson, A tropical mechanism for Northern Hemisphere deglaciation, *Geochemistry, Geophysics, Geosystems, 4,* doi:10.1029/2003GC000508, 2003.

Rodgers, K.B., C. Ritz, J.H. Yin, G. Lohmann, S.J. Lorenze and M. Khodri, Sensitivity of Northern Hemispheric continental ice sheets to tropical SST during deglaciation, *Geophys. Res. Let.*, 31, doi:10.129/2003GL018375, 2004.

Rohling, E.J., R. Marsh, N.C. Wells, M. Siddall, and N.R. Edwards, Similar meltwater contributions to glacial sea level changes from Antarctic and northern ice sheets, *Nature*, 430, 1016-1021, 2004.

Ruhlemann, C., S. Mulitza, P.J. Muller, G. Wefer, and R. Zahn, Warming of the tropical Atlantic Ocean and slowdown of thermohaline circulation during the last deglaciation, *Nature*, 402, 511-514, 1999.

Rutberg, R.L., S.R. Hemming, and S.L. Goldstein, Reduced North Atlantic Deep Water flux to the glacial Southern Ocean inferred from neodymium isotope ratios, *Nature*, 405, 935-938, 2000.

Sachs, J.P., and R.F. Anderson, Increased productivity in the subantarctic ocean during Heinrich events, *Nature*, 434, 1118-1121, 2005.

Saenko, O.A., A. Schmittner, and A.J. Weaver, The Atlantic-Pacific Seesaw, *Jour. Clim.*, 17, 2033-2038, 2004.

Sarmiento, J.L., N. Gruber, M.A. Brzezinski, and J.P. Dunne, High-latitude controls of thermocline nutrients and low latitude biological productivity, *Nature,* 427, 56-60, 2004.

Sarnthein, M., K. Winn, S.J.A. Jung, J.C. Duplessy, H. Erlenkeuser, and G. Ganssen, Changes in east Atlantic deepwater circulation over the last 30,000 years: Eight time slice reconstructions, *Paleoceanography*, 9, 209-267, 1994.

Sarnthein, M. *et al.*, Fundamental modes and abrupt changes in North Atlantic circulation and climate over the last 60 ky - Concepts, reconstruction and numerical modeling, in *The Northern North Atlantic: A Changing Environment*, edited by P. Schafer et al., pp. 365-410, Springer, New York, 2001.

Schiller, A., U. Mikolajewicz, and R. Voss, The stability of the North Atlantic thermohaline circulation in a coupled ocean-atmosphere general circulation model, *Clim. Dyn.*, 13, 325-347, 1997.

Schmidt, M.W., M.J. Vautravers, and H.J. Spero, Rapid subtropical North Atlantic salinity oscillations across Dansgaard-Oeschger cycles, *Nature*, 443, 561-564, 2006.

Schmittner, A., and T.F. Stocker, The stability of the thermohaline circulation in global warming experiments, *Jour. Clim.*, 12, 1117-1133, 1999.

Schmittner, A., and A.C. Clement, Sensitivity of the thermohaline circulation to tropical and high latitude freshwater forcing during the last glacial-interglacial cycle, *Paleoceanography*, 17, doi:10.1029/2000PA000591, 2002.

Schmittner, A., M. Yoshimori, and A.J. Weaver, Instability of glacial climate in a model ofthe ocean–atmosphere–cryosphere system, *Science*, 295, 1493-1498, 2002.

Schmittner, A., O.A. Saenko, and A.J. Weaver, Coupling of the hemispheres in observations of glacial climate change, *Jour. Clim.*, 22, 659-671, 2003.

Schmittner, A., E.D. Galbraith, S.W. Hostetler, T.F. Pedersen, and R. Zhang, Large oxygen fluctuations in the Indian and Pacific Oceans caused by variations of North Atlantic Deep Water subduction, *Paleoceanography*, in press, 2007.

Schulz, H., U. von Rad, and H. Erlenkeuser, Correlation between Arabian Sea and Greenland climate oscillations of the past 110,000 years, *Nature*, 393, 54-57, 1998.

Schulz, M., W.H. Berger, M. Sarnthein, and P.M. Grootes, Amplitude variations of 1470-year climate oscillations during the last 100,000 years linked to fluctuations of continental ice mass, *Geophys. Res. Let.*, 26, 3385-3388, 1999.

Shackleton, N.J., M.A. Hall, and E. Vincent, Phase relationships between millennial scale events 64,000 to 24,000 years ago, *Paleoceanography*, 15, 565-569, 2000.

Shaffer, G., S.M. Olsen, and C.J. Bjerrum, Ocean subsurface warming as a mechanism for coupling Dansgaard-Oeschger climate cycles and ice-rafting events, *Geophys. Res. Lett.*, 31, L24202, doi:10.1029/2004GL020968, 2004.

Shemesh, A., D. Hodell, X. Crosta, S. Kanfoush, C. Charles, and T. Guilderson, Sequence of events during the last deglaciation in Southern Ocean sediments and Antarctic ice cores, *Paleoceanography*, 17, doi:10.1029/2000PA000599, 2002.

Siddall, M., E.J. Rohling, A. Almogi-Labin, Ch. Hemleben, D. Meischner, I. Schmelzer, and D.A. Smeed, Sea-level fluctuations during the last glacial cycle, *Nature*, 423, 853-858, 2003.

Siddall, M.E., E.J. Rohling, W.G. Thompson, and C. Waelbroeck, in review, MIS 3 sea level changes: synthesis and new outlook, *Rev. Geophys.*

Sigman, D.M., and E.A. Boyle, Glacial/interglacial variations in atmospheric carbon dioxide, *Nature*, 407, 859-869, 2000.

Skinner, L.C., and H. Elderfield, Rapid fluctuations in the deep North Atlantic heat budget during the last glacial period, *Paleoceanography*, 22, PA1205, doi:10.1029/ 2006PA001338, 2007.

Sowers, T., and M. Bender, Climate records covering the last deglaciation, *Science*, 269, 210-214, 1995.

Stauffer, B. *et al.*, Atmospheric CO_2 concentration and millennial-scale climate change during the last glacial period, *Nature*, 392, 59-62, 1998.

Steig, E.J., D.L. Morse, E.D. Waddington, M. Stuiver, P.M. Grootes, P.A. Mayewski, M.S. Twickler, and A.I. Whitlow, Wisconsinan and Holocene climate history from an ice core at Taylor Dome, western Ross embayment, Antarctica, *Geografiska Annaler*, 82A, 213-235, 2000.

Stocker, T.F., and S.J. Johnsen, A minimum thermodynamic model for the bipolar seesaw, *Paleoceanography*, 18, doi:10.1029/2003PA000920, 2003.

Stocker, T.F., D.G. Wright, and L.A. Mysak, A zonally averaged, coupled ocean atmosphere model for paleoclimate studies, *Jour. Clim.*, 5, 773-797, 1992.

Stocker, T.F., The seesaw effect, *Science*, 282, 61-62, 1998.

Stocker, T.F, North-south connections, *Science*, 297, 1814-1815, 2002.

Stoner, J.S., J.E.T. Channell, and C. Hillaire-Marcel, A 200 kyr geomagnetic stratigraphy for the Labrador Sea: indirect correlation of the sediment record to SPECMAP, *Earth Planet. Sci. Let.*, 159, 165-181, 1998.

Stoner, J.S., J.E.T. Channell, C. Hillaire-Marcel, and C. Kissel, Geomagnetic paleointensity and environmental record from Labrador Sea core MD95-2024: global marine sediment and ice core chronostratigraphy for the last 110 kyr, *Earth Planet. Sci. Let.*, 183, 161-177, 2000.

Stott, L., C. Poulsen, S. Lund, and R. Thunell, Super ENSO and global climate oscillations at millennial time scales, *Science*, 297, 222-226, 2002.

Stouffer, R.J. *et al.*, Investigating the causes of the response of the thermohaline circulation to past and future climate changes, *Jour. Climate*, 19, 1365-1387, 2006.

Stuiver, M., and P.M., Grootes, GISP2 oxygen isotope ratios, *Quat. Res.*, 53, 277-284, 2000.

Thompson, S.L., and D. Pollard, A global climate model (GENESIS) with a land-surface transfer scheme (LSX). Part I: present climate simulation, *Jour. Clim.*, 8, 732-761, 1995.

Timmermann, A., U. Krebs, F. Justino, H. Goosse, and T. Ivanochko, Mechanisms for millennial-scale global synchronization during the last glacial period, *Paleoceanography*, 20, PA4008, doi:10.1029/2004PA001090, 2005.

Toggweiler, J.R., K. Dixon, and W.S. Broecker, The Peru upwelling and the ventilation of the South-Pacific thermocline, *Jour. Geophys. Res.*, 96, 20467-20497, 1991.

Trenberth, K., G.W. Branstator, D. Karoly, A. Kumar, N.-C. Lau, and C. Ropelewski, Progress during TOGA in understanding and modeling global teleconnections associated with sea surface temperatures, *Jour. Geophys. Res.*, 103, 14,291,14,324, 1998.

Vellinga, M., and R.A. Wood, Global climatic impacts of a collapse of the Atlantic thermohaline circulation, *Climatic Change*, 54, 251-267, 2002.

Visser, K., R. Thunell, and L. Stott, Magnitude and timing of temperature change in the Indo-Pacific warm pool during deglaciation, *Nature*, 421, 152-155, 2003.

Wang, Y.J., H. Cheng, R.L. Edwards, Z.S. An, J.Y. Wu, C.-C. Shen, and J.A. Dorale, A high-resolution absolute-dated late Pleistocene monsoon record from Hulu Cave, China, *Science*, 294, 2345-2348, 2001.

Wang, X., A.S. Auler, R.L. Edwards, H. Cheng, P.S. Cristalli, P.L. Smart, D.A. Richards, and C.-C. Shen, Wet periods in northeastern Brazil over the past 210 kyr linked to distant climate anomalies, *Nature,* 432, 740-743, 2004.

Weaver, A.J., Extratropical subduction and decadal modulation of El Nino, *Geophys. Res. Let.*, 26, 743-746, 1999.

Weaver, A.J., and E.S. Sarachik, The role of mixed boundary conditions in numerical models of the ocean's climate, *Jour. Phys. Ocean.*, 21, 1470-1493, 1991.

Weaver, A.J. *et al.*, The UVic Earth System Climate Model: model description, climatology, and applications to past, present and future climates, *Atmosphere-Ocean*, 39, 361-428, 2001.

Weaver, A.J., O.A. Saenko, P.U. Clark, and J.X. Mitrovica, Meltwater pulse 1A from Antarctica as a trigger of the Bølling-Allerød warm period, *Science*, 299, 1709-1713, 2003.

Wilson, G.C., A.E. Litherland, and J.C. Rucklidge, Dating of sediments using accelerator mass spectrometry, *Chem. Geol.*, 44, 1-17, 1984.

Winton, M., The effect of cold climate upon North Atlantic Deep Water formation in a simple ocean– atmosphere model, *Jour. Clim.*, 10, 37-51, 1997.

Wunsch, C., Greenland-Antarctic phase relations and millennial timescale fluctuations in the Greenland cores, *Quat. Sci. Rev.,* 22, 1631-1646, 2003.

Wunsch, C., Abrupt climate change: An alternative view, *Quat. Res.*, 65, 191-203, 2006.

Yin, J., and D.S. Battisti, The importance of tropical sea surface temperature patterns in simulations of the Last Glacial Maximum climate, *Jour. Climate*, 14, 565-581, 2001.

Yokoyama, Y., K. Lambeck, P. De Deckker, P. Johnston, and L.K. Fifield, Timing of the Last Glacial Maximum from observed sea-level minima, *Nature*, 406, 713-716, 2000.

Yokoyama, Y., T.M. Esat, and K. Lambeck, Coupled climate and sea-level changes deduced from Huon Peninsula coral terraces of the last ice age, *Earth Planet. Sci. Let.*, 193, 579-587, 2001.

Zahn, R., J. Schonfeld, H.-R. Kudrass, M.-H. Park, H. Erlenkeuser, and P. Grootes, Thermohaline instability in the North Atlantic during meltwater events: Stable isotope and ice-rafted detritus records from core S075-26KL, Portugese margin, *Paleoceanography*, 12, 696-710, 1997.

Zhang, R., and T.L. Delworth, Simulated tropical response to a substantial weakening of the Atlantic thermohaline circulation, *Jour. Clim.*, 18, 1853-1860, 2005.

Zhao, P., X. Zhou, Z. Jiam, M. Sparrow, and Y. Han, Modeling the tropical climate and the impact of the western Pacific sea surface temperature at the Last Glacial Maximum, *Jour. Geophys. Res.*, 109, doi:10.1029/ 2003JD004095, 2004.

Zweck, C., and P. Huybrechts, Modeling of the northern hemisphere ice sheets during the last glacial cycle and glaciological sensitivity, *Jour. Geophys. Res.*, 110, doi:10.1029/ 2004JD005489, 2005.

P. U. Clark, Department of Geosciences, Oregon State University, Corvallis, Oregon 97331, USA. (clarkp@onid.orst.edu)

S. W. Hostetler, U.S. Geological Survey, Department of Geosciences, Oregon State University, Corvallis, Oregon 97331, USA.

K. J. Meissner, School of Earth and Ocean Sciences, University of Victoria, Victoria, British Columbia V8W 3P6, Canada.

N. G. Pisias and A. Schmittner, College of Oceanic and Atmospheric Sciences, Oregon State University, Corvallis, Oregon 97331, USA.